



Search for pair production of higgsinos in events with two Higgs bosons and missing transverse momentum in $\sqrt{s} = 13$ TeV pp collisions at the ATLAS experiment

The ATLAS Collaboration

This paper presents a search for pair production of higgsinos, the supersymmetric partners of the Higgs bosons, in scenarios with gauge-mediated supersymmetry breaking. Each higgsino is assumed to decay into a Higgs boson and a nearly massless gravitino. The search targets events where each Higgs boson decays into $b\bar{b}$, leading to a reconstructed final state with at least three energetic b -jets and missing transverse momentum. Two complementary analysis channels are used, with each channel specifically targeting either low or high values of the higgsino mass. The low-mass (high-mass) channel exploits 126 (139) fb^{-1} of $\sqrt{s} = 13$ TeV data collected by the ATLAS detector during Run 2 of the Large Hadron Collider. No significant excess above the Standard Model prediction is found. At 95% confidence level, masses between 130 GeV and 940 GeV are excluded for higgsinos decaying exclusively into Higgs bosons and gravitinos. Exclusion limits as a function of the higgsino decay branching ratio to a Higgs boson are also reported.

1 Introduction

Supersymmetry (SUSY) [1–6] is an extension of the Standard Model (SM) predicting the existence of a bosonic (fermionic) partner for each fermionic (bosonic) particle of the SM. If R -parity is conserved [7], the lightest supersymmetric particle (LSP) cannot decay solely into lighter SM particles and consequently is stable, making it a potential dark matter candidate. The Higgs boson “mass hierarchy problem” could be resolved by supersymmetry, with the divergent Higgs mass diagrams being cancelled out by their SUSY counterparts [8–11]. This class of “natural” SUSY models requires the superpartners of the top and bottom quarks (i.e., the stop \tilde{t} and sbottom \tilde{b}), the gluon (i.e., the gluino \tilde{g}), and the bosons of an extended Higgs sector (i.e., the higgsinos \tilde{H}) to be light [12]. Such particles should be produced abundantly in proton–proton (pp) collisions at the Large Hadron Collider (LHC). While the ATLAS and CMS collaborations have set strong limits on the masses of the gluino and the stop particles, the exclusion limits on the higgsino masses are much less stringent [13–18], motivating searches for higgsinos at the LHC.

This paper presents a search for higgsino pair production inspired by models of general gauge mediation (GGM) [19–23] or gauge-mediated symmetry breaking (GMSB) [24, 25]. In these models, the lightest neutralino $\tilde{\chi}_1^0$, a neutral particle resulting from mixing between the SUSY partners of the SM electroweak bosons, is the next-to-lightest SUSY particle (NLSP), while the LSP is the particle associated with spontaneous breaking of the global supersymmetry. The $\tilde{\chi}_1^0$ in these models is dominated by the higgsino component and treated as a pure higgsino. In many GMSB models where the SUSY breaking is mediated at low energy, the LSP is nearly massless. When SUSY is promoted to a local symmetry, the LSP is absorbed by the superpartner of the graviton, the gravitino \tilde{G} . This allows the higgsino, which is produced via mass-degenerate pairs of charginos (the charged particles resulting from mixing between the SUSY partners of the SM electroweak bosons) or neutralinos, to decay into a SM Higgs boson and a nearly massless gravitino. The $\tilde{H} \rightarrow h + \tilde{G}$ mode dominates when $m_{\tilde{H}}$ is greater than the Higgs mass and when $\tan\beta$ (the ratio of the vacuum expectation values of the Higgs doublets) is small [26]. This specific scenario is implemented in this search through the simplified model represented in Figure 1. The \tilde{G} of the resulting model is effectively massless, with the mass set to 1 MeV for this analysis. The only free parameter in the model is the mass of the degenerate higgsino states, $m_{\tilde{H}}$.

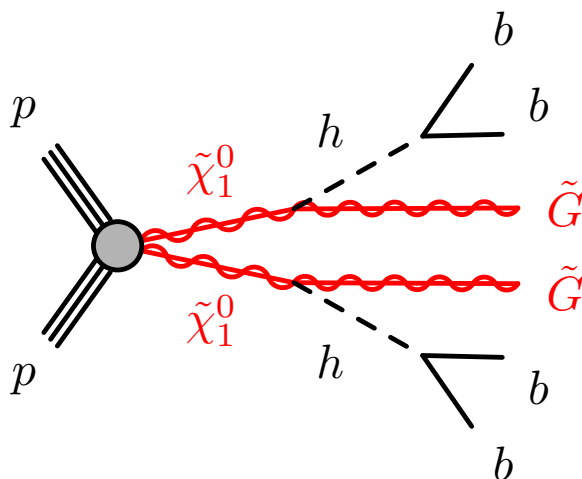


Figure 1: Diagram of a signal event in the simplified SUSY model targeted by this analysis, where the $\tilde{\chi}_1^0$ neutralino is treated as a pure higgsino.

In this search, higgsinos are assumed to be produced in pairs, resulting in an experimental signature including two SM Higgs bosons and missing transverse momentum (E_T^{miss}). Due to its high branching ratio, the $h \rightarrow b\bar{b}$ decay channel is an ideal target for this model, resulting in a final state with multiple b -jets (jets tagged as originating from b -quarks) and E_T^{miss} . The search is conducted in two complementary channels, each specifically targeting the production of either two high-mass or two low-mass higgsinos. Depending on the mass of the higgsino, the experimental signature can vary significantly, which motivates the use of different experimental approaches. The high-mass channel is characterized by significant E_T^{miss} in the final state, and relies on E_T^{miss} -based triggers [27]. The low-mass channel employs a combination of b -jet triggers [28] because of the significantly lower E_T^{miss} produced by low-mass higgsinos. For a higgsino decay branching ratio of $\mathcal{B}(\tilde{H} \rightarrow h + \tilde{G}) = 100\%$, the high-mass channel becomes the more sensitive one for $m_{\tilde{H}}$ values above about 250 GeV. The low-mass channel is used for results below this mass point, while the high-mass channel is used for results at all higher $m_{\tilde{H}}$ values. This strategy is used because the channels are not orthogonal and the sensitivity of the high-mass channel decreases rapidly as $m_{\tilde{H}}$ falls below 250 GeV. A similar search using the full Run 2 dataset was performed by the CMS Collaboration [14]. Compared to the previous ATLAS search using 24.3–36.1 fb⁻¹ of Run 2 data [13], the present ATLAS search includes multiple improvements beyond the use of a larger dataset. These include a new method for pairing b -jets into Higgs boson candidates, significantly improved jet reconstruction and b -tagging, optimized b -tagging requirements in the low-mass channel, and improved discrimination between signal and background in the high-mass channel through the use of multivariate techniques.

This paper is organized as follows. Section 2 describes the ATLAS detector, while Section 3 describes the data and simulated samples. Section 4 defines the objects and other inputs used in reconstructing events for the two channels, Section 5 describes the event selection and background estimation, and Section 6 the systematic uncertainties associated with this search. The results are reported in Section 7, while model-independent and model-dependent statistical interpretations are presented in Section 8. The conclusions are given in Section 9.

2 ATLAS detector

The ATLAS experiment [29] at the LHC is a multipurpose particle detector with a forward–backward symmetric cylindrical geometry and a near 4π coverage in solid angle.¹ It consists of an inner detector (ID) surrounded by a thin superconducting solenoid providing a 2 T axial magnetic field, electromagnetic and hadron calorimeters, and a muon spectrometer. The ID covers the pseudorapidity range $|\eta| < 2.5$ and it consists of silicon pixel, silicon microstrip, and transition radiation tracking detectors. Lead/liquid-argon (LAr) sampling calorimeters provide electromagnetic (EM) energy measurements with high granularity. A steel/scintillator-tile hadron calorimeter covers the central pseudorapidity range ($|\eta| < 1.7$). The endcap and forward regions are instrumented with LAr calorimeters for both the EM and hadronic energy measurements up to $|\eta| = 4.9$. The muon spectrometer (MS) surrounds the calorimeters and is based on three large superconducting air-core toroidal magnets with eight coils each. The field integral of the toroids ranges between 2.0 and 6.0 T m across most of the detector. The MS includes a system of precision chambers for tracking and fast detectors for triggering. A two-level trigger system is used to select events. The first-level

¹ ATLAS uses a right-handed coordinate system with its origin at the nominal interaction point (IP) in the center of the detector and the z -axis along the beam pipe. The x -axis points from the IP to the center of the LHC ring, and the y -axis points upwards. Cylindrical coordinates (r, ϕ) are used in the transverse plane, ϕ being the azimuthal angle around the z -axis. The pseudorapidity is defined in terms of the polar angle θ as $\eta = -\ln \tan(\theta/2)$. Angular distance is measured in units of $\Delta R \equiv \sqrt{(\Delta\eta)^2 + (\Delta\phi)^2}$.

trigger is implemented in hardware and uses a subset of the detector information to accept events at a rate below 100 kHz. This is followed by a software-based “high-level” trigger that reduces the accepted event rate to 1 kHz on average depending on the data-taking conditions. An extensive software suite [30] is used in data simulation, in the reconstruction and analysis of real and simulated data, in detector operations, and in the trigger and data acquisition systems of the experiment.

3 Data and simulated samples

The data used in this search were collected by the ATLAS detector from pp collisions produced during Run 2 of the LHC, from 2015 to 2018. During this period, the LHC collided proton bunches at a center-of-mass energy of $\sqrt{s} = 13$ TeV with a bunch-crossing separation of 25 ns. The high-mass channel uses the complete Run 2 dataset of pp collisions, corresponding to an integrated luminosity of 139 fb^{-1} after requiring all detector subsystems to be operational and recording good quality data [31]. The data for this channel were collected with a combination of $E_{\text{T}}^{\text{miss}}$ triggers. The low-mass channel uses data collected through a combination of b -jet triggers, enabling it to focus on signal-like events with lower $E_{\text{T}}^{\text{miss}}$ than in the high-mass channel, but with a lower integrated luminosity of 126 fb^{-1} due to some temporary operational issues associated with the b -jet trigger selections. The trigger selections, referred to as “online” selections, and the selections for fully reconstructed events, referred to as “offline” selections, are presented in Table 1. The offline thresholds are tighter than the online ones in order to select events with a well-understood trigger efficiency. Additional offline selections are applied in the low-mass channel to provide independent event samples for each trigger employed. This approach allows each b -jet trigger to receive an independent efficiency correction for differences between data and Monte Carlo (MC) simulation.

MC simulations are used to model the signals and the high-mass channel background processes in this search. The signal samples consist of pair-produced higgsinos as described in Section 1. These include both $\tilde{H} \rightarrow h + \tilde{G}$ and $\tilde{H} \rightarrow Z + \tilde{G}$ decays in order to test multiple values of the $\tilde{H} \rightarrow h + \tilde{G}$ branching ratio. In addition, MC simulations of dijet processes are used to validate the background modeling for the high-mass channel. Table 2 shows the generator, set of tuned parameters (tune), parton distribution function (PDF) set, and cross-section normalization order used for each sample. These samples were passed through a detailed simulation of the ATLAS detector and its response [32] based on GEANT4 [33]. A faster simulation relying on a parameterization of the calorimeter’s response [34] is used to estimate the effect of the noninterference theory uncertainties in $t\bar{t}$ and single-top production described in Section 6.2.

The effect of multiple interactions in the same and neighboring bunch crossings (pileup) was modeled by overlaying each simulated hard-scattering event with inelastic pp events generated with PYTHIA 8.186 [35] using the NNPDF2.3LO set of PDFs [36] and the A3 tune [37]. The MC events were weighted to reproduce the distribution of the average number of interactions per bunch crossing observed in the data. In all samples using the PYTHIA parton shower model, the decays of bottom and charm hadrons were performed by EVTGEN [38]. In the generation of $t\bar{t}$ events, the h_{damp} parameter² is set to $1.5 m_{\text{top}}$ [39]. In samples produced with the SHERPA generator, the matrix element calculations were matched and merged with the SHERPA parton shower based on Catani–Seymour dipole factorization [40, 41] using the MEPS@NLO prescription [42–45]. The virtual QCD corrections were provided by the OPENLOOPS library [46–48]. In the signal simulations, matrix elements for higgsino pairs were generated with up to two additional partons.

² The h_{damp} parameter is a resummation damping factor and one of the parameters that controls the matching of POWHEG matrix elements to the parton shower and thus effectively regulates the high- p_{T} radiation against which the $t\bar{t}$ system recoils.

Table 1: Online and offline selections used for the high- and low-mass channels of the analysis. The second column, entitled “Year”, refers to the year the data were recorded. The E_T^{miss} trigger requirement is listed in terms of $E_T^{\text{miss}}(\mu \text{ inv.})$ because the trigger treats muons as being invisible [27]. The offline selections listed for the low-mass channel are only those required to ensure orthogonality between different trigger selections. The H_T variable corresponds to the scalar sum of the p_T of jets in the event. When a p_T selection is listed for multiple jets, it is applied to each jet. The $p_{T,j1}$ variable is the p_T of the leading jet in an event.

Category	Year	Online selections	Offline selections
Low-mass channel			
$2b1j$	2016	1 jet ($p_T > 100 \text{ GeV}$), 2 b -jets (60% b -jet efficiency, $p_T > 55 \text{ GeV}$)	$p_{T,j1} > 150 \text{ GeV}$
	2017	1 jet ($p_T > 150 \text{ GeV}$),	$p_{T,j1} > 350 \text{ GeV}$
	2018	2 b -jets (70% b -jet efficiency, $p_T > 55 \text{ GeV}$)	$p_{T,j1} > 500 \text{ GeV}$
$2bH_T$	2017	$H_T > 300 \text{ GeV}$,	$p_{T,j1} < 350 \text{ GeV}$, $H_T > 850 \text{ GeV}$
	2018	2 b -jets (50% b -jet efficiency, $p_T > 55 \text{ GeV}$)	$p_{T,j1} < 500 \text{ GeV}$, $H_T > 700 \text{ GeV}$
$2b2j$	2016	2 jets ($p_T > 35 \text{ GeV}$), 2 b -jets (60% b -jet efficiency, $p_T > 35 \text{ GeV}$)	$p_{T,j1} < 150 \text{ GeV}$
	2017	2 jets ($p_T > 35 \text{ GeV}$), 2 b -jets (40% b -jet efficiency, $p_T > 35 \text{ GeV}$)	$p_{T,j1} < 350 \text{ GeV}$, $H_T < 850 \text{ GeV}$
	2018	2 jets ($p_T > 35 \text{ GeV}$), 2 b -jets (60% b -jet efficiency, $p_T > 35 \text{ GeV}$)	$p_{T,j1} < 500 \text{ GeV}$, $H_T < 700 \text{ GeV}$
High-mass channel			
E_T^{miss}	2015	$E_T^{\text{miss}}(\mu \text{ inv.}) > 70 \text{ GeV}$	$E_T^{\text{miss}} > 150 \text{ GeV}$
	2016	$E_T^{\text{miss}}(\mu \text{ inv.}) > 90 \text{ GeV}$	
	2017	$E_T^{\text{miss}}(\mu \text{ inv.}) > 100 \text{ GeV}$	
	2018	$E_T^{\text{miss}}(\mu \text{ inv.}) > 110 \text{ GeV}$	

Signal cross sections are calculated to next-to-leading order (NLO) in the strong coupling constant, adding the resummation of soft gluon emission at next-to-leading-logarithm accuracy (NLO+NLL) [49–54].

While simulations are used to estimate the high-mass channel backgrounds, the low-mass channel background is dominated by multijet processes that are not reliably modeled in simulation. A fully data-driven technique is used for background estimation in the low-mass channel as described in Section 5.

4 Object reconstruction

Charged-particle tracks are required to have $p_T > 0.5 \text{ GeV}$. Primary vertex candidates are reconstructed from at least two charged-particle tracks [85]. To identify the hard-scattering interaction, the event’s primary vertex is chosen as the vertex with the largest sum of squared track p_T ($\sum p_{T,\text{track}}^2$).

Small-radius jets are reconstructed using the anti- k_t algorithm [86] with a radius parameter of $R = 0.4$, with particle-flow objects as inputs. These objects are created by the particle-flow algorithm, which combines calorimeter energy clusters and ID tracks, improving the resolution of the combined energy measurement by subtracting the energy deposited by well-measured tracks in the calorimeter and using their p_T instead [87]. Jets produced by collisions other than the hard scattering (i.e., pileup jets) are removed by testing their compatibility with the primary vertex using the Jet Vertex Tagger (JVT) discriminant [88]. Jets with $p_T < 60 \text{ GeV}$ and $|\eta| < 2.4$ are required to pass the “Medium” JVT working point. Different

Table 2: List of generators used for the processes considered in this search, with MG5 standing for MADGRAPH5. The underlying-event (UE) tune, the PDF sets for the matrix element (ME) and UE, and the pQCD highest-order normalization accuracy used for each sample are also shown. Henceforth, the $t\bar{t}W$, $t\bar{t}Z$, $t\bar{t}t\bar{t}$, and $t\bar{t}h$ processes are grouped into a single $t\bar{t}+X$ category. The SUSY signals consist of pair-produced higgsinos. The dijet samples are only used for validation.

Process	Generator + fragmentation/hadronization	Tune	PDF set	Order of cross section
SUSY signals	MG5_AMC@NLO 2.6.1/2.6.2 [55] + PYTHIA 8.230 [66]	A14 [56]	NNPDF2.3LO [36]	NNLO _{approx} +NNLL [57–65]
Dibosons WW, WZ, ZZ	SHERPA 2.2.1 [40–48, 67]	Default	NNPDF3.0 _{NNLO} [68]	NLO [43, 69]
W/Z+jets	SHERPA 2.2.1	Default	NNPDF3.0 _{NNLO}	NNLO [46–48]
Top pairs: $t\bar{t}$	POWHEG BOX v2 [70–73] + PYTHIA 8.230	A14	NNPDF3.0 _{NLO} (ME) NNPDF2.3LO (UE)	NNLO+NNLL [74–80]
Single top	POWHEG BOX v2 + PYTHIA 8.230	A14	NNPDF3.0 _{NLO} (ME) NNPDF2.3LO (UE)	NLO [81] (t/s -channel) NLO+NNLL [82, 83] (Wt)
$t\bar{t}W/t\bar{t}Z$	MG5_AMC@NLO 2.3.3 [55] + PYTHIA 8.210	A14	NNPDF3.0 _{NLO} (ME) NNPDF2.3LO (UE)	NLO [84]
$t\bar{t}t\bar{t}$	MG5_AMC@NLO 2.2.2 + PYTHIA 8.186	A14	NNPDF2.3LO	NLO [55]
$t\bar{t}h$	POWHEG BOX v2 + PYTHIA 8.230	A14	NNPDF3.0 _{NLO} (ME) NNPDF2.3LO (UE)	NLO [84]
Dijet	PYTHIA 8.230	A14	NNPDF2.3LO	LO

MC-based calibration steps are applied to the reconstructed jets [89], including an area-based correction to account for energy contributions from pileup interactions, a p_T - and η -dependent calibration to match the generator-level energy scale of the jets, and the “global sequential calibration” (GSC) to minimize energy calibration differences between quark- and gluon-initiated jets. Finally, an *in situ* calibration is applied to jets in data to match the energy scale in simulation. Sensitivity to signal scenarios where jets are close to each other due to large higgsino–gravitino mass splittings is enhanced by using large-radius jets produced by reclustering $R = 0.4$ jets [90] through another iteration of the anti- k_t algorithm with a radius parameter of $R = 0.8$. Calibrations are propagated through that iteration. The reclustered jets are trimmed [91] by removing any small-radius jets whose p_T falls below $f_{\text{cut}} = 10\%$ of the p_T of the large-radius jet. After this procedure, reclustered jets are required to have $p_T > 100$ GeV and $|\eta| < 2.0$. The high-mass channel requires $R = 0.4$ jets to have $p_T > 25$ GeV and $|\eta| < 2.8$, while the low-mass channel uses jets with $p_T > 40$ GeV and $|\eta| < 2.8$ because of requirements from its jet-based trigger strategy. The high-mass channel uses as a discriminant the total mass of the large-radius jets in the event, as explained later in Section 5.1.1.

Small-radius jets initiated by b -quarks and decaying within the ID acceptance ($|\eta| < 2.5$) are identified as b -tagged jets using the DL1r classifier set to a working point of 77% efficiency for simulated $t\bar{t}$ events [92]. This classification algorithm uses various types of inputs, including information about the impact parameters

of ID tracks, the presence of displaced secondary vertices, and the reconstructed flight paths of b - and c -hadrons inside the jet. At the selected working point, the light-jet (charm-jet) rejection factor measured in $t\bar{t}$ events is approximately 130 (4.9) [92–95]. Correction factors are applied to the simulated samples to account for differences in the b -tagging efficiencies between data and simulation. For the low-mass channel, additional correction factors are applied to account for differences in the online b -tagging efficiencies. Correlations between the trigger correction factors and offline correction factors are taken into account.

Three types of electrons and muons, “loose”, “baseline”, and “signal-quality”, are defined for this analysis. Electron candidates are built from energy deposits in the EM calorimeter that are matched to ID tracks [96]. Loose electrons are required to pass the *LooseLH* likelihood identification criteria [97] and to have $p_T > 7$ GeV and $|\eta| < 2.47$. Further rejection of fake or nonprompt electrons is achieved by requiring electron tracks to match the primary vertex through a cut of $|z_0 \sin \theta| < 0.5$ mm on the longitudinal impact parameter z_0 . Loose electrons with $p_T > 20$ GeV, called “baseline” electrons, are used to calculate the E_T^{miss} . To be considered as “signal-quality” objects, candidates are required to survive the overlap removal procedure defined below, satisfy the *MediumLH* likelihood identification criteria [97], pass the *Loose* isolation requirements, and have $p_T > 20$ GeV and $|\eta| < 2.47$. Signal-quality electrons are also required to have a transverse impact parameter significance $|d_0|/\sigma(d_0) < 5$.

Muon candidates are reconstructed by matching an ID track with an MS track or performing a combined fit of an ID track with the aligned individual hits found in the MS. After reconstruction, loose muons are required to have $p_T > 6$ GeV and $|\eta| < 2.7$, and to pass the *Medium* identification requirement based on track quality variables [98]. Further rejection of fake or nonprompt muons is achieved by requiring muon tracks to match the primary vertex through a cut of $|z_0 \sin \theta| < 0.5$ mm on the longitudinal impact parameter z_0 . Loose muons with $p_T > 20$ GeV, called “baseline” muons, are used to calculate the E_T^{miss} and to correct the four-momentum of jets to account for semileptonic b -hadron decays. This correction adds the muon four-momentum to the jet if a muon is found within $\Delta R = 0.4$ of that jet. Signal-quality muons are the subset of loose muons that survive the overlap removal procedure defined below, pass the *TightTrackOnly* (with variable radius) isolation requirements [98], and have $p_T > 20$ GeV and $|\eta| < 2.5$. Signal-quality muons are also required to have a transverse impact parameter significance $|d_0|/\sigma(d_0) < 3$.

An overlap removal procedure is applied to resolve reconstruction ambiguities between electrons, muons, and small-radius jets. First, any baseline electron sharing an ID track with a baseline muon is rejected. Then, if a jet is found to be within $\Delta R = 0.2$ of a baseline electron, the jet is removed. If a baseline electron is found to lie $\Delta R < \min(0.4, 0.04 + 10 \text{ GeV}/p_T^e)$ from a remaining jet, where p_T^e is the transverse momentum of the electron, the electron is removed. Next, any jet with an associated muon ID track or a baseline muon within $\Delta R = 0.2$ of its axis is removed if the jet has less than three tracks. Lastly, the muon is removed if it lies $\Delta R < \min(0.4, 0.04 + 10 \text{ GeV}/p_T^\mu)$ from any remaining jet, where p_T^μ is the transverse momentum of the muon.

The missing transverse momentum \vec{p}_T^{miss} , with magnitude E_T^{miss} , is built from the negative vector sum of the transverse momenta of all well-identified and calibrated physics objects in the event, plus an extra “ E_T^{miss} soft term” [99] accounting for remaining low-energy charged particles. The *Tight* working point [99] is used to reduce pileup effects. The track-based soft term is calculated from ID tracks matched to the primary vertex but not to any physics object. Baseline identification criteria, which are looser than the signal-quality criteria described above, are applied to muons and electrons used in these calculations.

5 Event selection and background estimation

Prior to any channel-specific selections, both channels impose data quality requirements to ensure that only events recorded when the entire ATLAS detector was fully operational are used [31]. These selections reject events containing corrupted data from the ID and calorimeters, as well as spurious jets caused by noncollision backgrounds [100, 101]. Events containing signal-quality leptons (electrons or muons) are discarded to reduce backgrounds due to leptonically decaying W bosons. Events are also discarded if they contain more than one loose lepton with $p_T > 8$ GeV; a single loose lepton is allowed so as to avoid rejecting events containing a semileptonic b -hadron decay. The loose-lepton criteria employed also minimize overlaps with ATLAS analyses using leptonic final states to target the same signal [15, 17].

5.1 High-mass channel

The high-mass channel focuses on detecting final states characterized by high E_T^{miss} , a minimum of three b -jets, and no signal-quality leptons. It relies on reconstructing the Higgs bosons resulting from the decay of higgsinos. To estimate the main backgrounds, MC simulations are used, with adjustments made to the normalization of $t\bar{t}$ and Z +jets processes derived from data control samples. A boosted decision tree (BDT) is employed to distinguish between the signal and background events. A set of higgsino mass points, referred to as “mass hypotheses”, are considered, and for each of them control regions (CRs), validation regions (VRs), and up to four distinct signal regions (SRs) are defined by using the BDT score. The mass hypotheses are given by

$$m_{\tilde{H}} = \{200, 250, 300, 400, 500, 600, 700, 800, 900, 1000, 1100\} \text{ GeV}.$$

In addition, the three of these signal regions that have the highest expected sensitivity for the 250 GeV, 500 GeV, and 1000 GeV mass hypotheses, referred to as “discovery signal regions”, are used to search for, and set limits on, an excess of “beyond the Standard Model” (BSM) events in this phase space in a more model-independent manner.

5.1.1 Event selection

After the common selections described above and the trigger selections described in Section 3, signal-like events are required to satisfy the following “standard preselection” requirements:

- between four and seven small-radius jets with $p_T > 25$ GeV are reconstructed in the event, to reduce backgrounds with a large number of additional jets;
- at least three of these jets are b -tagged according to the requirements described in Section 4, as expected for the signal topology;
- E_T^{miss} is greater than 150 GeV, for consistency with the production of invisible particles;
- the minimum azimuthal angle between E_T^{miss} and any of the four leading jets ($\Delta\phi_{\text{min}}^{4j}$) is greater than 0.4, to reduce backgrounds with spuriously large E_T^{miss} resulting from mismeasurement of the momentum of a jet.

Scaling factors are applied to MC simulations to correct for discrepancies between simulated and data-based trigger efficiencies. Such corrections are negligible for events with $E_T^{\text{miss}} \geq 200$ GeV and reach a maximum of about 10% for events with $E_T^{\text{miss}} \simeq 150$ GeV and a scalar sum of jet p_T below 250 GeV.

A key element of this analysis is the identification of the Higgs bosons originating from the higgsino decays. This is essential because the masses of the higher- and lower-mass Higgs boson candidates, denoted by $m(h_1^{\text{HM}})$ and $m(h_2^{\text{HM}})$, respectively, are used to discriminate between signal and background. In order to obtain these values, the jets originating from the Higgs boson candidates must be identified and then paired. If there are exactly four b -jets in an event, those four are used. If there are more than four b -jets, the four with the highest p_T are used. If only three b -jets are reconstructed, and one of these jets has a mass greater than 100 GeV, it is considered to be a boosted Higgs boson candidate and no additional jets are considered. Otherwise, the fourth jet is selected as the untagged small-radius jet that minimizes the value of $m(h_1^{\text{HM}})$ that would be obtained from the pairing algorithm discussed in the next paragraph.

The selected jets are paired to create Higgs boson candidates. If only three jets are selected (in the case where one jet has a mass greater than 100 GeV), the heaviest jet is considered to be a Higgs boson candidate and the remaining two jets are paired to form the second candidate. Otherwise, the quantity $\Delta R_{\text{max}}^{bb}(h_1^{\text{HM}}, h_2^{\text{HM}}) = \max(\Delta R(h_1^{\text{HM}}), \Delta R(h_2^{\text{HM}}))$ is calculated for each of the three possible pairings of the four jets, where $\Delta R(h)$ is the ΔR separation of the jets coming from the same Higgs boson candidate. The pairing that minimizes $\Delta R_{\text{max}}^{bb}$ is used, because pairs of jets have a more collimated topology in signal events than in background events.

In order to maximize the sensitivity to a broad set of higgsino masses, a BDT is used to discriminate between background and signal events and define the various regions for the high-mass channel. The BDT was trained, using the XGBoost algorithm [102], on inclusive background and signal datasets, properly reweighted to account for the different cross sections of the simulated processes. For the classification, the BDT exploited the following inputs:

- the number of jets N_{jets} and b -jets $N_{b\text{-jets}}$ in the event,
- the scalar sum of the transverse momenta associated with small-radius jets in the event, H_T ,
- the magnitude E_T^{miss} of the missing transverse momentum, and the object-based E_T^{miss} significance, $\mathcal{S}(E_T^{\text{miss}})$ [103],
- the minimum azimuthal angle between E_T^{miss} and any of the four highest- p_T jets in the event, $\Delta\phi_{\text{min}}^{4j}$,
- the minimum transverse mass of the E_T^{miss} and the three leading b -jets in the event,

$$m_{T,\text{min}}^{b\text{-jets}} = \min_{i \leq 3} \sqrt{(E_T^{\text{miss}} + p_T^{j_i})^2 - (E_{T_x}^{\text{miss}} + p_x^{j_i})^2 - (E_{T_y}^{\text{miss}} + p_y^{j_i})^2},$$

- the minimum angular distance between any two b -jets in the event, $\Delta R_{\text{min}}^{bb}$,
- the scalar sum of the masses of the reclustered large-radius jets in the event, M_J^Σ ,
- the masses of the reconstructed Higgs boson candidates, $m(h_1^{\text{HM}})$ and $m(h_2^{\text{HM}})$, and the angular distances between the associated jets, $\Delta R(h_1^{\text{HM}})$ and $\Delta R(h_2^{\text{HM}})$.

The BDT was also parameterized with the generator-level higgsino mass $m_{\tilde{H}}^{\text{gen}}$ in order to define signal regions (SRs) that each target a specific mass hypothesis. The most discriminating variables for low-higgsino-mass hypotheses are N_{jets} , $N_{b\text{-jets}}$, and $m_{T,\text{min}}^{b\text{-jets}}$, while E_T^{miss} , $S(E_T^{\text{miss}})$, and $m_{T,\text{min}}^{b\text{-jets}}$ are the most discriminating variables for intermediate-to-high-higgsino-mass hypotheses. The optimization of the BDT hyperparameters was performed through a scan to optimize the discovery significance for the benchmark signal $m_{\tilde{H}} = 1000$ GeV. The selected parameters are 500 trees, a learning rate of 0.5, a maximum of 50 bins, and a maximum tree depth of six.

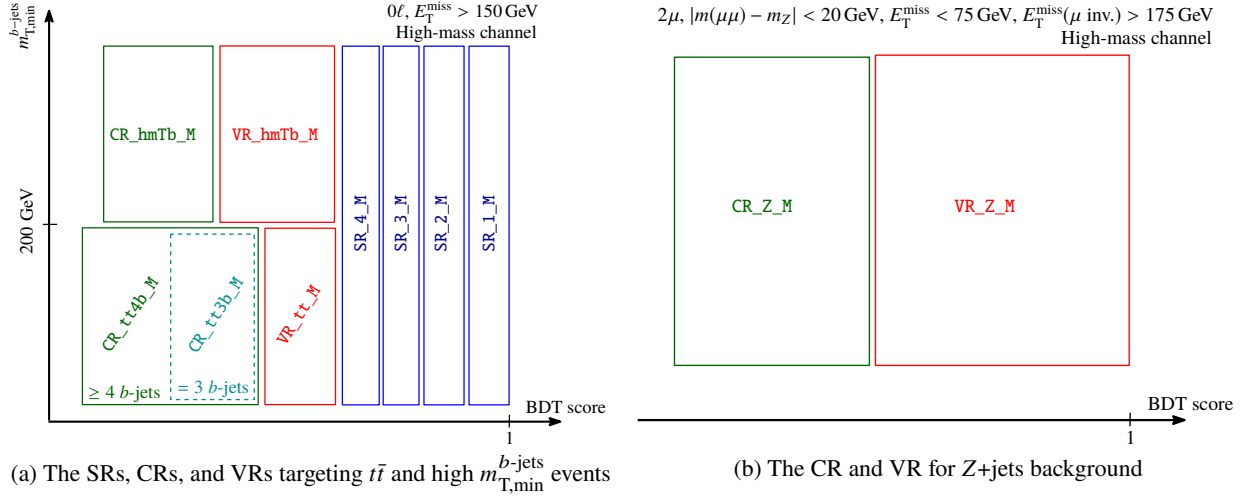


Figure 2: General scheme followed in the definition of SRs, VRs, and CRs for each mass hypothesis of the high-mass channel. The left plot shows the SRs, $t\bar{t}$ CRs and VR, and high $m_{T,\text{min}}^{b\text{-jets}}$ CR and VR. The SRs are constructed with all the events with BDT output scores in a specific range that maximizes the expected significance in the SR. Up to four SRs are defined that way. After finding all SRs, the lowest BDT-score threshold of any SR for that specific mass hypothesis is used as the upper bound for the VRs, and the procedure is repeated separately in regions of low and high $m_{T,\text{min}}^{b\text{-jets}}$ to define VRs targeting the $t\bar{t}$ background and high $m_{T,\text{min}}^{b\text{-jets}}$ selections, as shown in the figure. Once the VRs are found, the process is repeated to define CRs targeting $t\bar{t}$ and high $m_{T,\text{min}}^{b\text{-jets}}$ events, with a further splitting of the $t\bar{t}$ CRs in b -jet multiplicity. The right plot shows the Z+jets CR and VR. These are defined using the same procedure as for the $t\bar{t}$ and high $m_{T,\text{min}}^{b\text{-jets}}$ regions, but with no SRs and a different preselection designed to capture $Z(\rightarrow \mu\mu)$ +jets events. $E_T^{\text{miss}}(\mu \text{ inv.})$ is used in place of E_T^{miss} for the BDT input variables for the right plot to emulate the behavior of $Z(\rightarrow \nu\nu)$ +jets. The BDT-score thresholds for the CRs are not shown in either plot; this is because they depend on the mass hypothesis and the type of CR.

The SRs are defined using the BDT output scores of the preselected events. For each mass hypothesis, the SRs are built with an iterative procedure that begins with the highest BDT scores. The iterative process determines BDT-score thresholds for the SRs by requiring at least 0.5 background events and maximizing the statistical significance Z calculated from the BinomialExpZ function of RooStats [104]. For mass hypotheses that were excluded by the previous ATLAS search using 24.3–36.1 fb^{-1} of Run 2 data [13], the cross sections for the signals are scaled down to the minimum previously excluded values for the purposes of this calculation. After an SR is formed, subsequent SRs are created by repeating the procedure on events with BDT scores below the values used in the previous SR. If this would result in a significance Z of less than one, no SR is created and no further SRs are made for that mass hypothesis. If more than four SRs are created for a given mass hypothesis, the SRs with the lowest BDT scores are merged until there are only four SRs. The SRs are named as SR_i_M, where M corresponds to the signal mass hypothesis of the region and i is an integer between one and four that labels the SR, with lower values of i corresponding to SRs

Table 3: Summary of criteria applied to construct the CRs, VRs, and SRs of the high-mass channel. The considered variables are the statistical significance Z , the number of background events n_{bkg} , the ratio of signal events to background events S/B , the number of b -jets $N_{b\text{-jets}}$, and $m_{T,\text{min}}^{b\text{-jets}}$. The Z +jets preselection is discussed in Section 5.1.2. Additional selections based on the BDT score are included in the definitions of the CRs, VRs, and SRs, as shown in Figure 2; these are mass-dependent and are therefore omitted from the table.

Region name	Fixed Requirements			Boundary Conditions		
	Preselection	$m_{T,\text{min}}^{b\text{-jets}}$	$N_{b\text{-jets}}$	Z	n_{bkg}	S/B
SR_i_M	Standard	–	–	max.	≥ 0.5	–
VR_tt_M	Standard	< 200 GeV	–	–	≥ 25	< 0.2
VR_hmTb_M	Standard	> 200 GeV	–	–	≥ 25	< 0.2
VR_Z_M	Z+jets	–	–	–	≥ 25	< 0.2
CR_tt3b_M	Standard	< 200 GeV	$= 3$	–	≥ 100	< 0.1
CR_tt4b_M	Standard	< 200 GeV	≥ 4	–	≥ 100	< 0.1
CR_hmTb_M	Standard	> 200 GeV	–	–	≥ 100	< 0.1
CR_Z_M	Z+jets	–	–	–	≥ 100	< 0.1

with higher-BDT-score requirements. Using different SRs for different signal mass hypotheses improves the sensitivity of the high-mass channel to low higgsino masses by approximately 20% compared to using the same SRs for all mass hypotheses. The SRs corresponding to different signal mass hypotheses are not required to be orthogonal. These requirements are shown in Table 3, with a diagram of the SRs in Figure 2(a). The signal regions SR_1_250, SR_1_500, and SR_1_1000 are additionally used to search for excesses with minimal model dependence and are called discovery regions when used in this context.

5.1.2 Background estimation strategy

The background estimation in the high-mass channel relies almost entirely on MC simulation with data-driven normalization corrections. After preselection, the main background is $t\bar{t}$, followed by QCD multijet processes, primarily at low E_T^{miss} , as well as single top and Z +jets, which contribute at high E_T^{miss} . Smaller contributions arise from $t\bar{t}+X$ and diboson production. Distributions of the data and simulated backgrounds after preselection are shown in Figure 3. The data and background predictions agree within 10% after taking the statistical uncertainties into account. The normalizations of the dominant $t\bar{t}$ and Z +jets processes are measured through a combined maximum-likelihood fit which includes the high-mass channel's SRs, as well as a dedicated set of control regions (CRs) with separately enhanced purity of each background component. Three additional parameters are included in the fit to constrain the normalizations of the single-top backgrounds, which make large but subleading contributions to the SRs, and the $t\bar{t}+\geq 1b$ and $t\bar{t}+\geq 1c$ components of the $t\bar{t}$ background, to improve the modeling in heavy-flavor-dominated regions. The level of agreement between the adjusted background prediction and the data is checked through dedicated validation regions (VRs). These are named as CR_PROC_M and VR_PROC_M, where PROC labels the physical process and M denotes the signal mass hypothesis. The $t\bar{t}$ and high- $m_{T,\text{min}}^{b\text{-jets}}$ CRs and VRs are defined using the same selections as the SRs, except for the BDT score requirements. An additional requirement of $m_{T,\text{min}}^{b\text{-jets}} < 200$ GeV ($m_{T,\text{min}}^{b\text{-jets}} > 200$ GeV) is used to enhance the purity of the $t\bar{t}$ (high $m_{T,\text{min}}^{b\text{-jets}}$) CRs and VRs. The $t\bar{t}$ CRs are further split into $3b$ and $4b$ CRs to constrain the normalizations of the $t\bar{t}+\geq 1b$ and $t\bar{t}+\geq 1c$ backgrounds separately from the overall $t\bar{t}$ background.

The Z +jets background is estimated using a separate data sample enriched in events containing muons. The

dominant component of the Z +jets background in the SRs is $Z(\rightarrow \nu\nu)$ +jets. The “ Z +jets preselection” has the same requirements as the standard preselection described above, except for requiring two opposite-sign muons satisfying $|m(\mu\mu) - m_Z| < 20$ GeV, where m_Z is the mass of the Z boson, and $E_T^{\text{miss}} < 75$ GeV. The E_T^{miss} requirement is imposed to suppress the contamination from $t\bar{t}$ background and increase the sample’s purity in Z +jets events. In addition to the E_T^{miss} requirement, the cut $E_T^{\text{miss}}(\mu \text{ inv.}) > 175$ GeV is applied, where $E_T^{\text{miss}}(\mu \text{ inv.})$ is computed with muons treated as invisible particles to emulate a boosted $Z \rightarrow \nu\nu$ decay. The $E_T^{\text{miss}}(\mu \text{ inv.})$ requirement also allows events to be selected by the E_T^{miss} trigger, which treats muons as being invisible [27]. Once these events are selected, the same BDT used for the signal selection is used to create the CRs and VRs of the Z +jets process. All BDT input variables using E_T^{miss} are adjusted to use $E_T^{\text{miss}}(\mu \text{ inv.})$ instead.

For each signal mass hypothesis, the VR for a given background is defined to contain all events with BDT scores below the SR values and greater than a threshold value. The threshold BDT scores are selected such that each VR has at least a specific number of background events, denoted by n_{bkg} in Table 3, and a signal contamination less than a threshold value, denoted by S/B in Table 3. The CR is then defined using BDT scores below the values for the VR, with a minimum BDT score selected such that the CR has at least a specific number of background events and a signal contamination less than a threshold value, as indicated in Table 3. The strategy is illustrated graphically in Figure 2. For the Z +jets CRs and VRs, S/B is estimated to be zero and the signal contamination condition is therefore always satisfied. Due to their different preselection, the Z +jets VRs are not required to have BDT scores below the SR values.

A data-driven technique is used to estimate the QCD multijet background. This method exploits a template created by subtracting non-QCD-multijet backgrounds estimated with MC simulations from data in a kinematic regime dominated by QCD multijet processes. These events are obtained by replacing the selection $\Delta\phi_{\text{min}}^{4j} > 0.4$ with $\Delta\phi_{\text{min}}^{4j} < 0.2$. In order to estimate the contribution of this background to the CRs, VRs, and SRs, the template needs to be evaluated with the discriminating BDT. For this reason, a fake $\Delta\phi_{\text{min}}^{4j}$ distribution is generated for the events in the template, sampled randomly from the expected $\Delta\phi_{\text{min}}^{4j}$ distribution observed in dijet MC simulated samples. This template, however, does not correctly reproduce the correlations between $\Delta\phi_{\text{min}}^{4j}$ and other kinematic variables that are used in the BDT training. Additionally, given the exponentially falling shape of the $\Delta\phi_{\text{min}}^{4j}$ distribution for QCD multijet events, the template is not expected to accurately describe the normalization of this background in the targeted kinematic regime. These issues are resolved by applying a neural-network-assisted reweighting to the template. The neural network (NN) is trained on simulated dijet events to separate $\Delta\phi_{\text{min}}^{4j} < 0.2$ events from $\Delta\phi_{\text{min}}^{4j} > 0.4$ events, and an event weight based on the per-event NN output score is applied to the data-driven template to correct the normalization and the correlations between kinematic variables. The reweighted template is the final estimate for the QCD multijet background. This is validated in kinematic regimes enriched in QCD multijet events and is found to describe the data well, with up to 10% differences. A nonclosure uncertainty of 50% is applied to the QCD multijet prediction in the CRs, VRs, and SRs, found by comparing the performance of the NN-assisted reweighting with the prediction from dijet MC simulation in the analysis regions.

5.2 Low-mass channel

The low-mass channel focuses on final states characterized by four or more b -jets and the absence of signal-quality leptons. Two Higgs boson candidates are reconstructed from the b -jets in the event. Signal, control, and validation regions are defined in the phase space of leading and subleading Higgs masses.

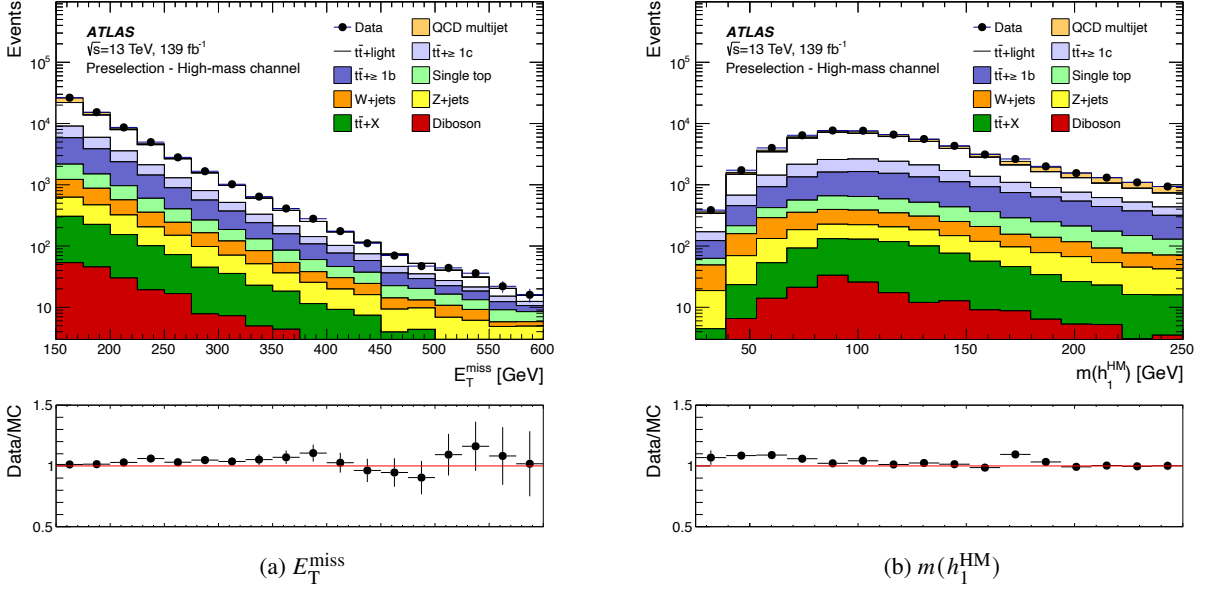


Figure 3: Comparisons of data and MC simulations for the standard preselection of the high-mass channel. The backgrounds are normalized to their theory cross sections. The left plot shows the distribution of E_T^{miss} while the right plot shows the distribution of $m(h_1^{\text{HM}})$. The lower panels show the ratios of data to MC simulations. The uncertainties in the ratios include the statistical uncertainties from both the data and MC simulations.

In the low-mass channel, the primary sources of background are QCD multijet events and $t\bar{t}$ processes. To estimate these backgrounds, an “ABCD” method is employed and a model is trained to adjust the kinematics across control regions with different b -jet multiplicities. The effectiveness of this adjustment is evaluated in validation regions. Within the signal region, two inclusive regions are defined in order to set model-independent limits on BSM physics. These regions are called “discovery regions” and are optimized to target higgsino mass hypotheses of 150 GeV and 300 GeV, respectively.

5.2.1 Event selection

The search in the low-mass channel uses events collected by the b -jet triggers listed in Table 1. Events are required to pass at least one of these triggers. Different offline kinematic requirements are also applied to ensure orthogonality between the different trigger selections, allowing correlations between the different trigger scale factors to be ignored.

Events are required to have at least four b -jets in order to reconstruct the Higgs boson candidates. These events are referred to as the “4 b ” sample. In events with more than four b -jets, only the four b -jets with the highest p_T are considered. The four jets are then paired to form Higgs boson candidates. For each possible pairing, the quantity $\Delta R_{\text{max}}^{bb}(h_1^{\text{LM}}, h_2^{\text{LM}})$ is calculated, where h_1^{LM} is defined as the Higgs boson candidate with the higher reconstructed p_T and h_2^{LM} is defined as the one with lower p_T . The pairing that yields the smallest value of $\Delta R_{\text{max}}^{bb}$ is used.

The largest backgrounds passing these selections are QCD multijet and $t\bar{t}$ events. The leptonic $t\bar{t}$ background is reduced through the signal-quality and loose-lepton vetoes included in the common selections. Events

are also required to have at most two loose leptons.³ In order to reduce the hadronic $t\bar{t}$ background, a discriminant based on the reconstruction of the top quark decay is used. Top quark candidates are reconstructed using three jets. One of these jets must be from a Higgs boson candidate and is considered to be the b -jet from the top quark decay. The other two jets are considered to form a W boson candidate. Since a W boson cannot decay into more than one b -jet, at least one of the W boson candidate jets must not be associated with a Higgs boson candidate. The quantity

$$X_{Wt} = \sqrt{\left(\frac{m_{jj} - m_W}{0.1 \cdot m_{jj}}\right)^2 + \left(\frac{m_{jjb} - m_t}{0.1 \cdot m_{jjb}}\right)^2}$$

is then calculated for each possible combination of jets, subject to the restrictions described above, and where m_{jj} and m_{jjb} are the masses of the reconstructed W boson and top quark candidates, and $m_W = 80.4$ GeV and $m_t = 172.5$ GeV are the nominal masses of the W boson and top quark. The factor of 0.1 approximates the fractional mass resolution for the reconstructed particle candidates. Events are vetoed if $X_{Wt} < 1.8$ for any of these combinations.

The low-mass SRs are defined by the requirement $X_{hh}^{\text{SR}} < 1.6$, where X_{hh}^{SR} is given by

$$X_{hh}^{\text{SR}} = \sqrt{\left(\frac{m(h_1^{\text{LM}}) - 120 \text{ GeV}}{0.1 \cdot m(h_1^{\text{LM}})}\right)^2 + \left(\frac{m(h_2^{\text{LM}}) - 110 \text{ GeV}}{0.1 \cdot m(h_2^{\text{LM}})}\right)^2},$$

where the denominators are the approximate mass resolutions for the Higgs boson candidates. A separate SR is created for each of the 2016, 2017, and 2018 data-taking periods to account for differences in the triggers and the background estimation procedure. The central values of 120 GeV and 110 GeV are offset from the true Higgs mass because of reconstruction inefficiencies such as from neutrinos produced in b -hadron semileptonic decays. The SR is the region within the innermost contour in Figure 4.

The SRs are binned in $E_{\text{T}}^{\text{miss}}$ and m_{eff} , where m_{eff} is defined as the $E_{\text{T}}^{\text{miss}}$ plus the scalar sum of the p_{T} values of the jets associated with Higgs boson candidates. A fit is performed over the two-dimensional distribution of these variables, with lower bin edges given by

$$E_{\text{T}}^{\text{miss}} = \{0, 20, 40, 60, 80, 100, 120, 140, 160, 180, 200\} \text{ GeV}$$

$$m_{\text{eff}} = \{160, 200, 260, 340, 440, 560, 700, 860\} \text{ GeV},$$

where the last bin is inclusive. In addition, two discovery regions are defined in order to obtain limits in model-independent scenarios. These regions are optimized for the $m_{\tilde{H}} = 150$ GeV (SR_LM_150) and $m_{\tilde{H}} = 300$ GeV (SR_LM_300) mass points, although they are also sensitive at nearby $m_{\tilde{H}}$ values. The region definitions are shown in Table 4.

³ This veto uses all loose leptons, while the common loose-lepton veto only uses loose leptons with $p_{\text{T}} > 8$ GeV.

Table 4: Discovery region definitions for the low-mass channel.

Region	E_T^{miss}	m_{eff}
SR_LM_150	$> 20 \text{ GeV}$	$> 560 \text{ GeV}$
SR_LM_300	$> 150 \text{ GeV}$	$> 340 \text{ GeV}$

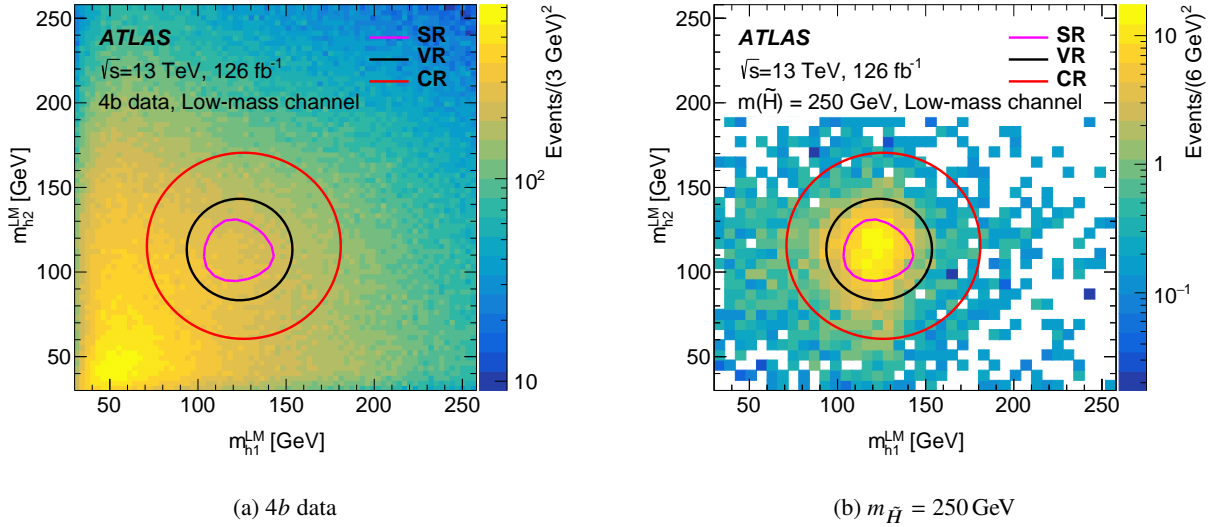


Figure 4: Reconstructed Higgs boson masses in the low-mass channel. The left plot shows the $4b$ data, while the right plot shows the $4b$ MC signal sample for a higgsino mass of 250 GeV. The red, black, and pink (i.e., innermost) contours correspond to the outer boundaries of the control, validation, and signal regions respectively.

5.2.2 Background estimation strategy

The dominant background in the low- E_T^{miss} regime of the low-mass channel comes from QCD multijet processes. Because these processes are difficult to model sufficiently well in simulation, a purely data-driven approach is used to estimate the background from all sources. This estimate makes use of an alternative set of regions with exactly two b -jets and two or more non- b -tagged jets instead of four or more b -jets. All other analysis selections are the same as those previously described in Section 5.2.1. These alternative regions, called the “ $2b$ ” sample, have more events than provided by the nominal $4b$ sample while also having significantly less signal contamination.

The Higgs boson candidates for the $2b$ sample are reconstructed using the two b -jets plus two jets selected randomly from the event’s non- b -tagged jets. The additional jets are required to have $|\eta| < 2.5$ to match the η requirements for b -tagging. The mass values of the reconstructed Higgs bosons are used to create the VRs and CRs. The VRs are defined for each data-taking period by $R_{hh}^{\text{VR}} < 30 \text{ GeV}$ and $X_{hh}^{\text{SR}} \geq 1.6$, where R_{hh}^{VR} is given by

$$R_{hh}^{\text{VR}} = \sqrt{(m(h_1^{\text{LM}}) - 123.6 \text{ GeV})^2 + (m(h_2^{\text{LM}}) - 113.3 \text{ GeV})^2}.$$

The CRs are defined by $R_{hh}^{\text{CR}} < 55 \text{ GeV}$ and $R_{hh}^{\text{VR}} \geq 30 \text{ GeV}$, where R_{hh}^{CR} is given by

$$R_{hh}^{\text{CR}} = \sqrt{(m(h_1^{\text{LM}}) - 126.0 \text{ GeV})^2 + (m(h_2^{\text{LM}}) - 115.5 \text{ GeV})^2}.$$

The VRs and CRs form ellipses around the SRs with the central values shifted by factors of 1.03 and 1.05, respectively. These shifts avoid over-representing low $(m(h_1^{\text{LM}}), m(h_2^{\text{LM}}))$ values, which have a higher density of events. The SRs, VRs, and CRs are each defined for both the $2b$ and $4b$ samples. The $2b$ CRs, $4b$ CRs, and $2b$ SRs are used to create a background model for the $4b$ SRs, where the search is performed. Figure 4 shows the $m(h_1^{\text{LM}})$ versus $m(h_2^{\text{LM}})$ distributions for both the $4b$ data and the 250 GeV signal simulation with the region definitions overlaid.

The background model is created by normalizing and reweighting the $2b$ SR to estimate the behavior of the background in the $4b$ SR. The normalization factor is determined from the CRs as

$$\mu_{\text{CR}} = \frac{N_{\text{CR}}^{4b}}{N_{\text{CR}}^{2b}},$$

where N_{CR}^{4b} (N_{CR}^{2b}) is the observed number of data events in the $4b$ ($2b$) CR. The parameter μ_{CR} is measured separately for the 2016, 2017, and 2018 data-taking periods because of the differences in the triggers used to record the data.

The $2b$ regions are reweighted using BDTs [105] to correct for any kinematic differences between the $2b$ and $4b$ regions. The BDTs are trained on data events in the CRs separately for the 2016, 2017, and 2018 data-taking periods. The hyperparameters used in common for each year are the maximum number of layers (5), the minimum number of events per node (250), the learning rate (0.3), and the sampling fraction (0.4). The number of trees was set to 50 for 2016, 75 for 2017, and 100 for 2018. A greater number of trees are used for later years because the data samples are larger. A large set of 51 input variables is provided, as the BDT training can select which variables to weight most strongly. These include the mass, energy, p_{T} , η , and ϕ of each Higgs boson candidate and Higgs boson candidate jet; the mass and p_{T} of the di-Higgs system; the number of jets; the $E_{\text{T}}^{\text{miss}}$; X_{Wt} without the light-jet requirement; the number of track-jets associated with each Higgs boson candidate; and 14 angular variables.

For each tree of the BDT, events are separated into two nodes using the input variable and the cut value maximizing the χ^2 difference between the nodes. This process repeats at each resulting node until either the maximum number of layers or minimum number of events per node is reached.

Each of the final nodes (or leaves) is given a weight

$$w = e^{\lambda \cdot \log(N_{\text{CR,leaf}}^{4b}/N_{\text{CR,leaf}}^{2b})},$$

where λ is the learning rate and $N_{\text{CR,leaf}}^{4b}$ ($N_{\text{CR,leaf}}^{2b}$) is the number of events in the leaf for the $4b$ ($2b$) CR. The results are then inputted into a new decision tree. This process iterates until the desired number of trees is reached. The final weight for each event is the product of the event's weight in each tree, normalized such that the number of events in the reweighted $2b$ CR matches that of the $4b$ CR. After training on data events in the CR, the BDT is used to calculate weights for all $2b$ events. The reweighted $2b$ SR then forms the background estimate for the $4b$ SR.

A bootstrapping procedure is used to increase the stability of the BDT reweighting and estimate its statistical uncertainty. In addition to the nominal BDT, an ensemble of 100 BDTs were trained for each year. These

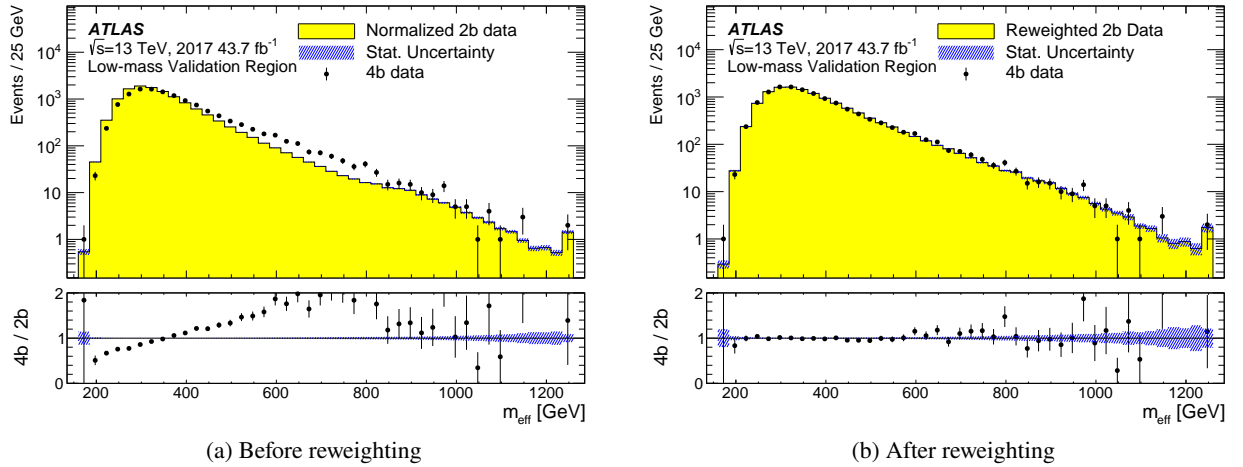


Figure 5: Comparison of the $2b$ and $4b$ m_{eff} distributions in the 2017 VR of the low-mass channel. The left plot shows the m_{eff} distribution before BDT reweighting. The right plot illustrates the same distribution, with the $2b$ events having the reweighting applied to match the $4b$ data. The final non-empty bin contains overflow events. The $2b$ distribution is normalized to the $4b$ integral to show the shape differences. The blue shading shows the uncertainty due to the $2b$ sample size for the left plot and both the reweighting and the $2b$ sample size for the right plot.

BDTs were trained using the same input events but with random Poisson weights with a mean of 1 to model the effect of statistical variations on the training data. The background estimate in any region of phase space is then set to the value obtained from the median of the $100 + 1$ variations. Half of the difference between the 84th percentile and 16th percentile of the $100 + 1$ bootstrap variations is taken to be the statistical uncertainty due to the reweighting. This is combined in quadrature with the Poisson uncertainties from the $2b$ samples.

Figure 5 shows the m_{eff} distribution in the VR for the 2017 dataset before and after the reweighting is applied. Excellent agreement is observed between the reweighted m_{eff} distributions of the $2b$ and $4b$ data. Good agreement was also found in all cases for other years and input variables.

6 Systematic uncertainties

Systematic uncertainties from various sources are evaluated for this analysis. Uncertainties are divided into three types: experimental uncertainties, theoretical uncertainties, and uncertainties in the data-driven background estimate. Experimental uncertainties quantify systematic effects due to the ATLAS detector and LHC conditions. Theoretical uncertainties account for possible mismodeling in the simulations of various physical processes. Experimental and theoretical uncertainties apply to the signal models used by the two channels as well as to the MC background estimates for the high-mass channel. Uncertainties in the data-driven background estimate are applied to the low-mass channel to account for potential mismodeling from the normalization factors and the BDTs used to estimate the background.

6.1 Experimental uncertainties

Systematic uncertainties associated with the jet energy scale and resolution [89], jet mass scale [106], flavor-tagging efficiencies [93], trigger efficiencies, soft E_T^{miss} terms [107], pileup conditions [108, 109], and luminosity are included in this analysis. Apart from the 1.7% uncertainty in the combined 2015–2018 integrated luminosity [110], obtained using the LUCID-2 detector [111] for the primary luminosity measurements, these uncertainties are assessed separately for each signal and background process. For the high-mass channel, experimental uncertainties are correlated across all of the SRs, VRs, and CRs for the higgsino mass hypothesis being tested. For the low-mass channel, these uncertainties are only applied to the $4b$ SRs as no other regions are used in the fit. For the high-mass channel, the jet energy scale, jet energy resolution, and jet mass scale uncertainties are estimated using a single enlarged CR, VR, and SR for each mass point. These three regions are created for each mass point by merging each of the mass point’s CRs, VRs, and SRs, respectively, and are used to avoid large statistical fluctuations that could cause instabilities in the fit. For the low-mass channel, the trigger and offline flavor-tagging uncertainties are calculated jointly in order to properly account for correlations. The jet energy resolution uncertainties for the low-mass channel are smoothed with a Gaussian kernel to mitigate the effect of statistical fluctuations.

6.2 Theoretical uncertainties

The signal models used by the two channels are also subject to theoretical uncertainties. MC generator-level samples for a representative set of mass points are used to assess the effect of varying the factorization and renormalization scales, merging scale, parton shower tuning, and initial- and final-state radiation parameters. The differences resulting from these variations are applied as the systematic uncertainties. For the low-mass channel, these differences are smoothed using a Gaussian kernel.

Theoretical uncertainties are also applied to the background samples for the high-mass channel. Uncertainties quantifying the systematic effects due to possible mismodeling associated with the MC generator and parton shower models, as well as with the modeling of initial- and final-state radiation, are applied to the $t\bar{t}$ and single-top backgrounds. For the tW process, the uncertainty associated with interference with $t\bar{t}$ production was estimated by comparing the nominal sample with an alternative sample generated using the diagram subtraction scheme [39, 112]. Uncertainties related to the renormalization, factorization, resummation, and matching scales are applied to the W +jets and Z +jets backgrounds. Uncertainties of 50% are applied to the $t\bar{t}+X$ and diboson backgrounds. Since the $t\bar{t}+X$ and diboson backgrounds make up a small fraction of the overall background, these uncertainties have no significant impact on the analysis.

Figure 6 illustrates the total post-fit uncertainties in the high-mass channel’s SRs, as well as the dominant components in each. Statistical uncertainties dominate. At masses below 1000 GeV, theoretical uncertainties associated with the generation and parton showering of $t\bar{t}$ events are one of the most important systematic uncertainty components, due to the dominance of this background process. In contrast, signal regions with $m_{\tilde{H}} \geq 1000$ GeV are more affected by uncertainties in Z +jets processes because of the increasing importance of the $Z \rightarrow \nu\nu$ background at higher E_T^{miss} .

6.3 Data-driven background uncertainties

In the low-mass channel, three sources of systematic uncertainty affect the data-driven background estimate. Their effects are estimated separately for the 2016, 2017, and 2018 data-taking periods.

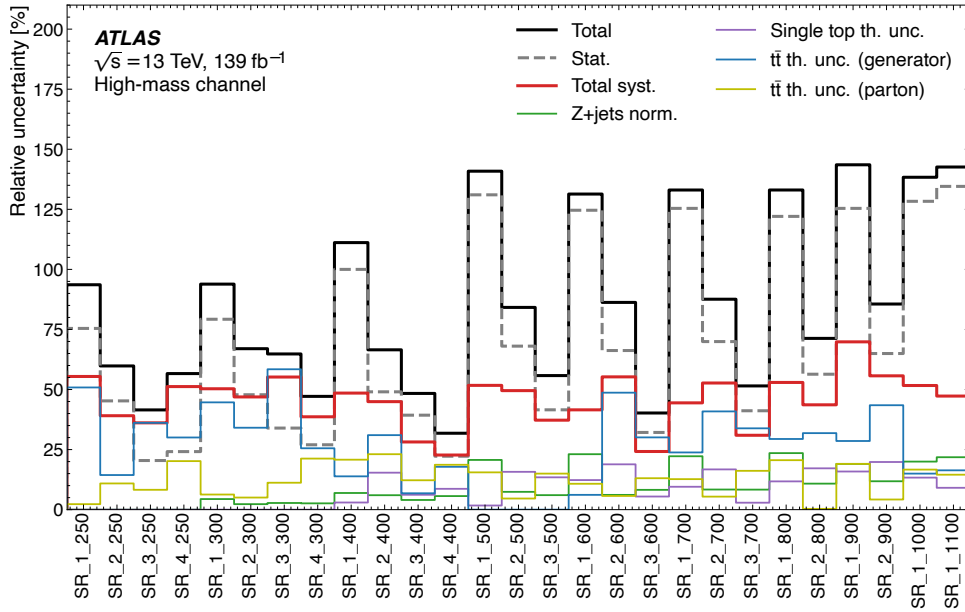


Figure 6: Breakdown of the dominant post-fit systematic uncertainties in the SRs of the high-mass channel. Because of their correlations, the total systematic uncertainty may exceed the quadrature sum of its components. The total uncertainty shown is the quadrature sum of the statistical and total systematic uncertainties.

A nonclosure uncertainty is assigned to account for imperfections in the reweighting procedure. This is estimated by evaluating the bin-by-bin differences between the $4b$ and reweighted $2b$ samples in the CRs. A nuisance parameter corresponding to the discrepancy is assigned to each bin where the difference is greater than the combined statistical uncertainty of the $2b$ and $4b$ samples. No nuisance parameters are assigned to bins where the discrepancy is less than this uncertainty. The nonclosure uncertainties are treated as uncorrelated in the statistical analysis.

A transfer uncertainty is assigned to the extrapolation of results from the CRs to the SRs. This transfer uncertainty is divided into a normalization component and a shape component. To estimate the transfer shape uncertainty, the BDTs were retrained using data from the VRs instead of the CRs. All other aspects of the training, including the bootstrapping procedure, were unchanged. This creates alternative background estimates with weights derived closer to the SRs. Each VR-derived estimate is then normalized to the corresponding nominal (CR-derived) estimate in the SR to separate this uncertainty from the normalization uncertainty. The difference between the two estimates is calculated for each bin and applied as an uncertainty if the difference is greater than the combined statistical uncertainty of the estimates. As with the nonclosure uncertainty, the transfer shape uncertainty is treated as uncorrelated across bins and is not applied to bins where the difference is less than the combined statistical uncertainty of the estimates.

The third source is the transfer normalization uncertainty, which is computed using two methods. In the first method, the uncertainty is taken to be the fractional difference between the numbers of SR events predicted by using the nominal and VR-derived background estimates. In the second method, the uncertainty for each data-taking period is taken to be the fractional difference between the predicted and observed numbers of events in the VR. The normalization uncertainty is taken to be the larger of its two estimated values.

A slightly different treatment is used to assign transfer uncertainties to the discovery regions. Since the discovery regions each consist of a single bin, the transfer normalization and shape uncertainties are

calculated jointly as the difference between the numbers of SR events predicted by using the nominal and VR-derived background estimates. In addition, the VR nonclosure is calculated as the difference between the numbers of predicted and observed events in the VR. The transfer uncertainties for the discovery regions are then taken to be the larger of the calculated transfer and VR nonclosure uncertainties. The bootstrap and nonclosure uncertainties are assigned in the same way as in the exclusion regions, except that the nonclosure uncertainty is applied even if it is less than the statistical uncertainty.

The components of the background uncertainty for the low-mass channel are shown in Figure 7. Considering all sources of systematic uncertainty, the nonclosure, jet energy resolution, and jet flavor composition uncertainties tend to have the greatest effect, the last being a component of the jet energy scale uncertainty.

A 50% uncertainty is applied to the QCD multijet prediction for the high-mass channel to account for potential mismodeling from the NN-assisted reweighting.

7 Results

7.1 High-mass channel

The level of agreement between the data and the post-fit background prediction is shown for each VR of the high-mass channel in Figure 8. All data observations are found to be in agreement with the background prediction within the analysis uncertainties. The $t\bar{t}$ and Z +jets normalization factors are measured to be between 0.9 and 1.3 for all mass hypotheses.

The SR observations are shown in Figure 9, together with the post-fit background predictions. No statistically significant excess is found, and the largest excess is observed in SR_1_1000 with a local statistical significance of 1.9σ . The excesses seen in SR_1_900, SR_1_1000 and SR_1_1100 are, however, similar due to the highly correlated SR definitions. The same three data events are observed in the first two of these SRs, and one of those events fails the SR_1_1100 selection.

7.2 Low-mass channel

The observations and normalized background predictions are shown for each E_T^{miss} and m_{eff} bin of the VRs in Figure 10. The lower panel shows the significance of the differences, using the profile likelihood method from Ref. [113]. No significant mismodeling is observed.

Figure 11 shows the results for each E_T^{miss} and m_{eff} bin of the SRs. No significant excess above the Standard Model prediction is observed. The largest upward fluctuation in the 213 kinematically allowed bins is observed in the $E_T^{\text{miss}} > 200$ GeV, $m_{\text{eff}} > 860$ GeV bin for the 2017 data-taking period. This bin has 6 observed events and 1.51 ± 0.35 predicted background events, corresponding to a local significance of 2.6σ . This excess occurs for events with high E_T^{miss} , where the high-mass channel has greater sensitivity.

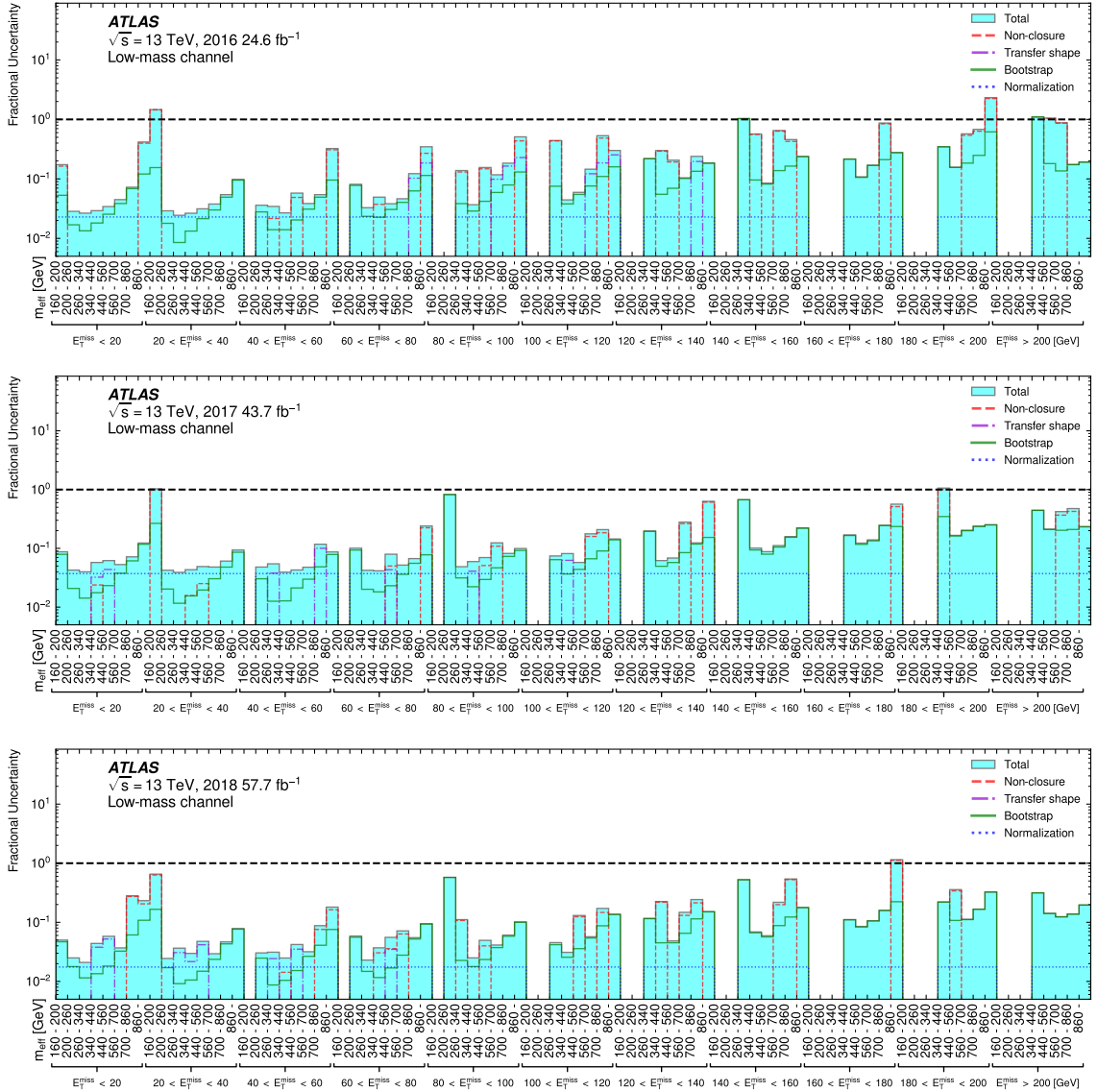


Figure 7: Background uncertainties as a fraction of background yields for the 2016, 2017, and 2018 SRs. Pre-fit values are shown. The bootstrap component also includes the Poisson component of the statistical uncertainty of the $2b$ sample. No uncertainties are shown for bins predicted to have no background events. The total uncertainty shown is the quadrature sum of the individual uncertainties. All uncertainties are treated as symmetric.

8 Statistical interpretation

Following the Neyman–Pearson lemma, upper limits on higgsino pair-production cross sections are set using test statistics [114] based on the profile likelihood ratio. The p -values of the statistical tests are obtained by following the CL_s prescription [115] and, unless stated otherwise, using the asymptotic approximation described in Ref. [114]. Results obtained using the asymptotic approximation were confirmed with pseudo-experiments. The HistFitter framework [116] is used for the high-mass channel and the pyhf framework [117, 118] is used for the low-mass channel. Two different types of upper limits are provided

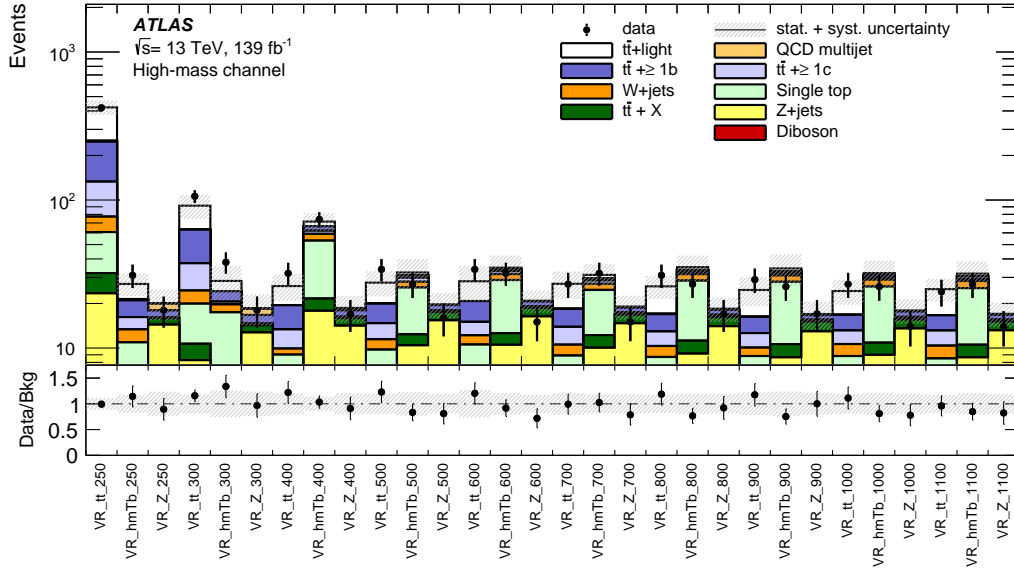


Figure 8: Post-fit VR yields in the high-mass channel. The upper panel shows the observed number of events, as well as the post-fit background predictions in each region. The bottom panel shows the ratio of the observed data to the total background prediction. The shaded areas correspond to the total statistical and systematic uncertainties obtained after the fit and described in Section 6.

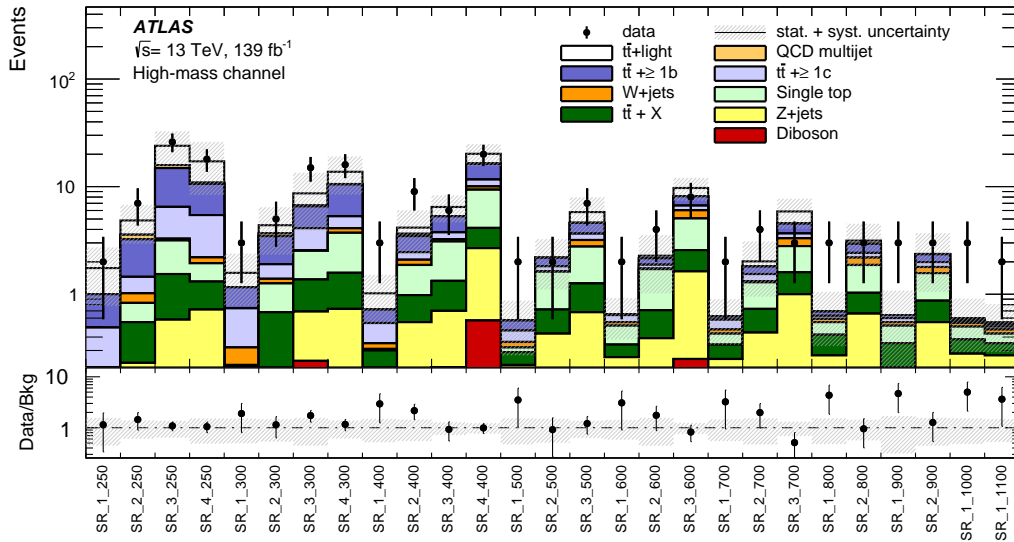


Figure 9: Post-fit SR yields in the high-mass channel. The upper panel shows the observed number of events, as well as the post-fit background predictions in each region. The bottom panel shows the ratio of the observed data to the total background prediction. The shaded areas correspond to the total statistical and systematic uncertainties obtained after the fit and described in Section 6.

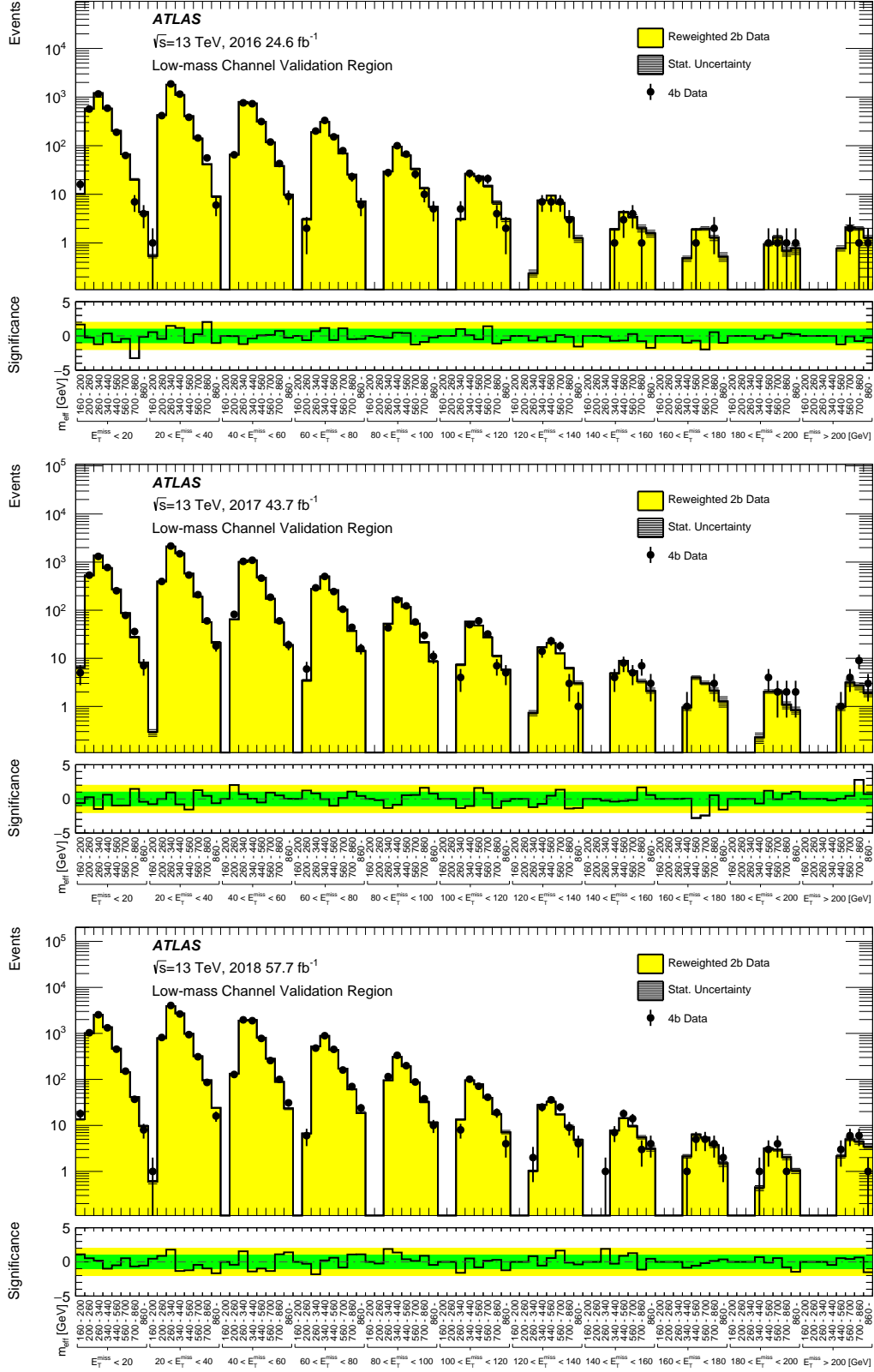


Figure 10: Data and background (reweighted 2b) predictions for each 4b VR E_T^{miss} and m_{eff} bin of the low-mass channel for the 2016, 2017, and 2018 data-taking periods. The background is normalized to the 4b data. The bottom panel shows the significance of any differences between the observed 4b data and the background prediction. The 1 σ and 2 σ bands are shown in green and yellow, respectively.

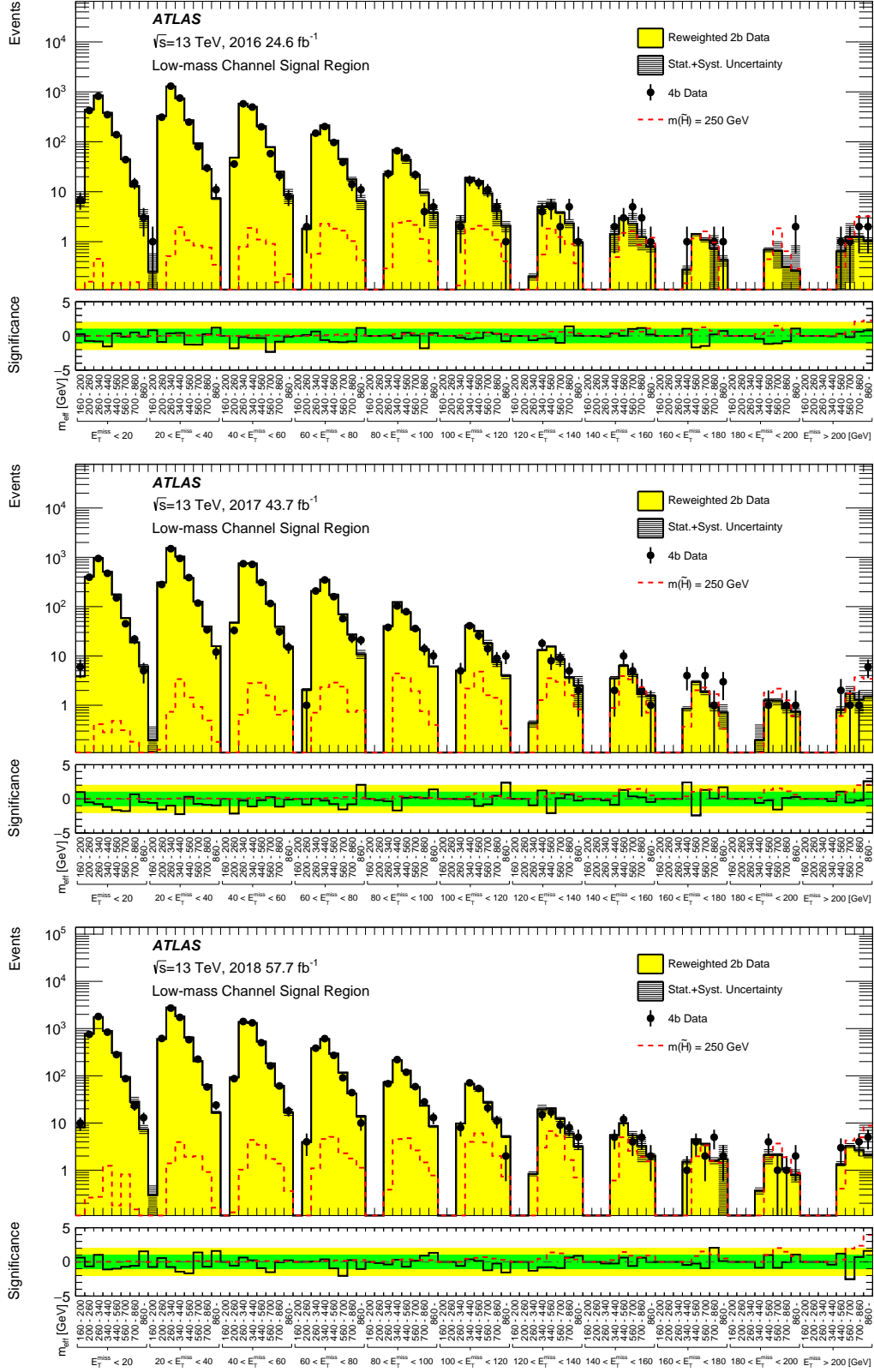


Figure 11: Pre-fit data and background (reweighted $2b$) predictions for each $4b$ SR E_T^{miss} and m_{eff} bin of the low-mass channel for the 2016, 2017, and 2018 data-taking periods. The bottom panel shows the significance of any differences between the observed $4b$ data and the background prediction. The 1σ and 2σ bands are shown in green and yellow, respectively.

Table 5: Results from the high-mass and low-mass channel discovery regions. The columns include, from left to right: the observed number of events N_{obs} , predicted number of events N_{pred} , and 95% CL upper limits on the visible cross section ($\langle\epsilon\sigma\rangle_{\text{obs}}^{95}$) and on the number of signal events (S_{obs}^{95}). The S_{exp}^{95} column shows the 95% CL upper limit on the number of signal events, given the expected number (and $\pm 1\sigma$ excursions of the expectation) of background events. The last column indicates the discovery p -value (denoted by $p(s=0)$) and its corresponding significance in parentheses. The p -values are capped at 0.5.

Signal channel	N_{obs}	N_{pred}	$\langle\epsilon\sigma\rangle_{\text{obs}}^{95}$ [fb]	S_{obs}^{95}	S_{exp}^{95}	$p(s=0)$
SR_1_250	2	1.8 ± 1.0	0.04	6.2	$5.9_{-0.9}^{+1.7}$	0.48 (0.05)
SR_1_500	2	0.58 ± 0.30	0.04	5.5	$4.0_{-0.6}^{+1.7}$	0.18 (0.92)
SR_1_1000	3	0.60 ± 0.31	0.05	6.7	$4.3_{-0.9}^{+0.9}$	0.03 (1.9)
SR_LM_150	1790	1860 ± 50	0.73	92	127_{-34}^{+48}	0.5 (0.00)
SR_LM_300	97	77.0 ± 5.3	0.31	39	22_{-6}^{+9}	0.03 (1.8)

for each channel: model-independent limits and model-dependent limits for the various simulated higgsino masses $m_{\tilde{H}}$.

8.1 Model-independent limits

Model-independent limits on the number of beyond-the-SM physics events are set for each discovery SR of the analysis. The upper limits are obtained by assuming no signal contamination in the analysis CRs, and assigning to each SR a number of signal events corresponding to the fit’s BSM signal strength μ . The different backgrounds and model-independent signals are then adjusted to determine the 95% confidence level (CL) upper limits. Results are calculated using 5000 pseudo-experiments for the high-mass discovery regions SR_1_250, SR_1_500, and SR_1_1000 and 20000 pseudo-experiments for the low-mass discovery regions SR_LM_150 and SR_LM_300. The upper limits for the discovery regions of the two channels are summarized in Table 5.

8.2 Model-dependent exclusion limits

Since no significant excess above the SM prediction is observed, 95% CL upper limits are calculated for the simplified signal models described in Section 1. Each mass point uses the channel with the better expected limit, with the transition between the low-mass and high-mass channel interpretations occurring at $m_{\tilde{H}} = 250$ GeV. Figure 12(a) shows the upper limit on the higgsino pair-production cross section for a branching ratio of $\mathcal{B}(\tilde{H} \rightarrow h + \tilde{G}) = 100\%$. Higgsino masses below 940 GeV and, owing to the mass of the Higgs boson, above 130 GeV are excluded.

The results are also interpreted for the case where $\mathcal{B}(\tilde{H} \rightarrow h + \tilde{G})$ is allowed to vary, with all other decays assumed to create Z bosons through $\tilde{H} \rightarrow Z + \tilde{G}$. The higgsino pair-production cross section is assumed to match the theoretical prediction. Limits for this interpretation are shown in Figure 12(b). For the low-mass channel, the Z decays peak outside of the SRs in the $(m(h_1^{\text{LM}}), m(h_2^{\text{LM}}))$ plane and would be included in the data-driven background estimate. The limit on the branching ratio is therefore equal to the square root of the limit on $\sigma/\sigma_{\text{theory}}$ shown in Figure 12(a). For the high-mass channel, both the Higgs boson and the Z boson decays are included in the signal model, leading to additional sensitivity in the branching ratio plane and the exclusion of $\tilde{H} \rightarrow h + \tilde{G}$ branching ratios as low as 14%.

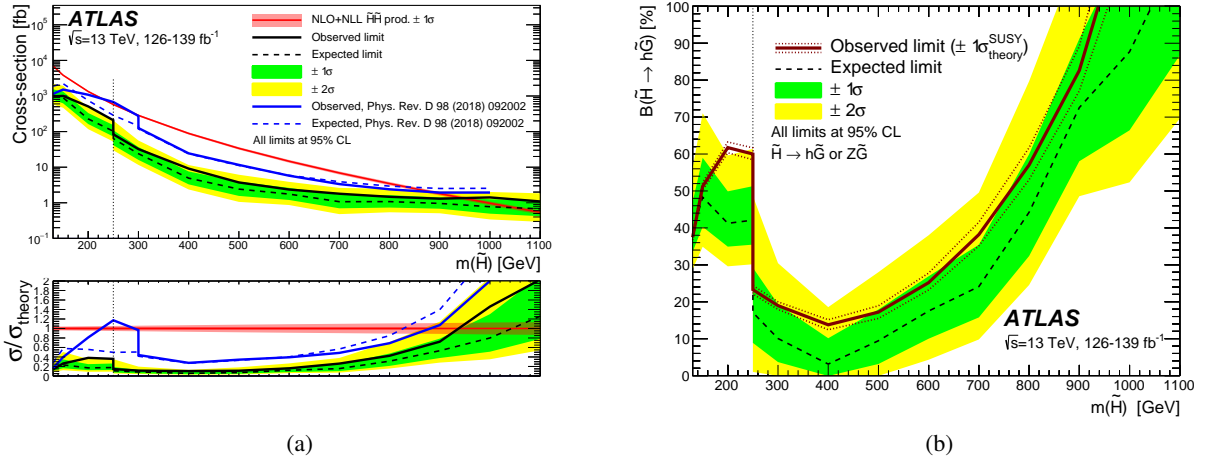


Figure 12: Exclusion limits in the low-mass and high-mass channels. The low-mass channel is used for $m_{\tilde{H}} < 250$ GeV, while the high-mass channel is used for $m_{\tilde{H}} \geq 250$ GeV. The left plot shows the observed (solid) and expected (dashed) 95% CL upper limits on the higgsino pair-production cross section, assuming a higgsino decay branching ratio of $\mathcal{B}(\tilde{H} \rightarrow h + \tilde{G}) = 100\%$. The theory cross section and its uncertainty are shown by the solid red line and red shading. Results from a previous ATLAS search using $24.3\text{--}36.1$ fb $^{-1}$ of Run 2 data [13] are shown by the solid (observed) and dashed (expected) blue lines. The bottom panel shows the ratio of the limits to the theory cross section. The right plot shows the 95% CL observed (solid) and expected (dashed) upper limits on $\mathcal{B}(\tilde{H} \rightarrow h + \tilde{G})$, assuming the theory cross section for higgsino pair production. The higgsinos are assumed to decay as $\tilde{H} \rightarrow h + \tilde{G}$ or $\tilde{H} \rightarrow Z + \tilde{G}$. For both plots, the phase space above the lines is excluded.

9 Conclusion

A search for pair-produced and mass-degenerate higgsinos decaying to gravitinos and Higgs bosons was performed using the ≥ 3 b -jets + E_T^{miss} final state. The search uses two separate channels optimized for either low-mass or high-mass higgsinos and exploits the 139 fb $^{-1}$ of $\sqrt{s} = 13$ TeV proton–proton collision data collected by the ATLAS detector during Run 2 of the LHC. This analysis improves upon the previous ATLAS search in several ways, including using a boosted decision tree to provide enhanced background rejection for the high-mass channel, reoptimizing the b -tagging efficiency working point and binning structure for the low-mass channel, implementing a new method for reconstructing Higgs boson candidates, and using improved jet reconstruction and b -tagging algorithms.

No significant excess above the SM prediction is observed. Higgsinos with masses between 130 GeV and 940 GeV are excluded at 95% confidence level for the $\mathcal{B}(\tilde{H} \rightarrow h + \tilde{G}) = 100\%$ hypothesis. For this hypothesis, this search is the most sensitive to date across the mass range investigated, and provides the most stringent constraints in the $130\text{--}800$ GeV higgsino mass range. Upper limits are set on $\mathcal{B}(\tilde{H} \rightarrow h + \tilde{G})$, reaching as low as 14% for a higgsino mass of 400 GeV. Model-independent limits are also set on the visible cross section for new physics processes.

Acknowledgements

We thank CERN for the very successful operation of the LHC, as well as the support staff from our institutions without whom ATLAS could not be operated efficiently.

We acknowledge the support of ANPCyT, Argentina; YerPhI, Armenia; ARC, Australia; BMFWF and FWF, Austria; ANAS, Azerbaijan; CNPq and FAPESP, Brazil; NSERC, NRC and CFI, Canada; CERN; ANID, Chile; CAS, MOST and NSFC, China; Minciencias, Colombia; MEYS CR, Czech Republic; DNRF and DNSRC, Denmark; IN2P3-CNRS and CEA-DRF/IRFU, France; SRNSFG, Georgia; BMBF, HGF and MPG, Germany; GSRI, Greece; RGC and Hong Kong SAR, China; ISF and Benozziyo Center, Israel; INFN, Italy; MEXT and JSPS, Japan; CNRST, Morocco; NWO, Netherlands; RCN, Norway; MEiN, Poland; FCT, Portugal; MNE/IFA, Romania; MESTD, Serbia; MSSR, Slovakia; ARRS and MIZŠ, Slovenia; DSI/NRF, South Africa; MICINN, Spain; SRC and Wallenberg Foundation, Sweden; SERI, SNSF and Cantons of Bern and Geneva, Switzerland; MOST, Taipei; TENMAK, Türkiye; STFC, United Kingdom; DOE and NSF, United States of America. In addition, individual groups and members have received support from BCKDF, CANARIE, CRC and DRAC, Canada; PRIMUS 21/SCI/017 and UNCE SCI/013, Czech Republic; COST, ERC, ERDF, Horizon 2020, ICSC-NextGenerationEU and Marie Skłodowska-Curie Actions, European Union; Investissements d’Avenir Labex, Investissements d’Avenir Idex and ANR, France; DFG and AvH Foundation, Germany; Herakleitos, Thales and Aristeia programmes co-financed by EU-ESF and the Greek NSRF, Greece; BSF-NSF and MINERVA, Israel; Norwegian Financial Mechanism 2014-2021, Norway; NCN and NAWA, Poland; La Caixa Banking Foundation, CERCA Programme Generalitat de Catalunya and PROMETEO and GenT Programmes Generalitat Valenciana, Spain; Göran Gustafssons Stiftelse, Sweden; The Royal Society and Leverhulme Trust, United Kingdom.

The crucial computing support from all WLCG partners is acknowledged gratefully, in particular from CERN, the ATLAS Tier-1 facilities at TRIUMF/SFU (Canada), NDGF (Denmark, Norway, Sweden), CC-IN2P3 (France), KIT/GridKA (Germany), INFN-CNAF (Italy), NL-T1 (Netherlands), PIC (Spain), RAL (UK) and BNL (USA), the Tier-2 facilities worldwide and large non-WLCG resource providers. Major contributors of computing resources are listed in Ref. [119].

References

- [1] Y. Golfand and E. Likhtman, *Extension of the Algebra of Poincare Group Generators and Violation of P Invariance*, JETP Lett. **13** (1971) 323, [Pisma Zh. Eksp. Teor. Fiz. **13** (1971) 452].
- [2] D. Volkov and V. Akulov, *Is the neutrino a goldstone particle?* Phys. Lett. B **46** (1973) 109.
- [3] J. Wess and B. Zumino, *Supergauge transformations in four dimensions*, Nucl. Phys. B **70** (1974) 39.
- [4] J. Wess and B. Zumino, *Supergauge invariant extension of quantum electrodynamics*, Nucl. Phys. B **78** (1974) 1.
- [5] S. Ferrara and B. Zumino, *Supergauge invariant Yang-Mills theories*, Nucl. Phys. B **79** (1974) 413.
- [6] A. Salam and J. Strathdee, *Super-symmetry and non-Abelian gauges*, Phys. Lett. B **51** (1974) 353.
- [7] G. R. Farrar and P. Fayet, *Phenomenology of the production, decay, and detection of new hadronic states associated with supersymmetry*, Phys. Lett. B **76** (1978) 575.
- [8] N. Sakai, *Naturalness in supersymmetric GUTS*, Z. Phys. C **11** (1981) 153.
- [9] S. Dimopoulos, S. Raby, and F. Wilczek, *Supersymmetry and the scale of unification*, Phys. Rev. D **24** (1981) 1681.
- [10] L. E. Ibáñez and G. G. Ross, *Low-energy predictions in supersymmetric grand unified theories*, Phys. Lett. B **105** (1981) 439.
- [11] S. Dimopoulos and H. Georgi, *Softly broken supersymmetry and SU(5)*, Nucl. Phys. B **193** (1981) 150.
- [12] R. Barbieri and G. Giudice, *Upper bounds on supersymmetric particle masses*, Nucl. Phys. B **306** (1988) 63.
- [13] ATLAS Collaboration, *Search for pair production of higgsinos in final states with at least three b-tagged jets in $\sqrt{s} = 13$ TeV pp collisions using the ATLAS detector*, Phys. Rev. D **98** (2018) 092002, arXiv: 1806.04030 [hep-ex].
- [14] CMS Collaboration, *Search for higgsinos decaying to two Higgs bosons and missing transverse momentum in proton–proton collisions at $\sqrt{s} = 13$ TeV*, JHEP **05** (2022) 014, arXiv: 2201.04206 [hep-ex].
- [15] ATLAS Collaboration, *Search for supersymmetry in events with four or more charged leptons in 139fb^{-1} of $\sqrt{s} = 13$ TeV pp collisions with the ATLAS detector*, JHEP **07** (2021) 167, arXiv: 2103.11684 [hep-ex].
- [16] ATLAS Collaboration, *Search for charginos and neutralinos in final states with two boosted hadronically decaying bosons and missing transverse momentum in pp collisions at $\sqrt{s} = 13$ TeV with the ATLAS detector*, Phys. Rev. D **104** (2021) 112010, arXiv: 2108.07586 [hep-ex].
- [17] ATLAS Collaboration, *Searches for new phenomena in events with two leptons, jets, and missing transverse momentum in 139fb^{-1} of $\sqrt{s} = 13$ TeV pp collisions with the ATLAS detector*, Eur. Phys. J. C **83** (2023) 515, arXiv: 2204.13072 [hep-ex].
- [18] ATLAS Collaboration, *Search for pair-produced Higgsinos decaying via Higgs or Z bosons to final states containing a pair of photons and a pair of b-jets with the ATLAS detector*, ATLAS-CONF-2023-009, 2023, URL: <https://cds.cern.ch/record/2854839>.

- [19] P. Meade, N. Seiberg, and D. Shih, *General Gauge Mediation*, *Prog. Theor. Phys. Suppl.* **177** (2009) 143, arXiv: [0801.3278 \[hep-ph\]](#).
- [20] C. Cheung, A. L. Fitzpatrick, and D. Shih, *(Extra)ordinary gauge mediation*, *JHEP* **07** (2008) 054, arXiv: [0710.3585 \[hep-ph\]](#).
- [21] M. Dine and W. Fischler, *A phenomenological model of particle physics based on supersymmetry*, *Phys. Lett. B* **110** (1982) 227.
- [22] L. Alvarez-Gaumé, M. Claudson, and M. B. Wise, *Low-energy supersymmetry*, *Nucl. Phys. B* **207** (1982) 96.
- [23] C. R. Nappi and B. A. Ovrut, *Supersymmetric extension of the $SU(3) \times SU(2) \times U(1)$ model*, *Phys. Lett. B* **113** (1982) 175.
- [24] S. Dimopoulos, M. Dine, S. Raby, and S. Thomas, *Experimental Signatures of Low Energy Gauge-Mediated Supersymmetry Breaking*, *Phys. Rev. Lett.* **76** (1996) 3494, arXiv: [hep-ph/9601367](#).
- [25] K. T. Matchev and S. Thomas, *Higgs and Z-boson signatures of supersymmetry*, *Phys. Rev. D* **62** (2000) 077702, arXiv: [hep-ph/9908482](#).
- [26] P. Meade, M. Reece, and D. Shih, *Prompt Decays of General Neutralino NLSPs at the Tevatron*, *JHEP* **05** (2010) 105, arXiv: [0911.4130 \[hep-ph\]](#).
- [27] ATLAS Collaboration, *Performance of the missing transverse momentum triggers for the ATLAS detector during Run-2 data taking*, *JHEP* **08** (2020) 080, arXiv: [2005.09554 \[hep-ex\]](#).
- [28] ATLAS Collaboration, *Configuration and performance of the ATLAS b-jet triggers in Run 2*, *Eur. Phys. J. C* **81** (2021) 1087, arXiv: [2106.03584 \[hep-ex\]](#).
- [29] ATLAS Collaboration, *The ATLAS Experiment at the CERN Large Hadron Collider*, *JINST* **3** (2008) S08003.
- [30] ATLAS Collaboration, *The ATLAS Collaboration Software and Firmware*, ATL-SOFT-PUB-2021-001, 2021, URL: <https://cds.cern.ch/record/2767187>.
- [31] ATLAS Collaboration, *ATLAS data quality operations and performance for 2015–2018 data-taking*, *JINST* **15** (2020) P04003, arXiv: [1911.04632 \[physics.ins-det\]](#).
- [32] ATLAS Collaboration, *The ATLAS Simulation Infrastructure*, *Eur. Phys. J. C* **70** (2010) 823, arXiv: [1005.4568 \[physics.ins-det\]](#).
- [33] S. Agostinelli et al., *GEANT4 – a simulation toolkit*, *Nucl. Instrum. Meth. A* **506** (2003) 250.
- [34] ATLAS Collaboration, *The simulation principle and performance of the ATLAS fast calorimeter simulation FastCaloSim*, ATL-PHYS-PUB-2010-013, 2010, URL: <https://cds.cern.ch/record/1300517>.
- [35] T. Sjöstrand, S. Mrenna, and P. Skands, *A brief introduction to PYTHIA 8.1*, *Comput. Phys. Commun.* **178** (2008) 852, arXiv: [0710.3820 \[hep-ph\]](#).
- [36] NNPDF Collaboration, R. D. Ball, et al., *Parton distributions with LHC data*, *Nucl. Phys. B* **867** (2013) 244, arXiv: [1207.1303 \[hep-ph\]](#).
- [37] ATLAS Collaboration, *The Pythia 8 A3 tune description of ATLAS minimum bias and inelastic measurements incorporating the Donnachie–Landshoff diffractive model*, ATL-PHYS-PUB-2016-017, 2016, URL: <https://cds.cern.ch/record/2206965>.

- [38] D. J. Lange, *The EvtGen particle decay simulation package*, *Nucl. Instrum. Meth. A* **462** (2001) 152.
- [39] ATLAS Collaboration, *Studies on top-quark Monte Carlo modelling for Top2016*, ATL-PHYS-PUB-2016-020, 2016, URL: <https://cds.cern.ch/record/2216168>.
- [40] T. Gleisberg and S. Höche, *Comix, a new matrix element generator*, *JHEP* **12** (2008) 039, arXiv: [0808.3674](https://arxiv.org/abs/0808.3674) [[hep-ph](#)].
- [41] S. Schumann and F. Krauss, *A parton shower algorithm based on Catani–Seymour dipole factorisation*, *JHEP* **03** (2008) 038, arXiv: [0709.1027](https://arxiv.org/abs/0709.1027) [[hep-ph](#)].
- [42] S. Höche, F. Krauss, M. Schönherr, and F. Siegert, *A critical appraisal of NLO+PS matching methods*, *JHEP* **09** (2012) 049, arXiv: [1111.1220](https://arxiv.org/abs/1111.1220) [[hep-ph](#)].
- [43] S. Höche, F. Krauss, M. Schönherr, and F. Siegert, *QCD matrix elements + parton showers. The NLO case*, *JHEP* **04** (2013) 027, arXiv: [1207.5030](https://arxiv.org/abs/1207.5030) [[hep-ph](#)].
- [44] S. Catani, F. Krauss, B. R. Webber, and R. Kuhn, *QCD Matrix Elements + Parton Showers*, *JHEP* **11** (2001) 063, arXiv: [hep-ph/0109231](https://arxiv.org/abs/hep-ph/0109231).
- [45] S. Höche, F. Krauss, S. Schumann, and F. Siegert, *QCD matrix elements and truncated showers*, *JHEP* **05** (2009) 053, arXiv: [0903.1219](https://arxiv.org/abs/0903.1219) [[hep-ph](#)].
- [46] F. Buccioni et al., *OpenLoops 2*, *Eur. Phys. J. C* **79** (2019) 866, arXiv: [1907.13071](https://arxiv.org/abs/1907.13071) [[hep-ph](#)].
- [47] F. Cascioli, P. Maierhöfer, and S. Pozzorini, *Scattering Amplitudes with Open Loops*, *Phys. Rev. Lett.* **108** (2012) 111601, arXiv: [1111.5206](https://arxiv.org/abs/1111.5206) [[hep-ph](#)].
- [48] A. Denner, S. Dittmaier, and L. Hofer, *COLLIER: A fortran-based complex one-loop library in extended regularizations*, *Comput. Phys. Commun.* **212** (2017) 220, arXiv: [1604.06792](https://arxiv.org/abs/1604.06792) [[hep-ph](#)].
- [49] W. Beenakker et al., *Production of Charginos, Neutralinos, and Stopped at Hadron Colliders*, *Phys. Rev. Lett.* **83** (1999) 3780, arXiv: [hep-ph/9906298](https://arxiv.org/abs/hep-ph/9906298),
Erratum: *Phys. Rev. Lett.* **100** (2008) 029901.
- [50] G. Bozzi, B. Fuks, and M. Klasen, *Threshold Resummation for Slepton-Pair Production at Hadron Colliders*, *Nucl. Phys. B* **777** (2007) 157, arXiv: [hep-ph/0701202](https://arxiv.org/abs/hep-ph/0701202) [[hep-ph](#)].
- [51] B. Fuks, M. Klasen, D. R. Lamprea, and M. Rothering, *Gaugino production in proton-proton collisions at a center-of-mass energy of 8 TeV*, *JHEP* **10** (2012) 081, arXiv: [1207.2159](https://arxiv.org/abs/1207.2159) [[hep-ph](#)].
- [52] B. Fuks, M. Klasen, D. R. Lamprea, and M. Rothering, *Precision predictions for electroweak superpartner production at hadron colliders with RESUMMINO*, *Eur. Phys. J. C* **73** (2013) 2480, arXiv: [1304.0790](https://arxiv.org/abs/1304.0790) [[hep-ph](#)].
- [53] B. Fuks, M. Klasen, D. R. Lamprea, and M. Rothering, *Revisiting slepton pair production at the Large Hadron Collider*, *JHEP* **01** (2014) 168, arXiv: [1310.2621](https://arxiv.org/abs/1310.2621) [[hep-ph](#)].

- [54] J. Fiaschi and M. Klasen, *Slepton pair production at the LHC in NLO+NLL with resummation-improved parton densities*, *JHEP* **03** (2018) 094, arXiv: [1801.10357 \[hep-ph\]](#).
- [55] J. Alwall et al., *The automated computation of tree-level and next-to-leading order differential cross sections, and their matching to parton shower simulations*, *JHEP* **07** (2014) 079, arXiv: [1405.0301 \[hep-ph\]](#).
- [56] ATLAS Collaboration, *ATLAS Pythia 8 tunes to 7 TeV data*, ATL-PHYS-PUB-2014-021, 2014, URL: <https://cds.cern.ch/record/1966419>.
- [57] W. Beenakker, C. Borschensky, M. Krämer, A. Kulesza, and E. Laenen, *NNLL-fast: predictions for coloured supersymmetric particle production at the LHC with threshold and Coulomb resummation*, *JHEP* **12** (2016) 133, arXiv: [1607.07741 \[hep-ph\]](#).
- [58] W. Beenakker et al., *NNLL resummation for squark and gluino production at the LHC*, *JHEP* **12** (2014) 023, arXiv: [1404.3134 \[hep-ph\]](#).
- [59] W. Beenakker et al., *Towards NNLL resummation: hard matching coefficients for squark and gluino hadroproduction*, *JHEP* **10** (2013) 120, arXiv: [1304.6354 \[hep-ph\]](#).
- [60] W. Beenakker et al., *NNLL resummation for squark-antisquark pair production at the LHC*, *JHEP* **01** (2012) 076, arXiv: [1110.2446 \[hep-ph\]](#).
- [61] W. Beenakker et al., *Soft-gluon resummation for squark and gluino hadroproduction*, *JHEP* **12** (2009) 041, arXiv: [0909.4418 \[hep-ph\]](#).
- [62] A. Kulesza and L. Motyka, *Soft gluon resummation for the production of gluino-gluino and squark-antisquark pairs at the LHC*, *Phys. Rev. D* **80** (2009) 095004, arXiv: [0905.4749 \[hep-ph\]](#).
- [63] A. Kulesza and L. Motyka, *Threshold Resummation for Squark-Antisquark and Gluino-Pair Production at the LHC*, *Phys. Rev. Lett.* **102** (2009) 111802, arXiv: [0807.2405 \[hep-ph\]](#).
- [64] W. Beenakker, R. Höpker, M. Spira, and P. Zerwas, *Squark and gluino production at hadron colliders*, *Nucl. Phys. B* **492** (1997) 51, arXiv: [hep-ph/9610490](#).
- [65] J. Butterworth et al., *PDF4LHC recommendations for LHC Run II*, *J. Phys. G* **43** (2016) 023001, arXiv: [1510.03865 \[hep-ph\]](#).
- [66] T. Sjöstrand et al., *An introduction to PYTHIA 8.2*, *Comput. Phys. Commun.* **191** (2015) 159, arXiv: [1410.3012 \[hep-ph\]](#).
- [67] E. Bothmann et al., *Event generation with Sherpa 2.2*, *SciPost Phys.* **7** (2019) 034, arXiv: [1905.09127 \[hep-ph\]](#).
- [68] NNPDF Collaboration, R. D. Ball, et al., *Parton distributions for the LHC run II*, *JHEP* **04** (2015) 040, arXiv: [1410.8849 \[hep-ph\]](#).
- [69] T. Gleisberg et al., *Event generation with SHERPA 1.1*, *JHEP* **02** (2009) 007, arXiv: [0811.4622 \[hep-ph\]](#).
- [70] S. Frixione, G. Ridolfi, and P. Nason, *A positive-weight next-to-leading-order Monte Carlo for heavy flavour hadroproduction*, *JHEP* **09** (2007) 126, arXiv: [0707.3088 \[hep-ph\]](#).

- [71] P. Nason, *A new method for combining NLO QCD with shower Monte Carlo algorithms*, *JHEP* **11** (2004) 040, arXiv: [hep-ph/0409146](#).
- [72] S. Frixione, P. Nason, and C. Oleari, *Matching NLO QCD computations with parton shower simulations: the POWHEG method*, *JHEP* **11** (2007) 070, arXiv: [0709.2092 \[hep-ph\]](#).
- [73] S. Alioli, P. Nason, C. Oleari, and E. Re, *A general framework for implementing NLO calculations in shower Monte Carlo programs: the POWHEG BOX*, *JHEP* **06** (2010) 043, arXiv: [1002.2581 \[hep-ph\]](#).
- [74] M. Beneke, P. Falgari, S. Klein, and C. Schwinn, *Hadronic top-quark pair production with NNLL threshold resummation*, *Nucl. Phys. B* **855** (2012) 695, arXiv: [1109.1536 \[hep-ph\]](#).
- [75] M. Cacciari, M. Czakon, M. Mangano, A. Mitov, and P. Nason, *Top-pair production at hadron colliders with next-to-next-to-leading logarithmic soft-gluon resummation*, *Phys. Lett. B* **710** (2012) 612, arXiv: [1111.5869 \[hep-ph\]](#).
- [76] P. Bärnreuther, M. Czakon, and A. Mitov, *Percent-Level-Precision Physics at the Tevatron: Next-to-Next-to-Leading Order QCD Corrections to $q\bar{q} \rightarrow t\bar{t} + X$* , *Phys. Rev. Lett.* **109** (2012) 132001, arXiv: [1204.5201 \[hep-ph\]](#).
- [77] M. Czakon and A. Mitov, *NNLO corrections to top-pair production at hadron colliders: the all-fermionic scattering channels*, *JHEP* **12** (2012) 054, arXiv: [1207.0236 \[hep-ph\]](#).
- [78] M. Czakon and A. Mitov, *NNLO corrections to top pair production at hadron colliders: the quark-gluon reaction*, *JHEP* **01** (2013) 080, arXiv: [1210.6832 \[hep-ph\]](#).
- [79] M. Czakon, P. Fiedler, and A. Mitov, *Total Top-Quark Pair-Production Cross Section at Hadron Colliders Through $O(\alpha_S^4)$* , *Phys. Rev. Lett.* **110** (2013) 252004, arXiv: [1303.6254 \[hep-ph\]](#).
- [80] M. Czakon and A. Mitov, *Top++: A program for the calculation of the top-pair cross-section at hadron colliders*, *Comput. Phys. Commun.* **185** (2014) 2930, arXiv: [1112.5675 \[hep-ph\]](#).
- [81] P. Kant et al., *HatHor for single top-quark production: Updated predictions and uncertainty estimates for single top-quark production in hadronic collisions*, *Comput. Phys. Commun.* **191** (2015) 74, arXiv: [1406.4403 \[hep-ph\]](#).
- [82] N. Kidonakis, *Two-loop soft anomalous dimensions for single top quark associated production with a W^- or H^-* , *Phys. Rev. D* **82** (2010) 054018, arXiv: [1005.4451 \[hep-ph\]](#).
- [83] N. Kidonakis, “Top Quark Production,” *Proceedings, Helmholtz International Summer School on Physics of Heavy Quarks and Hadrons (HQ 2013)* (JINR, Dubna, Russia, July 15–28, 2013) 139, arXiv: [1311.0283 \[hep-ph\]](#).
- [84] D. de Florian et al., *Handbook of LHC Higgs Cross Sections: 4. Deciphering the Nature of the Higgs Sector*, (2016), arXiv: [1610.07922 \[hep-ph\]](#).
- [85] ATLAS Collaboration, *Vertex Reconstruction Performance of the ATLAS Detector at $\sqrt{s} = 13$ TeV*, ATL-PHYS-PUB-2015-026, 2015, URL: <https://cds.cern.ch/record/2037717>.

- [86] M. Cacciari, G. P. Salam, and G. Soyez, *The anti- k_t jet clustering algorithm*, **JHEP** **04** (2008) 063, arXiv: [0802.1189 \[hep-ph\]](#).
- [87] ATLAS Collaboration, *Jet reconstruction and performance using particle flow with the ATLAS Detector*, **Eur. Phys. J. C** **77** (2017) 466, arXiv: [1703.10485 \[hep-ex\]](#).
- [88] ATLAS Collaboration, *Tagging and suppression of pileup jets with the ATLAS detector*, ATLAS-CONF-2014-018, 2014, URL: <https://cds.cern.ch/record/1700870>.
- [89] ATLAS Collaboration, *Jet energy scale and resolution measured in proton–proton collisions at $\sqrt{s} = 13$ TeV with the ATLAS detector*, **Eur. Phys. J. C** **81** (2021) 689, arXiv: [2007.02645 \[hep-ex\]](#).
- [90] ATLAS Collaboration, *Jet reclustering and close-by effects in ATLAS Run 2*, ATLAS-CONF-2017-062, 2017, URL: <https://cds.cern.ch/record/2275649>.
- [91] D. Krohn, J. Thaler, and L.-T. Wang, *Jet trimming*, **JHEP** **02** (2010) 084, arXiv: [0912.1342 \[hep-ph\]](#).
- [92] ATLAS Collaboration, *ATLAS flavour-tagging algorithms for the LHC Run 2 pp collision dataset*, **Eur. Phys. J. C** **83** (2023) 681, arXiv: [2211.16345 \[physics.data-an\]](#).
- [93] ATLAS Collaboration, *ATLAS b-jet identification performance and efficiency measurement with $t\bar{t}$ events in pp collisions at $\sqrt{s} = 13$ TeV*, **Eur. Phys. J. C** **79** (2019) 970, arXiv: [1907.05120 \[hep-ex\]](#).
- [94] ATLAS Collaboration, *Measurement of the c-jet mistagging efficiency in $t\bar{t}$ events using pp collision data at $\sqrt{s} = 13$ TeV collected with the ATLAS detector*, **Eur. Phys. J. C** **82** (2022) 95, arXiv: [2109.10627 \[hep-ex\]](#).
- [95] ATLAS Collaboration, *Calibration of the light-flavour jet mistagging efficiency of the b-tagging algorithms with Z+jets events using 139fb^{-1} of ATLAS proton–proton collision data at $\sqrt{s} = 13$ TeV*, **Eur. Phys. J. C** **83** (2023) 728, arXiv: [2301.06319 \[hep-ex\]](#).
- [96] ATLAS Collaboration, *Electron and photon performance measurements with the ATLAS detector using the 2015–2017 LHC proton–proton collision data*, **JINST** **14** (2019) P12006, arXiv: [1908.00005 \[hep-ex\]](#).
- [97] ATLAS Collaboration, *Electron efficiency measurements with the ATLAS detector using 2012 LHC proton–proton collision data*, **Eur. Phys. J. C** **77** (2017) 195, arXiv: [1612.01456 \[hep-ex\]](#).
- [98] ATLAS Collaboration, *Muon reconstruction and identification efficiency in ATLAS using the full Run 2 pp collision data set at $\sqrt{s} = 13$ TeV*, **Eur. Phys. J. C** **81** (2021) 578, arXiv: [2012.00578 \[hep-ex\]](#).
- [99] ATLAS Collaboration, *E_T^{miss} performance in the ATLAS detector using 2015–2016 LHC pp collisions*, ATLAS-CONF-2018-023, 2018, URL: <https://cds.cern.ch/record/2625233>.
- [100] ATLAS Collaboration, *Characterisation and mitigation of beam-induced backgrounds observed in the ATLAS detector during the 2011 proton–proton run*, **JINST** **8** (2013) P07004, arXiv: [1303.0223 \[hep-ex\]](#).
- [101] ATLAS Collaboration, *Selection of jets produced in 13 TeV proton–proton collisions with the ATLAS detector*, ATLAS-CONF-2015-029, 2015, URL: <https://cds.cern.ch/record/2037702>.

- [102] T. Chen and C. Guestrin, *XGBoost: A Scalable Tree Boosting System*, (2016), arXiv: [1603.02754](https://arxiv.org/abs/1603.02754) [[cs.LG](https://arxiv.org/archive/cs)].
- [103] ATLAS Collaboration, *Object-based missing transverse momentum significance in the ATLAS Detector*, ATLAS-CONF-2018-038, 2018, URL: <https://cds.cern.ch/record/2630948>.
- [104] L. Moneta et al., *The RooStats Project*, *PoS ACAT2010 (2011) 057*, ed. by T. Speer et al., arXiv: [1009.1003](https://arxiv.org/abs/1009.1003) [[physics.data-an](https://arxiv.org/archive/physics)].
- [105] A. Rogozhnikov, *Reweighting with Boosted Decision Trees*, *J. Phys. Conf. Ser.* **762** (2016) 012036, ed. by L. Salinas and C. Torres, arXiv: [1608.05806](https://arxiv.org/abs/1608.05806) [[physics.data-an](https://arxiv.org/archive/physics)].
- [106] ATLAS Collaboration, *In situ calibration of large-radius jet energy and mass in 13 TeV proton–proton collisions with the ATLAS detector*, *Eur. Phys. J. C* **79** (2019) 135, arXiv: [1807.09477](https://arxiv.org/abs/1807.09477) [[hep-ex](https://arxiv.org/archive/hep)].
- [107] ATLAS Collaboration, *Performance of missing transverse momentum reconstruction with the ATLAS detector using proton–proton collisions at $\sqrt{s} = 13$ TeV*, *Eur. Phys. J. C* **78** (2018) 903, arXiv: [1802.08168](https://arxiv.org/abs/1802.08168) [[hep-ex](https://arxiv.org/archive/hep)].
- [108] ATLAS Collaboration, *Performance of pile-up mitigation techniques for jets in pp collisions at $\sqrt{s} = 8$ TeV using the ATLAS detector*, *Eur. Phys. J. C* **76** (2016) 581, arXiv: [1510.03823](https://arxiv.org/abs/1510.03823) [[hep-ex](https://arxiv.org/archive/hep)].
- [109] ATLAS Collaboration, *Measurement of the Inelastic Proton–Proton Cross Section at $\sqrt{s} = 13$ TeV with the ATLAS Detector at the LHC*, *Phys. Rev. Lett.* **117** (2016) 182002, arXiv: [1606.02625](https://arxiv.org/abs/1606.02625) [[hep-ex](https://arxiv.org/archive/hep)].
- [110] ATLAS Collaboration, *Luminosity determination in pp collisions at $\sqrt{s} = 13$ TeV using the ATLAS detector at the LHC*, ATLAS-CONF-2019-021, 2019, URL: <https://cds.cern.ch/record/2677054>.
- [111] G. Avoni et al., *The new LUCID-2 detector for luminosity measurement and monitoring in ATLAS*, *JINST* **13** (2018) P07017.
- [112] S. Frixione, E. Laenen, P. Motylinski, C. White, and B. R. Webber, *Single-top hadroproduction in association with a W boson*, *JHEP* **07** (2008) 029, arXiv: [0805.3067](https://arxiv.org/abs/0805.3067) [[hep-ph](https://arxiv.org/archive/hep)].
- [113] R. D. Cousins, J. T. Linnemann, and J. Tucker, *Evaluation of three methods for calculating statistical significance when incorporating a systematic uncertainty into a test of the background-only hypothesis for a Poisson process*, *Nucl. Instrum. Meth. A* **595** (2008) 480, arXiv: [physics/0702156](https://arxiv.org/abs/physics/0702156) [[physics.data-an](https://arxiv.org/archive/physics)].
- [114] G. Cowan, K. Cranmer, E. Gross, and O. Vitells, *Asymptotic formulae for likelihood-based tests of new physics*, *Eur. Phys. J. C* **71** (2011) 1554, arXiv: [1007.1727](https://arxiv.org/abs/1007.1727) [[physics.data-an](https://arxiv.org/archive/physics)], Erratum: *Eur. Phys. J. C* **73** (2013) 2501.
- [115] A. L. Read, *Presentation of search results: the CL_s technique*, *J. Phys. G* **28** (2002) 2693.
- [116] M. Baak et al., *HistFitter software framework for statistical data analysis*, *Eur. Phys. J. C* **75** (2015) 153, arXiv: [1410.1280](https://arxiv.org/abs/1410.1280) [[hep-ex](https://arxiv.org/archive/hep)].
- [117] L. Heinrich, M. Feickert, and G. Stark, *pyhf: v0.7.6*, version 0.7.6, <https://github.com/scikit-hep/pyhf/releases/tag/v0.7.6>, URL: <https://doi.org/10.5281/zenodo.1169739>.

- [118] L. Heinrich, M. Feickert, G. Stark, and K. Cranmer, *pyhf: pure-Python implementation of HistFactory statistical models*, *Journal of Open Source Software* **6** (2021) 2823, URL: <https://doi.org/10.21105/joss.02823>.
- [119] ATLAS Collaboration, *ATLAS Computing Acknowledgements*, ATL-SOFT-PUB-2023-001, 2023, URL: <https://cds.cern.ch/record/2869272>.

The ATLAS Collaboration

G. Aad ¹⁰², B. Abbott ¹²⁰, K. Abeling ⁵⁵, N.J. Abicht ⁴⁹, S.H. Abidi ²⁹, A. Abouhorma ^{35e}, H. Abramowicz ¹⁵¹, H. Abreu ¹⁵⁰, Y. Abulaiti ¹¹⁷, B.S. Acharya ^{69a,69b,m}, C. Adam Bourdarios ⁴, L. Adamczyk ^{86a}, S.V. Addepalli ²⁶, M.J. Addison ¹⁰¹, J. Adelman ¹¹⁵, A. Adiguzel ^{21c}, T. Adye ¹³⁴, A.A. Affolder ¹³⁶, Y. Afik ³⁶, M.N. Agaras ¹³, J. Agarwala ^{73a,73b}, A. Aggarwal ¹⁰⁰, C. Agheorghiesei ^{27c}, A. Ahmad ³⁶, F. Ahmadov ^{38,y}, W.S. Ahmed ¹⁰⁴, S. Ahuja ⁹⁵, X. Ai ^{62a}, G. Aielli ^{76a,76b}, A. Aikot ¹⁶³, M. Ait Tamlihat ^{35e}, B. Aitbenchikh ^{35a}, I. Aizenberg ¹⁶⁹, M. Akbiyik ¹⁰⁰, T.P.A. Åkesson ⁹⁸, A.V. Akimov ³⁷, D. Akiyama ¹⁶⁸, N.N. Akolkar ²⁴, S. Aktas ^{21a}, K. Al Houry ⁴¹, G.L. Alberghi ^{23b}, J. Albert ¹⁶⁵, P. Albicocco ⁵³, G.L. Albouy ⁶⁰, S. Alderweireldt ⁵², Z.L. Alegria ¹²¹, M. Aleksa ³⁶, I.N. Aleksandrov ³⁸, C. Alexa ^{27b}, T. Alexopoulos ¹⁰, F. Alfonsi ^{23b}, M. Algren ⁵⁶, M. Alhroob ¹²⁰, B. Ali ¹³², H.M.J. Ali ⁹¹, S. Ali ¹⁴⁸, S.W. Alibocus ⁹², M. Aliev ¹⁴⁵, G. Alimonti ^{71a}, W. Alkakhki ⁵⁵, C. Allaire ⁶⁶, B.M.M. Allbrooke ¹⁴⁶, J.F. Allen ⁵², C.A. Allendes Flores ^{137f}, P.P. Allport ²⁰, A. Aloisio ^{72a,72b}, F. Alonso ⁹⁰, C. Alpigiani ¹³⁸, M. Alvarez Estevez ⁹⁹, A. Alvarez Fernandez ¹⁰⁰, M. Alves Cardoso ⁵⁶, M.G. Alviggi ^{72a,72b}, M. Aly ¹⁰¹, Y. Amaral Coutinho ^{83b}, A. Ambler ¹⁰⁴, C. Amelung ³⁶, M. Amerl ¹⁰¹, C.G. Ames ¹⁰⁹, D. Amidei ¹⁰⁶, S.P. Amor Dos Santos ^{130a}, K.R. Amos ¹⁶³, V. Ananiev ¹²⁵, C. Anastopoulos ¹³⁹, T. Andeen ¹¹, J.K. Anders ³⁶, S.Y. Andreev ^{47a,47b}, A. Andreatta ^{71a,71b}, S. Angelidakis ⁹, A. Angerami ^{41,ab}, A.V. Anisenkov ³⁷, A. Annovi ^{74a}, C. Antel ⁵⁶, M.T. Anthony ¹³⁹, E. Antipov ¹⁴⁵, M. Antonelli ⁵³, F. Anulli ^{75a}, M. Aoki ⁸⁴, T. Aoki ¹⁵³, J.A. Aparisi Pozo ¹⁶³, M.A. Aparo ¹⁴⁶, L. Aperio Bella ⁴⁸, C. Appelt ¹⁸, A. Apyan ²⁶, N. Aranzabal ³⁶, S.J. Arbiol Val ⁸⁷, C. Arcangeletti ⁵³, A.T.H. Arce ⁵¹, E. Arena ⁹², J-F. Arguin ¹⁰⁸, S. Argyropoulos ⁵⁴, J.-H. Arling ⁴⁸, O. Arnaez ⁴, H. Arnold ¹¹⁴, G. Artoni ^{75a,75b}, H. Asada ¹¹¹, K. Asai ¹¹⁸, S. Asai ¹⁵³, N.A. Asbah ⁶¹, K. Assamagan ²⁹, R. Astalos ^{28a}, S. Atashi ¹⁶⁰, R.J. Atkin ^{33a}, M. Atkinson ¹⁶², H. Atmani ^{35f}, P.A. Atlasiddha ¹²⁸, K. Augsten ¹³², S. Auricchio ^{72a,72b}, A.D. Auriol ²⁰, V.A. Austrup ¹⁰¹, G. Avolio ³⁶, K. Axiotis ⁵⁶, G. Azuelos ^{108,af}, D. Babal ^{28b}, H. Bachacou ¹³⁵, K. Bachas ^{152,p}, A. Bachi ³⁴, F. Backman ^{47a,47b}, A. Badea ⁶¹, T.M. Baer ¹⁰⁶, P. Bagnaia ^{75a,75b}, M. Bahmani ¹⁸, D. Bahner ⁵⁴, A.J. Bailey ¹⁶³, V.R. Bailey ¹⁶², J.T. Baines ¹³⁴, L. Baines ⁹⁴, O.K. Baker ¹⁷², E. Bakos ¹⁵, D. Bakshi Gupta ⁸, V. Balakrishnan ¹²⁰, R. Balasubramanian ¹¹⁴, E.M. Baldin ³⁷, P. Balek ^{86a}, E. Ballabene ^{23b,23a}, F. Balli ¹³⁵, L.M. Baltes ^{63a}, W.K. Balunas ³², J. Balz ¹⁰⁰, E. Banas ⁸⁷, M. Bandieramonte ¹²⁹, A. Bandyopadhyay ²⁴, S. Bansal ²⁴, L. Barak ¹⁵¹, M. Barakat ⁴⁸, E.L. Barberio ¹⁰⁵, D. Barberis ^{57b,57a}, M. Barbero ¹⁰², M.Z. Barel ¹¹⁴, K.N. Barends ^{33a}, T. Barillari ¹¹⁰, M-S. Barisits ³⁶, T. Barklow ¹⁴³, P. Baron ¹²², D.A. Baron Moreno ¹⁰¹, A. Baroncelli ^{62a}, G. Barone ²⁹, A.J. Barr ¹²⁶, J.D. Barr ⁹⁶, L. Barranco Navarro ^{47a,47b}, F. Barreiro ⁹⁹, J. Barreiro Guimarães da Costa ^{14a}, U. Barron ¹⁵¹, M.G. Barros Teixeira ^{130a}, S. Barsov ³⁷, F. Bartels ^{63a}, R. Bartoldus ¹⁴³, A.E. Barton ⁹¹, P. Bartos ^{28a}, A. Basan ¹⁰⁰, M. Baselga ⁴⁹, A. Bassalat ^{66,b}, M.J. Basso ^{156a}, C.R. Basson ¹⁰¹, R.L. Bates ⁵⁹, S. Batlamous ^{35e}, J.R. Batley ³², B. Batool ¹⁴¹, M. Battaglia ¹³⁶, D. Battulga ¹⁸, M. Baunce ^{75a,75b}, M. Bauer ³⁶, P. Bauer ²⁴, L.T. Bazzano Hurrell ³⁰, J.B. Beacham ⁵¹, T. Beau ¹²⁷, J.Y. Beauchamp ⁹⁰, P.H. Beauchemin ¹⁵⁸, F. Becherer ⁵⁴, P. Bechtel ²⁴, H.P. Beck ^{19,o}, K. Becker ¹⁶⁷, A.J. Beddall ⁸², V.A. Bednyakov ³⁸, C.P. Bee ¹⁴⁵, L.J. Beamster ¹⁵, T.A. Beermann ³⁶, M. Begalli ^{83d}, M. Begel ²⁹, A. Behera ¹⁴⁵, J.K. Behr ⁴⁸, J.F. Beirer ³⁶, F. Beisiegel ²⁴, M. Belfkir ¹⁵⁹, G. Bella ¹⁵¹, L. Bellagamba ^{23b}, A. Bellerive ³⁴, P. Bellos ²⁰, K. Beloborodov ³⁷, D. Bencheikroun ^{35a}, F. Bendebba ^{35a}, Y. Benhammou ¹⁵¹, M. Benoit ²⁹, J.R. Bensinger ²⁶, S. Bentvelsen ¹¹⁴, L. Beresford ⁴⁸,

M. Beretta ⁵³, E. Bergeaas Kuutmann ¹⁶¹, N. Berger ⁴, B. Bergmann ¹³², J. Beringer ^{17a},
G. Bernardi ⁵, C. Bernius ¹⁴³, F.U. Bernlochner ²⁴, F. Bernon ^{36,102}, A. Berrocal Guardia ¹³,
T. Berry ⁹⁵, P. Berta ¹³³, A. Berthold ⁵⁰, I.A. Bertram ⁹¹, S. Bethke ¹¹⁰, A. Betti ^{75a,75b},
A.J. Bevan ⁹⁴, N.K. Bhalla ⁵⁴, M. Bhamjee ^{33c}, S. Bhatta ¹⁴⁵, D.S. Bhattacharya ¹⁶⁶,
P. Bhattarai ¹⁴³, V.S. Bhopatkar ¹²¹, R. Bi ^{29,ai}, R.M. Bianchi ¹²⁹, G. Bianco ^{23b,23a}, O. Biebel ¹⁰⁹,
R. Bielski ¹²³, M. Biglietti ^{77a}, M. Bindi ⁵⁵, A. Bingul ^{21b}, C. Bini ^{75a,75b}, A. Biondini ⁹²,
C.J. Birch-sykes ¹⁰¹, G.A. Bird ^{20,134}, M. Birman ¹⁶⁹, M. Biros ¹³³, S. Biryukov ¹⁴⁶,
T. Bisanz ⁴⁹, E. Bisceglie ^{43b,43a}, J.P. Biswal ¹³⁴, D. Biswas ¹⁴¹, A. Bitadze ¹⁰¹, K. Bjørke ¹²⁵,
I. Bloch ⁴⁸, A. Blue ⁵⁹, U. Blumenschein ⁹⁴, J. Blumenthal ¹⁰⁰, G.J. Bobbink ¹¹⁴,
V.S. Bobrovnikov ³⁷, M. Boehler ⁵⁴, B. Boehm ¹⁶⁶, D. Bogavac ³⁶, A.G. Bogdanchikov ³⁷,
C. Bohm ^{47a}, V. Boisvert ⁹⁵, P. Bokan ⁴⁸, T. Bold ^{86a}, M. Bomben ⁵, M. Bona ⁹⁴,
M. Boonekamp ¹³⁵, C.D. Booth ⁹⁵, A.G. Borbély ⁵⁹, I.S. Bordulev ³⁷, H.M. Borecka-Bielska ¹⁰⁸,
G. Borissov ⁹¹, D. Bortoletto ¹²⁶, D. Boscherini ^{23b}, M. Bosman ¹³, J.D. Bossio Sola ³⁶,
K. Bouaouda ^{35a}, N. Bouchhar ¹⁶³, J. Boudreau ¹²⁹, E.V. Bouhova-Thacker ⁹¹, D. Boumediene ⁴⁰,
R. Bouquet ¹⁶⁵, A. Boveia ¹¹⁹, J. Boyd ³⁶, D. Boye ²⁹, I.R. Boyko ³⁸, J. Bracinik ²⁰,
N. Brahimy ^{62d}, G. Brandt ¹⁷¹, O. Brandt ³², F. Braren ⁴⁸, B. Brau ¹⁰³, J.E. Brau ¹²³,
R. Brenner ¹⁶⁹, L. Brenner ¹¹⁴, R. Brenner ¹⁶¹, S. Bressler ¹⁶⁹, D. Britton ⁵⁹, D. Britzger ¹¹⁰,
I. Brock ²⁴, G. Brooijmans ⁴¹, W.K. Brooks ^{137f}, E. Brost ²⁹, L.M. Brown ¹⁶⁵, L.E. Bruce ⁶¹,
T.L. Bruckler ¹²⁶, P.A. Bruckman de Renstrom ⁸⁷, B. Brüers ⁴⁸, A. Bruni ^{23b}, G. Bruni ^{23b},
M. Bruschi ^{23b}, N. Bruscinò ^{75a,75b}, T. Buanes ¹⁶, Q. Buat ¹³⁸, D. Buchin ¹¹⁰, A.G. Buckley ⁵⁹,
O. Bulekov ³⁷, B.A. Bullard ¹⁴³, S. Burdin ⁹², C.D. Burgard ⁴⁹, A.M. Burger ⁴⁰,
B. Burghgrave ⁸, O. Burlayenko ⁵⁴, J.T.P. Burr ³², C.D. Burton ¹¹, J.C. Burzynski ¹⁴²,
E.L. Busch ⁴¹, V. Büscher ¹⁰⁰, P.J. Bussey ⁵⁹, J.M. Butler ²⁵, C.M. Buttar ⁵⁹,
J.M. Butterworth ⁹⁶, W. Buttinger ¹³⁴, C.J. Buxo Vazquez ¹⁰⁷, A.R. Buzykaev ³⁷,
S. Cabrera Urbán ¹⁶³, L. Cadamuro ⁶⁶, D. Caforio ⁵⁸, H. Cai ¹²⁹, Y. Cai ^{14a,14e}, Y. Cai ^{14c},
V.M.M. Cairo ³⁶, O. Cakir ^{3a}, N. Calace ³⁶, P. Calafiura ^{17a}, G. Calderini ¹²⁷, P. Calfayan ⁶⁸,
G. Callea ⁵⁹, L.P. Caloba ^{83b}, D. Calvet ⁴⁰, S. Calvet ⁴⁰, T.P. Calvet ¹⁰², M. Calvetti ^{74a,74b},
R. Camacho Toro ¹²⁷, S. Camarda ³⁶, D. Camarero Munoz ²⁶, P. Camarri ^{76a,76b},
M.T. Camerlingo ^{72a,72b}, D. Cameron ³⁶, C. Camincher ¹⁶⁵, M. Campanelli ⁹⁶, A. Camplani ⁴²,
V. Canale ^{72a,72b}, A. Canesse ¹⁰⁴, J. Cantero ¹⁶³, Y. Cao ¹⁶², F. Capocasa ²⁶, M. Capua ^{43b,43a},
A. Carbone ^{71a,71b}, R. Cardarelli ^{76a}, J.C.J. Cardenas ⁸, F. Cardillo ¹⁶³, G. Carducci ^{43b,43a},
T. Carli ³⁶, G. Carlino ^{72a}, J.I. Carlotto ¹³, B.T. Carlson ^{129,q}, E.M. Carlson ^{165,156a},
L. Carminati ^{71a,71b}, A. Carnelli ¹³⁵, M. Carnesale ^{75a,75b}, S. Caron ¹¹³, E. Carquin ^{137f},
S. Carrá ^{71a}, G. Carratta ^{23b,23a}, F. Carrio Argos ^{33g}, J.W.S. Carter ¹⁵⁵, T.M. Carter ⁵²,
M.P. Casado ^{13,i}, M. Caspar ⁴⁸, F.L. Castillo ⁴, L. Castillo Garcia ¹³, V. Castillo Gimenez ¹⁶³,
N.F. Castro ^{130a,130e}, A. Catinaccio ³⁶, J.R. Catmore ¹²⁵, V. Cavaliere ²⁹, N. Cavalli ^{23b,23a},
V. Cavasinni ^{74a,74b}, Y.C. Cekmecelioglu ⁴⁸, E. Celebi ^{21a}, F. Celli ¹²⁶, M.S. Centonze ^{70a,70b},
V. Cepaitis ⁵⁶, K. Cerny ¹²², A.S. Cerqueira ^{83a}, A. Cerri ¹⁴⁶, L. Cerrito ^{76a,76b}, F. Cerutti ^{17a},
B. Cervato ¹⁴¹, A. Cervelli ^{23b}, G. Cesarini ⁵³, S.A. Cetin ⁸², D. Chakraborty ¹¹⁵, J. Chan ¹⁷⁰,
W.Y. Chan ¹⁵³, J.D. Chapman ³², E. Chapon ¹³⁵, B. Chargeishvili ^{149b}, D.G. Charlton ²⁰,
M. Chatterjee ¹⁹, C. Chauhan ¹³³, S. Chekanov ⁶, S.V. Chekulaev ^{156a}, G.A. Chelkov ^{38,a},
A. Chen ¹⁰⁶, B. Chen ¹⁵¹, B. Chen ¹⁶⁵, H. Chen ^{14c}, H. Chen ²⁹, J. Chen ^{62c}, J. Chen ¹⁴²,
M. Chen ¹²⁶, S. Chen ¹⁵³, S.J. Chen ^{14c}, X. Chen ^{62c,135}, X. Chen ^{14b,ae}, Y. Chen ^{62a},
C.L. Cheng ¹⁷⁰, H.C. Cheng ^{64a}, S. Cheong ¹⁴³, A. Cheplakov ³⁸, E. Cheremushkina ⁴⁸,
E. Cherepanova ¹¹⁴, R. Cherkaoui El Moursli ^{35e}, E. Cheu ⁷, K. Cheung ⁶⁵, L. Chevalier ¹³⁵,
V. Chiarella ⁵³, G. Chiarelli ^{74a}, N. Chiedde ¹⁰², G. Chiodini ^{70a}, A.S. Chisholm ²⁰,
A. Chitan ^{27b}, M. Chitishvili ¹⁶³, M.V. Chizhov ³⁸, K. Choi ¹¹, A.R. Chomont ^{75a,75b},

Y. Chou [id](#)¹⁰³, E.Y.S. Chow [id](#)¹¹³, T. Chowdhury [id](#)^{33g}, K.L. Chu [id](#)¹⁶⁹, M.C. Chu [id](#)^{64a}, X. Chu [id](#)^{14a,14e},
 J. Chudoba [id](#)¹³¹, J.J. Chwastowski [id](#)⁸⁷, D. Cieri [id](#)¹¹⁰, K.M. Ciesla [id](#)^{86a}, V. Cindro [id](#)⁹³, A. Ciocio [id](#)^{17a},
 F. Cirotto [id](#)^{72a,72b}, Z.H. Citron [id](#)^{169,k}, M. Citterio [id](#)^{71a}, D.A. Ciubotaru^{27b}, A. Clark [id](#)⁵⁶, P.J. Clark [id](#)⁵²,
 C. Clarry [id](#)¹⁵⁵, J.M. Clavijo Columbie [id](#)⁴⁸, S.E. Clawson [id](#)⁴⁸, C. Clement [id](#)^{47a,47b}, J. Clercx [id](#)⁴⁸,
 Y. Coadou [id](#)¹⁰², M. Cobal [id](#)^{69a,69c}, A. Coccaro [id](#)^{57b}, R.F. Coelho Barrue [id](#)^{130a},
 R. Coelho Lopes De Sa [id](#)¹⁰³, S. Coelli [id](#)^{71a}, A.E.C. Coimbra [id](#)^{71a,71b}, B. Cole [id](#)⁴¹, J. Collot [id](#)⁶⁰,
 P. Conde Muiño [id](#)^{130a,130g}, M.P. Connell [id](#)^{33c}, S.H. Connell [id](#)^{33c}, I.A. Connelly [id](#)⁵⁹, E.I. Conroy [id](#)¹²⁶,
 F. Conventi [id](#)^{72a,ag}, H.G. Cooke [id](#)²⁰, A.M. Cooper-Sarkar [id](#)¹²⁶, A. Cordeiro Oudot Choi [id](#)¹²⁷,
 L.D. Corpe [id](#)⁴⁰, M. Corradi [id](#)^{75a,75b}, F. Corriveau [id](#)^{104,w}, A. Cortes-Gonzalez [id](#)¹⁸, M.J. Costa [id](#)¹⁶³,
 F. Costanza [id](#)⁴, D. Costanzo [id](#)¹³⁹, B.M. Cote [id](#)¹¹⁹, G. Cowan [id](#)⁹⁵, K. Cranmer [id](#)¹⁷⁰,
 D. Cremonini [id](#)^{23b,23a}, S. Crépe-Renaudin [id](#)⁶⁰, F. Crescioli [id](#)¹²⁷, M. Cristinziani [id](#)¹⁴¹,
 M. Cristoforetti [id](#)^{78a,78b}, V. Croft [id](#)¹¹⁴, J.E. Crosby [id](#)¹²¹, G. Crosetti [id](#)^{43b,43a}, A. Cueto [id](#)⁹⁹,
 T. Cuhadar Donszelmann [id](#)¹⁶⁰, H. Cui [id](#)^{14a,14e}, Z. Cui [id](#)⁷, W.R. Cunningham [id](#)⁵⁹, F. Curcio [id](#)^{43b,43a},
 P. Czodrowski [id](#)³⁶, M.M. Czurylo [id](#)^{63b}, M.J. Da Cunha Sargedas De Sousa [id](#)^{57b,57a},
 J.V. Da Fonseca Pinto [id](#)^{83b}, C. Da Via [id](#)¹⁰¹, W. Dabrowski [id](#)^{86a}, T. Dado [id](#)⁴⁹, S. Dahbi [id](#)^{33g},
 T. Dai [id](#)¹⁰⁶, D. Dal Santo [id](#)¹⁹, C. Dallapiccola [id](#)¹⁰³, M. Dam [id](#)⁴², G. D'amen [id](#)²⁹, V. D'Amico [id](#)¹⁰⁹,
 J. Damp [id](#)¹⁰⁰, J.R. Dandoy [id](#)³⁴, M.F. Daneri [id](#)³⁰, M. Danninger [id](#)¹⁴², V. Dao [id](#)³⁶, G. Darbo [id](#)^{57b},
 S. Darmora [id](#)⁶, S.J. Das [id](#)^{29,ai}, S. D'Auria [id](#)^{71a,71b}, C. David [id](#)^{156b}, T. Davidek [id](#)¹³³,
 B. Davis-Purcell [id](#)³⁴, I. Dawson [id](#)⁹⁴, H.A. Day-hall [id](#)¹³², K. De [id](#)⁸, R. De Asmundis [id](#)^{72a},
 N. De Biase [id](#)⁴⁸, S. De Castro [id](#)^{23b,23a}, N. De Groot [id](#)¹¹³, P. de Jong [id](#)¹¹⁴, H. De la Torre [id](#)¹¹⁵,
 A. De Maria [id](#)^{14c}, A. De Salvo [id](#)^{75a}, U. De Sanctis [id](#)^{76a,76b}, F. De Santis [id](#)^{70a,70b}, A. De Santo [id](#)¹⁴⁶,
 J.B. De Vivie De Regie [id](#)⁶⁰, D.V. Dedovich³⁸, J. Degens [id](#)¹¹⁴, A.M. Deiana [id](#)⁴⁴, F. Del Corso [id](#)^{23b,23a},
 J. Del Peso [id](#)⁹⁹, F. Del Rio [id](#)^{63a}, L. Delagrangé [id](#)¹²⁷, F. Deliot [id](#)¹³⁵, C.M. Delitzsch [id](#)⁴⁹,
 M. Della Pietra [id](#)^{72a,72b}, D. Della Volpe [id](#)⁵⁶, A. Dell'Acqua [id](#)³⁶, L. Dell'Asta [id](#)^{71a,71b}, M. Delmastro [id](#)⁴,
 P.A. Delsart [id](#)⁶⁰, S. Demers [id](#)¹⁷², M. Demichev [id](#)³⁸, S.P. Denisov [id](#)³⁷, L. D'Eramo [id](#)⁴⁰,
 D. Derendarz [id](#)⁸⁷, F. Derue [id](#)¹²⁷, P. Dervan [id](#)⁹², K. Desch [id](#)²⁴, C. Deutsch [id](#)²⁴, F.A. Di Bello [id](#)^{57b,57a},
 A. Di Ciaccio [id](#)^{76a,76b}, L. Di Ciaccio [id](#)⁴, A. Di Domenico [id](#)^{75a,75b}, C. Di Donato [id](#)^{72a,72b},
 A. Di Girolamo [id](#)³⁶, G. Di Gregorio [id](#)³⁶, A. Di Luca [id](#)^{78a,78b}, B. Di Micco [id](#)^{77a,77b}, R. Di Nardo [id](#)^{77a,77b},
 C. Diaconu [id](#)¹⁰², M. Diamantopoulou [id](#)³⁴, F.A. Dias [id](#)¹¹⁴, T. Dias Do Vale [id](#)¹⁴², M.A. Diaz [id](#)^{137a,137b},
 F.G. Diaz Capriles [id](#)²⁴, M. Didenko [id](#)¹⁶³, E.B. Diehl [id](#)¹⁰⁶, L. Diehl [id](#)⁵⁴, S. Díez Cornell [id](#)⁴⁸,
 C. Díez Pardos [id](#)¹⁴¹, C. Dimitriadi [id](#)^{161,24}, A. Dimitrievska [id](#)^{17a}, J. Dingfelder [id](#)²⁴, I-M. Dinu [id](#)^{27b},
 S.J. Dittmeier [id](#)^{63b}, F. Dittus [id](#)³⁶, F. Djama [id](#)¹⁰², T. Djobava [id](#)^{149b}, J.I. Djuvslund [id](#)¹⁶,
 C. Doglioni [id](#)^{101,98}, A. Dohnalova [id](#)^{28a}, J. Dolejsi [id](#)¹³³, Z. Dolezal [id](#)¹³³, K.M. Dona [id](#)³⁹,
 M. Donadelli [id](#)^{83c}, B. Dong [id](#)¹⁰⁷, J. Donini [id](#)⁴⁰, A. D'Onofrio [id](#)^{72a,72b}, M. D'Onofrio [id](#)⁹²,
 J. Dopke [id](#)¹³⁴, A. Doria [id](#)^{72a}, N. Dos Santos Fernandes [id](#)^{130a}, P. Dougan [id](#)¹⁰¹, M.T. Dova [id](#)⁹⁰,
 A.T. Doyle [id](#)⁵⁹, M.A. Draguet [id](#)¹²⁶, E. Dreyer [id](#)¹⁶⁹, I. Drivas-koulouris [id](#)¹⁰, M. Drnevich [id](#)¹¹⁷,
 A.S. Drobac [id](#)¹⁵⁸, M. Drozdova [id](#)⁵⁶, D. Du [id](#)^{62a}, T.A. du Pree [id](#)¹¹⁴, F. Dubinin [id](#)³⁷, M. Dubovsky [id](#)^{28a},
 E. Duchovni [id](#)¹⁶⁹, G. Duckeck [id](#)¹⁰⁹, O.A. Ducu [id](#)^{27b}, D. Duda [id](#)⁵², A. Dudarev [id](#)³⁶, E.R. Duden [id](#)²⁶,
 M. D'uffizi [id](#)¹⁰¹, L. Duflo [id](#)⁶⁶, M. Dührssen [id](#)³⁶, C. Dülsen [id](#)¹⁷¹, A.E. Dumitriu [id](#)^{27b}, M. Dunford [id](#)^{63a},
 S. Dungs [id](#)⁴⁹, K. Dunne [id](#)^{47a,47b}, A. Duperrin [id](#)¹⁰², H. Duran Yildiz [id](#)^{3a}, M. Düren [id](#)⁵⁸,
 A. Durglishvili [id](#)^{149b}, B.L. Dwyer [id](#)¹¹⁵, G.I. Dyckes [id](#)^{17a}, M. Dyndal [id](#)^{86a}, B.S. Dziedzic [id](#)⁸⁷,
 Z.O. Earnshaw [id](#)¹⁴⁶, G.H. Eberwein [id](#)¹²⁶, B. Eckerova [id](#)^{28a}, S. Eggebrecht [id](#)⁵⁵,
 E. Egidio Purcino De Souza [id](#)¹²⁷, L.F. Ehrke [id](#)⁵⁶, G. Eigen [id](#)¹⁶, K. Einsweiler [id](#)^{17a}, T. Ekelof [id](#)¹⁶¹,
 P.A. Ekman [id](#)⁹⁸, S. El Farkh [id](#)^{35b}, Y. El Ghazali [id](#)^{35b}, H. El Jarrari [id](#)³⁶, A. El Moussaouy [id](#)¹⁰⁸,
 V. Ellajosyula [id](#)¹⁶¹, M. Ellert [id](#)¹⁶¹, F. Ellinghaus [id](#)¹⁷¹, N. Ellis [id](#)³⁶, J. Elmsheuser [id](#)²⁹, M. Elsing [id](#)³⁶,
 D. Emelianov [id](#)¹³⁴, Y. Enari [id](#)¹⁵³, I. Ene [id](#)^{17a}, S. Epari [id](#)¹³, J. Erdmann [id](#)⁴⁹, P.A. Erland [id](#)⁸⁷,
 M. Errenst [id](#)¹⁷¹, M. Escalier [id](#)⁶⁶, C. Escobar [id](#)¹⁶³, E. Etzion [id](#)¹⁵¹, G. Evans [id](#)^{130a}, H. Evans [id](#)⁶⁸,

L.S. Evans ⁹⁵, M.O. Evans ¹⁴⁶, A. Ezhilov ³⁷, S. Ezzarqtouni ^{35a}, F. Fabbri ⁵⁹, L. Fabbri ^{23b,23a},
 G. Facini ⁹⁶, V. Fadeyev ¹³⁶, R.M. Fakhrutdinov ³⁷, D. Fakoudis ¹⁰⁰, S. Falciano ^{75a},
 L.F. Falda Ulhoa Coelho ³⁶, P.J. Falke ²⁴, J. Faltova ¹³³, C. Fan ¹⁶², Y. Fan ^{14a}, Y. Fang ^{14a,14e},
 M. Fanti ^{71a,71b}, M. Faraj ^{69a,69b}, Z. Farazpay ⁹⁷, A. Farbin ⁸, A. Farilla ^{77a}, T. Farooque ¹⁰⁷,
 S.M. Farrington ⁵², F. Fassi ^{35e}, D. Fassouliotis ⁹, M. Faucci Giannelli ^{76a,76b}, W.J. Fawcett ³²,
 L. Fayard ⁶⁶, P. Federic ¹³³, P. Federicova ¹³¹, O.L. Fedin ^{37,a}, G. Fedotov ³⁷, M. Feickert ¹⁷⁰,
 L. Feligioni ¹⁰², D.E. Fellers ¹²³, C. Feng ^{62b}, M. Feng ^{14b}, Z. Feng ¹¹⁴, M.J. Fenton ¹⁶⁰,
 A.B. Fenyuk ³⁷, L. Ferencz ⁴⁸, R.A.M. Ferguson ⁹¹, S.I. Fernandez Luengo ^{137f},
 P. Fernandez Martinez ¹³, M.J.V. Fernoux ¹⁰², J. Ferrando ⁴⁸, A. Ferrari ¹⁶¹, P. Ferrari ^{114,113},
 R. Ferrari ^{73a}, D. Ferrere ⁵⁶, C. Ferretti ¹⁰⁶, F. Fiedler ¹⁰⁰, P. Fiedler ¹³², A. Filipčič ⁹³,
 E.K. Filmer ¹, F. Filthaut ¹¹³, M.C.N. Fiolhais ^{130a,130c,c}, L. Fiorini ¹⁶³, W.C. Fisher ¹⁰⁷,
 T. Fitschen ¹⁰¹, P.M. Fitzhugh ¹³⁵, I. Fleck ¹⁴¹, P. Fleischmann ¹⁰⁶, T. Flick ¹⁷¹, M. Flores ^{33d,ac},
 L.R. Flores Castillo ^{64a}, L. Flores Sanz De Acedo ³⁶, F.M. Follega ^{78a,78b}, N. Fomin ¹⁶,
 J.H. Foo ¹⁵⁵, B.C. Forland ⁶⁸, A. Formica ¹³⁵, A.C. Forti ¹⁰¹, E. Fortin ³⁶, A.W. Fortman ⁶¹,
 M.G. Foti ^{17a}, L. Fountas ^{9,j}, D. Fournier ⁶⁶, H. Fox ⁹¹, P. Francavilla ^{74a,74b}, S. Francescato ⁶¹,
 S. Franchellucci ⁵⁶, M. Franchini ^{23b,23a}, S. Franchino ^{63a}, D. Francis ³⁶, L. Franco ¹¹³,
 V. Franco Lima ³⁶, L. Franconi ⁴⁸, M. Franklin ⁶¹, G. Frattari ²⁶, A.C. Freegard ⁹⁴,
 W.S. Freund ^{83b}, Y.Y. Frid ¹⁵¹, J. Friend ⁵⁹, N. Fritzsche ⁵⁰, A. Froch ⁵⁴, D. Froidevaux ³⁶,
 J.A. Frost ¹²⁶, Y. Fu ^{62a}, S. Fuenzalida Garrido ^{137f}, M. Fujimoto ¹⁰², K.Y. Fung ^{64a},
 E. Furtado De Simas Filho ^{83b}, M. Furukawa ¹⁵³, J. Fuster ¹⁶³, A. Gabrielli ^{23b,23a},
 A. Gabrielli ¹⁵⁵, P. Gadow ³⁶, G. Gagliardi ^{57b,57a}, L.G. Gagnon ^{17a}, E.J. Gallas ¹²⁶,
 B.J. Gallop ¹³⁴, K.K. Gan ¹¹⁹, S. Ganguly ¹⁵³, Y. Gao ⁵², F.M. Garay Walls ^{137a,137b}, B. Garcia ²⁹,
 C. García ¹⁶³, A. Garcia Alonso ¹¹⁴, A.G. Garcia Caffaro ¹⁷², J.E. García Navarro ¹⁶³,
 M. Garcia-Sciveres ^{17a}, G.L. Gardner ¹²⁸, R.W. Gardner ³⁹, N. Garelli ¹⁵⁸, D. Garg ⁸⁰,
 R.B. Garg ^{143,n}, J.M. Gargan ⁵², C.A. Garner ¹⁵⁵, C.M. Garvey ^{33a}, P. Gaspar ^{83b}, V.K. Gassmann ¹⁵⁸,
 G. Gaudio ^{73a}, V. Gautam ¹³, P. Gauzzi ^{75a,75b}, I.L. Gavrilenko ³⁷, A. Gavrilyuk ³⁷, C. Gay ¹⁶⁴,
 G. Gaycken ⁴⁸, E.N. Gazis ¹⁰, A.A. Geanta ^{27b}, C.M. Gee ¹³⁶, A. Gekow ¹¹⁹, C. Gemme ^{57b},
 M.H. Genest ⁶⁰, S. Gentile ^{75a,75b}, A.D. Gentry ¹¹², S. George ⁹⁵, W.F. George ²⁰, T. Geralis ⁴⁶,
 P. Gessinger-Befurt ³⁶, M.E. Geyik ¹⁷¹, M. Ghani ¹⁶⁷, M. Ghneimat ¹⁴¹, K. Ghorbanian ⁹⁴,
 A. Ghosal ¹⁴¹, A. Ghosh ¹⁶⁰, A. Ghosh ⁷, B. Giacobbe ^{23b}, S. Giagu ^{75a,75b}, T. Giani ¹¹⁴,
 P. Giannetti ^{74a}, A. Giannini ^{62a}, S.M. Gibson ⁹⁵, M. Gignac ¹³⁶, D.T. Gil ^{86b}, A.K. Gilbert ^{86a},
 B.J. Gilbert ⁴¹, D. Gillberg ³⁴, G. Gilles ¹¹⁴, N.E.K. Gillwald ⁴⁸, L. Ginabat ¹²⁷,
 D.M. Gingrich ^{2,af}, M.P. Giordani ^{69a,69c}, P.F. Giraud ¹³⁵, G. Giugliarelli ^{69a,69c}, D. Giugni ^{71a},
 F. Giuli ³⁶, I. Gkialas ^{9,j}, L.K. Gladilin ³⁷, C. Glasman ⁹⁹, G.R. Gledhill ¹²³, G. Glemža ⁴⁸,
 M. Glisic ¹²³, I. Gnesi ^{43b,f}, Y. Go ^{29,ai}, M. Goblirsch-Kolb ³⁶, B. Gocke ⁴⁹, D. Godin ¹⁰⁸,
 B. Gokturk ^{21a}, S. Goldfarb ¹⁰⁵, T. Golling ⁵⁶, M.G.D. Gololo ^{33g}, D. Golubkov ³⁷,
 J.P. Gombas ¹⁰⁷, A. Gomes ^{130a,130b}, G. Gomes Da Silva ¹⁴¹, A.J. Gomez Delegido ¹⁶³,
 R. Gonçalves ^{130a,130c}, G. Gonella ¹²³, L. Gonella ²⁰, A. Gongadze ^{149c}, F. Gonnella ²⁰,
 J.L. Gonski ⁴¹, R.Y. González Andana ⁵², S. González de la Hoz ¹⁶³, S. Gonzalez Fernandez ¹³,
 R. Gonzalez Lopez ⁹², C. Gonzalez Renteria ^{17a}, M.V. Gonzalez Rodrigues ⁴⁸,
 R. Gonzalez Suarez ¹⁶¹, S. Gonzalez-Sevilla ⁵⁶, G.R. Gonzalvo Rodriguez ¹⁶³, L. Goossens ³⁶,
 B. Gorini ³⁶, E. Gorini ^{70a,70b}, A. Gorišek ⁹³, T.C. Gosart ¹²⁸, A.T. Goshaw ⁵¹, M.I. Gostkin ³⁸,
 S. Goswami ¹²¹, C.A. Gottardo ³⁶, S.A. Gotz ¹⁰⁹, M. Gouighri ^{35b}, V. Goumarre ⁴⁸,
 A.G. Goussiou ¹³⁸, N. Govender ^{33c}, I. Grabowska-Bold ^{86a}, K. Graham ³⁴, E. Gramstad ¹²⁵,
 S. Grancagnolo ^{70a,70b}, M. Grandi ¹⁴⁶, C.M. Grant ^{1,135}, P.M. Gravila ^{27f}, F.G. Gravili ^{70a,70b},
 H.M. Gray ^{17a}, M. Greco ^{70a,70b}, C. Grefe ²⁴, I.M. Gregor ⁴⁸, P. Grenier ¹⁴³, S.G. Grewe ¹¹⁰,
 C. Grieco ¹³, A.A. Grillo ¹³⁶, K. Grimm ³¹, S. Grinstein ^{13,s}, J.-F. Grivaz ⁶⁶, E. Gross ¹⁶⁹,

J. Grosse-Knetter ⁵⁵, C. Grud ¹⁰⁶, J.C. Grundy ¹²⁶, L. Guan ¹⁰⁶, W. Guan ²⁹, C. Gubbels ¹⁶⁴,
 J.G.R. Guerrero Rojas ¹⁶³, G. Guerrieri ^{69a,69c}, F. Guescini ¹¹⁰, R. Gugel ¹⁰⁰, J.A.M. Guhit ¹⁰⁶,
 A. Guida ¹⁸, E. Guilloton ^{167,134}, S. Guindon ³⁶, F. Guo ^{14a,14e}, J. Guo ^{62c}, L. Guo ⁴⁸,
 Y. Guo ¹⁰⁶, R. Gupta ⁴⁸, R. Gupta ¹²⁹, S. Gurbuz ²⁴, S.S. Gurdasani ⁵⁴, G. Gustavino ³⁶,
 M. Guth ⁵⁶, P. Gutierrez ¹²⁰, L.F. Gutierrez Zagazeta ¹²⁸, M. Gutsche ⁵⁰, C. Gutschow ⁹⁶,
 C. Gwenlan ¹²⁶, C.B. Gwilliam ⁹², E.S. Haaland ¹²⁵, A. Haas ¹¹⁷, M. Habedank ⁴⁸,
 C. Haber ^{17a}, H.K. Hadavand ⁸, A. Hadeef ⁵⁰, S. Hadzic ¹¹⁰, A.I. Hagan ⁹¹, J.J. Hahn ¹⁴¹,
 E.H. Haines ⁹⁶, M. Haleem ¹⁶⁶, J. Haley ¹²¹, J.J. Hall ¹³⁹, G.D. Hallewell ¹⁰², L. Halser ¹⁹,
 K. Hamano ¹⁶⁵, M. Hamer ²⁴, G.N. Hamity ⁵², E.J. Hampshire ⁹⁵, J. Han ^{62b}, K. Han ^{62a},
 L. Han ^{14c}, L. Han ^{62a}, S. Han ^{17a}, Y.F. Han ¹⁵⁵, K. Hanagaki ⁸⁴, M. Hance ¹³⁶,
 D.A. Hangal ^{41,ab}, H. Hanif ¹⁴², M.D. Hank ¹²⁸, R. Hankache ¹⁰¹, J.B. Hansen ⁴²,
 J.D. Hansen ⁴², P.H. Hansen ⁴², K. Hara ¹⁵⁷, D. Harada ⁵⁶, T. Harenberg ¹⁷¹, S. Harkusha ³⁷,
 M.L. Harris ¹⁰³, Y.T. Harris ¹²⁶, J. Harrison ¹³, N.M. Harrison ¹¹⁹, P.F. Harrison ¹⁶⁷,
 N.M. Hartman ¹¹⁰, N.M. Hartmann ¹⁰⁹, Y. Hasegawa ¹⁴⁰, R. Hauser ¹⁰⁷, C.M. Hawkes ²⁰,
 R.J. Hawkings ³⁶, Y. Hayashi ¹⁵³, S. Hayashida ¹¹¹, D. Hayden ¹⁰⁷, C. Hayes ¹⁰⁶,
 R.L. Hayes ¹¹⁴, C.P. Hays ¹²⁶, J.M. Hays ⁹⁴, H.S. Hayward ⁹², F. He ^{62a}, M. He ^{14a,14e},
 Y. He ¹⁵⁴, Y. He ⁴⁸, N.B. Heatley ⁹⁴, V. Hedberg ⁹⁸, A.L. Heggelund ¹²⁵, N.D. Hehir ^{94,*},
 C. Heidegger ⁵⁴, K.K. Heidegger ⁵⁴, W.D. Heidorn ⁸¹, J. Heilman ³⁴, S. Heim ⁴⁸, T. Heim ^{17a},
 J.G. Heinlein ¹²⁸, J.J. Heinrich ¹²³, L. Heinrich ^{110,ad}, J. Hejbal ¹³¹, L. Helary ⁴⁸, A. Held ¹⁷⁰,
 S. Hellesund ¹⁶, C.M. Helling ¹⁶⁴, S. Hellman ^{47a,47b}, R.C.W. Henderson ⁹¹, L. Henkelmann ³²,
 A.M. Henriques Correia ³⁶, H. Herde ⁹⁸, Y. Hernández Jiménez ¹⁴⁵, L.M. Herrmann ²⁴,
 T. Herrmann ⁵⁰, G. Herten ⁵⁴, R. Hertenberger ¹⁰⁹, L. Hervas ³⁶, M.E. Hesping ¹⁰⁰,
 N.P. Hessey ^{156a}, H. Hibi ⁸⁵, E. Hill ¹⁵⁵, S.J. Hillier ²⁰, J.R. Hinds ¹⁰⁷, F. Hinterkeuser ²⁴,
 M. Hirose ¹²⁴, S. Hirose ¹⁵⁷, D. Hirschbuehl ¹⁷¹, T.G. Hitchings ¹⁰¹, B. Hiti ⁹³, J. Hobbs ¹⁴⁵,
 R. Hobincu ^{27e}, N. Hod ¹⁶⁹, M.C. Hodgkinson ¹³⁹, B.H. Hodgkinson ³², A. Hoecker ³⁶,
 D.D. Hofer ¹⁰⁶, J. Hofer ⁴⁸, T. Holm ²⁴, M. Holzbock ¹¹⁰, L.B.A.H. Hommels ³²,
 B.P. Honan ¹⁰¹, J. Hong ^{62c}, T.M. Hong ¹²⁹, B.H. Hooberman ¹⁶², W.H. Hopkins ⁶, Y. Horii ¹¹¹,
 S. Hou ¹⁴⁸, A.S. Howard ⁹³, J. Howarth ⁵⁹, J. Hoya ⁶, M. Hrabovsky ¹²², A. Hrynevich ⁴⁸,
 T. Hryn'ova ⁴, P.J. Hsu ⁶⁵, S.-C. Hsu ¹³⁸, Q. Hu ^{62a}, Y.F. Hu ^{14a,14e}, S. Huang ^{64b},
 X. Huang ^{14c}, X. Huang ^{14a,14e}, Y. Huang ¹³⁹, Y. Huang ^{14a}, Z. Huang ¹⁰¹, Z. Hubacek ¹³²,
 M. Huebner ²⁴, F. Huegging ²⁴, T.B. Huffman ¹²⁶, C.A. Hugli ⁴⁸, M. Huhtinen ³⁶,
 S.K. Huiberts ¹⁶, R. Hulsken ¹⁰⁴, N. Huseynov ¹², J. Huston ¹⁰⁷, J. Huth ⁶¹, R. Hyneman ¹⁴³,
 G. Iacobucci ⁵⁶, G. Iakovidis ²⁹, I. Ibragimov ¹⁴¹, L. Iconomidou-Fayard ⁶⁶, P. Iengo ^{72a,72b},
 R. Iguchi ¹⁵³, T. Iizawa ¹²⁶, Y. Ikegami ⁸⁴, N. Ilic ¹⁵⁵, H. Imam ^{35a}, M. Ince Lezki ⁵⁶,
 T. Ingebretsen Carlson ^{47a,47b}, G. Introzzi ^{73a,73b}, M. Iodice ^{77a}, V. Ippolito ^{75a,75b}, R.K. Irwin ⁹²,
 M. Ishino ¹⁵³, W. Islam ¹⁷⁰, C. Issever ^{18,48}, S. Istin ^{21a,ak}, H. Ito ¹⁶⁸, J.M. Iturbe Ponce ^{64a},
 R. Iuppa ^{78a,78b}, A. Ivina ¹⁶⁹, J.M. Izen ⁴⁵, V. Izzo ^{72a}, P. Jacka ^{131,132}, P. Jackson ¹,
 R.M. Jacobs ⁴⁸, B.P. Jaeger ¹⁴², C.S. Jagfeld ¹⁰⁹, G. Jain ^{156a}, P. Jain ⁵⁴, K. Jakobs ⁵⁴,
 T. Jakoubek ¹⁶⁹, J. Jamieson ⁵⁹, K.W. Janas ^{86a}, M. Javurkova ¹⁰³, F. Jeanneau ¹³⁵,
 L. Jeanty ¹²³, J. Jejelava ^{149a,z}, P. Jenni ^{54,g}, C.E. Jessiman ³⁴, S. Jézéquel ⁴, C. Jia ^{62b}, J. Jia ¹⁴⁵,
 X. Jia ⁶¹, X. Jia ^{14a,14e}, Z. Jia ^{14c}, S. Jiggins ⁴⁸, J. Jimenez Pena ¹³, S. Jin ^{14c}, A. Jinaru ^{27b},
 O. Jinnouchi ¹⁵⁴, P. Johansson ¹³⁹, K.A. Johns ⁷, J.W. Johnson ¹³⁶, D.M. Jones ³², E. Jones ⁴⁸,
 P. Jones ³², R.W.L. Jones ⁹¹, T.J. Jones ⁹², H.L. Joos ^{55,36}, R. Joshi ¹¹⁹, J. Jovicevic ¹⁵,
 X. Ju ^{17a}, J.J. Junggeburth ¹⁰³, T. Junkermann ^{63a}, A. Juste Rozas ^{13,s}, M.K. Juzek ⁸⁷,
 S. Kabana ^{137e}, A. Kaczmarska ⁸⁷, M. Kado ¹¹⁰, H. Kagan ¹¹⁹, M. Kagan ¹⁴³, A. Kahn ⁴¹,
 A. Kahn ¹²⁸, C. Kahra ¹⁰⁰, T. Kaji ¹⁵³, E. Kajomovitz ¹⁵⁰, N. Kakati ¹⁶⁹, I. Kalaitzidou ⁵⁴,
 C.W. Kalderon ²⁹, A. Kamenshchikov ¹⁵⁵, N.J. Kang ¹³⁶, D. Kar ^{33g}, K. Karava ¹²⁶,

M.J. Kareem [ID156b](#), E. Karentzos [ID54](#), I. Karkanias [ID152](#), O. Karkout [ID114](#), S.N. Karpov [ID38](#),
Z.M. Karpova [ID38](#), V. Kartvelishvili [ID91](#), A.N. Karyukhin [ID37](#), E. Kasimi [ID152](#), J. Katzy [ID48](#),
S. Kaur [ID34](#), K. Kawade [ID140](#), M.P. Kawale [ID120](#), C. Kawamoto [ID88](#), T. Kawamoto [ID62a](#), E.F. Kay [ID36](#),
F.I. Kaya [ID158](#), S. Kazakos [ID107](#), V.F. Kazanin [ID37](#), Y. Ke [ID145](#), J.M. Keaveney [ID33a](#), R. Keeler [ID165](#),
G.V. Kehris [ID61](#), J.S. Keller [ID34](#), A.S. Kelly [ID96](#), J.J. Kempster [ID146](#), K.E. Kennedy [ID41](#),
P.D. Kennedy [ID100](#), O. Kepka [ID131](#), B.P. Kerridge [ID167](#), S. Kersten [ID171](#), B.P. Kerševan [ID93](#),
S. Keshri [ID66](#), L. Keszeghova [ID28a](#), S. Ketabchi Haghighat [ID155](#), R.A. Khan [ID129](#), M. Khandoga [ID127](#),
A. Khanov [ID121](#), A.G. Kharlamov [ID37](#), T. Kharlamova [ID37](#), E.E. Khoda [ID138](#), M. Kholodenko [ID37](#),
T.J. Khoo [ID18](#), G. Khoraiuli [ID166](#), J. Khubua [ID149b](#), Y.A.R. Khwaira [ID66](#), A. Kilgallon [ID123](#),
D.W. Kim [ID47a,47b](#), Y.K. Kim [ID39](#), N. Kimura [ID96](#), M.K. Kingston [ID55](#), A. Kirchhoff [ID55](#), C. Kirfel [ID24](#),
F. Kirfel [ID24](#), J. Kirk [ID134](#), A.E. Kiryunin [ID110](#), C. Kitsaki [ID10](#), O. Kivernyk [ID24](#), M. Klassen [ID63a](#),
C. Klein [ID34](#), L. Klein [ID166](#), M.H. Klein [ID106](#), M. Klein [ID92](#), S.B. Klein [ID56](#), U. Klein [ID92](#),
P. Klimek [ID36](#), A. Klimentov [ID29](#), T. Klioutchnikova [ID36](#), P. Kluit [ID114](#), S. Kluth [ID110](#), E. Kneringer [ID79](#),
T.M. Knight [ID155](#), A. Knue [ID49](#), R. Kobayashi [ID88](#), D. Kobylanski [ID169](#), S.F. Koch [ID126](#),
M. Kocian [ID143](#), P. Kodyš [ID133](#), D.M. Koeck [ID123](#), P.T. Koenig [ID24](#), T. Koffas [ID34](#), O. Kolay [ID50](#),
I. Koletsou [ID4](#), T. Komarek [ID122](#), K. Köneke [ID54](#), A.X.Y. Kong [ID1](#), T. Kono [ID118](#), N. Konstantinidis [ID96](#),
P. Kontaxakis [ID56](#), B. Konya [ID98](#), R. Kopeliansky [ID68](#), S. Koperny [ID86a](#), K. Korcyl [ID87](#), K. Kordas [ID152,e](#),
G. Koren [ID151](#), A. Korn [ID96](#), S. Korn [ID55](#), I. Korolkov [ID13](#), N. Korotkova [ID37](#), B. Kortman [ID114](#),
O. Kortner [ID110](#), S. Kortner [ID110](#), W.H. Kostecka [ID115](#), V.V. Kostyukhin [ID141](#), A. Kotskechagia [ID135](#),
A. Kotwal [ID51](#), A. Koulouris [ID36](#), A. Kourkoumeli-Charalampidi [ID73a,73b](#), C. Kourkoumelis [ID9](#),
E. Kourlitis [ID110,ad](#), O. Kovanda [ID146](#), R. Kowalewski [ID165](#), W. Kozanecki [ID135](#), A.S. Kozhin [ID37](#),
V.A. Kramarenko [ID37](#), G. Kramberger [ID93](#), P. Kramer [ID100](#), M.W. Krasny [ID127](#), A. Krasznahorkay [ID36](#),
J.W. Kraus [ID171](#), J.A. Kremer [ID48](#), T. Kresse [ID50](#), J. Kretschmar [ID92](#), K. Kreul [ID18](#), P. Krieger [ID155](#),
S. Krishnamurthy [ID103](#), M. Krivos [ID133](#), K. Krizka [ID20](#), K. Kroeninger [ID49](#), H. Kroha [ID110](#), J. Kroll [ID131](#),
J. Kroll [ID128](#), K.S. Krowpman [ID107](#), U. Kruchonak [ID38](#), H. Krüger [ID24](#), N. Krumnack [ID81](#), M.C. Kruse [ID51](#),
O. Kuchinskaia [ID37](#), S. Kuday [ID3a](#), S. Kuehn [ID36](#), R. Kuesters [ID54](#), T. Kuhl [ID48](#), V. Kukhtin [ID38](#),
Y. Kulchitsky [ID37,a](#), S. Kuleshov [ID137d,137b](#), M. Kumar [ID33g](#), N. Kumari [ID48](#), P. Kumari [ID156b](#),
A. Kupco [ID131](#), T. Kupfer [ID49](#), A. Kupich [ID37](#), O. Kuprash [ID54](#), H. Kurashige [ID85](#), L.L. Kurchaninov [ID156a](#),
O. Kurdysh [ID66](#), Y.A. Kurochkin [ID37](#), A. Kurova [ID37](#), M. Kuze [ID154](#), A.K. Kvam [ID103](#), J. Kvitá [ID122](#),
T. Kwan [ID104](#), N.G. Kyriacou [ID106](#), L.A.O. Laatu [ID102](#), C. Lacasta [ID163](#), F. Lacava [ID75a,75b](#),
H. Lacker [ID18](#), D. Lacour [ID127](#), N.N. Lad [ID96](#), E. Ladygin [ID38](#), B. Laforge [ID127](#), T. Lagouri [ID137e](#),
F.Z. Lahbabi [ID35a](#), S. Lai [ID55](#), I.K. Lakomic [ID86a](#), N. Lalloue [ID60](#), J.E. Lambert [ID165](#), S. Lammers [ID68](#),
W. Lampl [ID7](#), C. Lampoudis [ID152,e](#), A.N. Lancaster [ID115](#), E. Lançon [ID29](#), U. Landgraf [ID54](#),
M.P.J. Landon [ID94](#), V.S. Lang [ID54](#), R.J. Langenberg [ID103](#), O.K.B. Langrekken [ID125](#), A.J. Lankford [ID160](#),
F. Lanni [ID36](#), K. Lantzs [ID24](#), A. Lanza [ID73a](#), A. Lapertosa [ID57b,57a](#), J.F. Laporte [ID135](#), T. Lari [ID71a](#),
F. Lasagni Manghi [ID23b](#), M. Lassnig [ID36](#), V. Latonova [ID131](#), A. Laudrain [ID100](#), A. Laurier [ID150](#),
S.D. Lawlor [ID139](#), Z. Lawrence [ID101](#), R. Lazaridou [ID167](#), M. Lazzaroni [ID71a,71b](#), B. Le [ID101](#),
E.M. Le Boulicaut [ID51](#), B. Leban [ID93](#), A. Lebedev [ID81](#), M. LeBlanc [ID101](#), F. Ledroit-Guillon [ID60](#),
A.C.A. Lee [ID96](#), S.C. Lee [ID148](#), S. Lee [ID47a,47b](#), T.F. Lee [ID92](#), L.L. Leeuw [ID33c](#), H.P. Lefebvre [ID95](#),
M. Lefebvre [ID165](#), C. Leggett [ID17a](#), G. Lehmann Miotto [ID36](#), M. Leigh [ID56](#), W.A. Leight [ID103](#),
W. Leinonen [ID113](#), A. Leisos [ID152,r](#), M.A.L. Leite [ID83c](#), C.E. Leitgeb [ID48](#), R. Leitner [ID133](#),
K.J.C. Leney [ID44](#), T. Lenz [ID24](#), S. Leone [ID74a](#), C. Leonidopoulos [ID52](#), A. Leopold [ID144](#), C. Leroy [ID108](#),
R. Les [ID107](#), C.G. Lester [ID32](#), M. Levchenko [ID37](#), J. Levêque [ID4](#), D. Levin [ID106](#), L.J. Levinson [ID169](#),
M.P. Lewicki [ID87](#), D.J. Lewis [ID4](#), A. Li [ID5](#), B. Li [ID62b](#), C. Li [ID62a](#), C-Q. Li [ID110](#), H. Li [ID62a](#), H. Li [ID62b](#),
H. Li [ID14c](#), H. Li [ID14b](#), H. Li [ID62b](#), J. Li [ID62c](#), K. Li [ID138](#), L. Li [ID62c](#), M. Li [ID14a,14e](#), Q.Y. Li [ID62a](#),
S. Li [ID14a,14e](#), S. Li [ID62d,62c,d](#), T. Li [ID5](#), X. Li [ID104](#), Z. Li [ID126](#), Z. Li [ID104](#), Z. Li [ID14a,14e](#), S. Liang [ID14a,14e](#),
Z. Liang [ID14a](#), M. Liberatore [ID135](#), B. Liberti [ID76a](#), K. Lie [ID64c](#), J. Lieber Marin [ID83b](#), H. Lien [ID68](#),

K. Lin ¹⁰⁷, R.E. Lindley ⁷, J.H. Lindon ², E. Lipeles ¹²⁸, A. Lipniacka ¹⁶, A. Lister ¹⁶⁴,
 J.D. Little ⁴, B. Liu ^{14a}, B.X. Liu ¹⁴², D. Liu ^{62d,62c}, J.B. Liu ^{62a}, J.K.K. Liu ³², K. Liu ^{62d,62c},
 M. Liu ^{62a}, M.Y. Liu ^{62a}, P. Liu ^{14a}, Q. Liu ^{62d,138,62c}, X. Liu ^{62a}, X. Liu ^{62b}, Y. Liu ^{14d,14e},
 Y.L. Liu ^{62b}, Y.W. Liu ^{62a}, J. Llorente Merino ¹⁴², S.L. Lloyd ⁹⁴, E.M. Lobodzinska ⁴⁸,
 P. Loch ⁷, T. Lohse ¹⁸, K. Lohwasser ¹³⁹, E. Loiacono ⁴⁸, M. Lokajicek ^{131,*}, J.D. Lomas ²⁰,
 J.D. Long ¹⁶², I. Longarini ¹⁶⁰, L. Longo ^{70a,70b}, R. Longo ¹⁶², I. Lopez Paz ⁶⁷,
 A. Lopez Solis ⁴⁸, N. Lorenzo Martinez ⁴, A.M. Lory ¹⁰⁹, G. Löschcke Centeno ¹⁴⁶, O. Loseva ³⁷,
 X. Lou ^{47a,47b}, X. Lou ^{14a,14e}, A. Lounis ⁶⁶, J. Love ⁶, P.A. Love ⁹¹, G. Lu ^{14a,14e}, M. Lu ⁸⁰,
 S. Lu ¹²⁸, Y.J. Lu ⁶⁵, H.J. Lubatti ¹³⁸, C. Luci ^{75a,75b}, F.L. Lucio Alves ^{14c}, A. Lucotte ⁶⁰,
 F. Luehring ⁶⁸, I. Luise ¹⁴⁵, O. Lukianchuk ⁶⁶, O. Lundberg ¹⁴⁴, B. Lund-Jensen ¹⁴⁴,
 N.A. Luongo ⁶, M.S. Lutz ¹⁵¹, A.B. Lux ²⁵, D. Lynn ²⁹, H. Lyons ⁹², R. Lysak ¹³¹, E. Lytken ⁹⁸,
 V. Lyubushkin ³⁸, T. Lyubushkina ³⁸, M.M. Lyukova ¹⁴⁵, H. Ma ²⁹, K. Ma ^{62a}, L.L. Ma ^{62b},
 W. Ma ^{62a}, Y. Ma ¹²¹, D.M. Mac Donell ¹⁶⁵, G. Maccarrone ⁵³, J.C. MacDonald ¹⁰⁰,
 P.C. Machado De Abreu Farias ^{83b}, R. Madar ⁴⁰, W.F. Mader ⁵⁰, T. Madula ⁹⁶, J. Maeda ⁸⁵,
 T. Maeno ²⁹, H. Maguire ¹³⁹, V. Maiboroda ¹³⁵, A. Maio ^{130a,130b,130d}, K. Maj ^{86a},
 O. Majersky ⁴⁸, S. Majewski ¹²³, N. Makovec ⁶⁶, V. Maksimovic ¹⁵, B. Malaescu ¹²⁷,
 Pa. Malecki ⁸⁷, V.P. Maleev ³⁷, F. Malek ⁶⁰, M. Mali ⁹³, D. Malito ⁹⁵, U. Mallik ⁸⁰,
 S. Maltezos ¹⁰, S. Malyukov ³⁸, J. Mamuzic ¹³, G. Mancini ⁵³, G. Manco ^{73a,73b}, J.P. Mandalia ⁹⁴,
 I. Mandić ⁹³, L. Manhaes de Andrade Filho ^{83a}, I.M. Maniatis ¹⁶⁹, J. Manjarres Ramos ^{102,aa},
 D.C. Mankad ¹⁶⁹, A. Mann ¹⁰⁹, B. Mansoulié ¹³⁵, S. Manzoni ³⁶, L. Mao ^{62c}, X. Mapekula ^{33c},
 A. Marantis ^{152,r}, G. Marchiori ⁵, M. Marcisovsky ¹³¹, C. Marcon ^{71a}, M. Marinescu ²⁰,
 S. Marium ⁴⁸, M. Marjanovic ¹²⁰, E.J. Marshall ⁹¹, Z. Marshall ^{17a}, S. Marti-Garcia ¹⁶³,
 T.A. Martin ¹⁶⁷, V.J. Martin ⁵², B. Martin dit Latour ¹⁶, L. Martinelli ^{75a,75b}, M. Martinez ^{13,s},
 P. Martinez Agullo ¹⁶³, V.I. Martinez Outschoorn ¹⁰³, P. Martinez Suarez ¹³, S. Martin-Haugh ¹³⁴,
 V.S. Martoiu ^{27b}, A.C. Martyniuk ⁹⁶, A. Marzin ³⁶, D. Mascione ^{78a,78b}, L. Masetti ¹⁰⁰,
 T. Mashimo ¹⁵³, J. Masik ¹⁰¹, A.L. Maslennikov ³⁷, L. Massa ^{23b}, P. Massarotti ^{72a,72b},
 P. Mastrandrea ^{74a,74b}, A. Mastroberardino ^{43b,43a}, T. Masubuchi ¹⁵³, T. Mathisen ¹⁶¹,
 J. Matousek ¹³³, N. Matsuzawa ¹⁵³, J. Maurer ^{27b}, B. Maček ⁹³, D.A. Maximov ³⁷, R. Mazini ¹⁴⁸,
 I. Maznas ¹⁵², M. Mazza ¹⁰⁷, S.M. Mazza ¹³⁶, E. Mazzeo ^{71a,71b}, C. Mc Ginn ²⁹,
 J.P. Mc Gowan ¹⁰⁴, S.P. Mc Kee ¹⁰⁶, C.C. McCracken ¹⁶⁴, E.F. McDonald ¹⁰⁵,
 A.E. McDougall ¹¹⁴, J.A. Mcfayden ¹⁴⁶, R.P. McGovern ¹²⁸, G. Mchedlidze ^{149b},
 R.P. Mckenzie ^{33g}, T.C. Mclachlan ⁴⁸, D.J. McLaughlin ⁹⁶, S.J. McMahon ¹³⁴,
 C.M. Mcpartland ⁹², R.A. McPherson ^{165,w}, S. Mehlhase ¹⁰⁹, A. Mehta ⁹², D. Melini ¹⁵⁰,
 B.R. Mellado Garcia ^{33g}, A.H. Melo ⁵⁵, F. Meloni ⁴⁸, A.M. Mendes Jacques Da Costa ¹⁰¹,
 H.Y. Meng ¹⁵⁵, L. Meng ⁹¹, S. Menke ¹¹⁰, M. Mentink ³⁶, E. Meoni ^{43b,43a}, G. Mercado ¹¹⁵,
 C. Merlassino ^{69a,69c}, L. Merola ^{72a,72b}, C. Meroni ^{71a,71b}, G. Merz ¹⁰⁶, J. Metcalfe ⁶, A.S. Mete ⁶,
 C. Meyer ⁶⁸, J-P. Meyer ¹³⁵, R.P. Middleton ¹³⁴, L. Mijović ⁵², G. Mikenberg ¹⁶⁹,
 M. Mikestikova ¹³¹, M. Mikuž ⁹³, H. Mildner ¹⁰⁰, A. Milic ³⁶, C.D. Milke ⁴⁴, D.W. Miller ³⁹,
 L.S. Miller ³⁴, A. Milov ¹⁶⁹, D.A. Milstead ^{47a,47b}, T. Min ^{14c}, A.A. Minaenko ³⁷,
 I.A. Minashvili ^{149b}, L. Mince ⁵⁹, A.I. Mincer ¹¹⁷, B. Mindur ^{86a}, M. Mineev ³⁸, Y. Mino ⁸⁸,
 L.M. Mir ¹³, M. Miralles Lopez ¹⁶³, M. Mironova ^{17a}, A. Mishima ¹⁵³, M.C. Missio ¹¹³,
 A. Mitra ¹⁶⁷, V.A. Mitsou ¹⁶³, Y. Mitsumori ¹¹¹, O. Miu ¹⁵⁵, P.S. Miyagawa ⁹⁴,
 T. Mkrtychyan ^{63a}, M. Mlinarevic ⁹⁶, T. Mlinarevic ⁹⁶, M. Mlynarikova ³⁶, S. Mobius ¹⁹,
 P. Moder ⁴⁸, P. Mogg ¹⁰⁹, M.H. Mohamed Farook ¹¹², A.F. Mohammed ^{14a,14e}, S. Mohapatra ⁴¹,
 G. Mokgatitswane ^{33g}, L. Moleri ¹⁶⁹, B. Mondal ¹⁴¹, S. Mondal ¹³², K. Mönig ⁴⁸,
 E. Monnier ¹⁰², L. Monsonis Romero ¹⁶³, J. Montejo Berlingen ¹³, M. Montella ¹¹⁹,
 F. Montereali ^{77a,77b}, F. Monticelli ⁹⁰, S. Monzani ^{69a,69c}, N. Morange ⁶⁶,

A.L. Moreira De Carvalho [ID130a](#), M. Moreno Llácer [ID163](#), C. Moreno Martinez [ID56](#), P. Morettini [ID57b](#),
 S. Morgenstern [ID36](#), M. Morii [ID61](#), M. Morinaga [ID153](#), A.K. Morley [ID36](#), F. Morodei [ID75a,75b](#),
 L. Morvaj [ID36](#), P. Moschovakos [ID36](#), B. Moser [ID36](#), M. Mosidze [ID149b](#), T. Moskalets [ID54](#),
 P. Moskvitina [ID113](#), J. Moss [ID31.1](#), E.J.W. Moyse [ID103](#), O. Mtintsilana [ID33g](#), S. Muanza [ID102](#),
 J. Mueller [ID129](#), D. Muenstermann [ID91](#), R. Müller [ID19](#), G.A. Mullier [ID161](#), A.J. Mullin³², J.J. Mullin¹²⁸,
 D.P. Mungo [ID155](#), D. Munoz Perez [ID163](#), F.J. Munoz Sanchez [ID101](#), M. Murin [ID101](#), W.J. Murray [ID167,134](#),
 A. Murrone [ID71a,71b](#), M. Muškinja [ID17a](#), C. Mwewa [ID29](#), A.G. Myagkov [ID37,a](#), A.J. Myers [ID8](#),
 G. Myers [ID68](#), M. Myska [ID132](#), B.P. Nachman [ID17a](#), O. Nackenhorst [ID49](#), A. Nag [ID50](#), K. Nagai [ID126](#),
 K. Nagano [ID84](#), J.L. Nagle [ID29,ai](#), E. Nagy [ID102](#), A.M. Nairz [ID36](#), Y. Nakahama [ID84](#), K. Nakamura [ID84](#),
 K. Nakkalil [ID5](#), H. Nanjo [ID124](#), R. Narayan [ID44](#), E.A. Narayanan [ID112](#), I. Naryshkin [ID37](#), M. Naseri [ID34](#),
 S. Nasri [ID159](#), C. Nass [ID24](#), G. Navarro [ID22a](#), J. Navarro-Gonzalez [ID163](#), R. Nayak [ID151](#), A. Nayaz [ID18](#),
 P.Y. Nechaeva [ID37](#), F. Nechansky [ID48](#), L. Nedic [ID126](#), T.J. Neep [ID20](#), A. Negri [ID73a,73b](#), M. Negrini [ID23b](#),
 C. Nellist [ID114](#), C. Nelson [ID104](#), K. Nelson [ID106](#), S. Nemecek [ID131](#), M. Nessi [ID36,h](#), M.S. Neubauer [ID162](#),
 F. Neuhaus [ID100](#), J. Neundorf [ID48](#), R. Newhouse [ID164](#), P.R. Newman [ID20](#), C.W. Ng [ID129](#), Y.W.Y. Ng [ID48](#),
 B. Ngair [ID35e](#), H.D.N. Nguyen [ID108](#), R.B. Nickerson [ID126](#), R. Nicolaidou [ID135](#), J. Nielsen [ID136](#),
 M. Niemeyer [ID55](#), J. Niermann [ID55,36](#), N. Nikiforou [ID36](#), V. Nikolaenko [ID37,a](#), I. Nikolic-Audit [ID127](#),
 K. Nikolopoulos [ID20](#), P. Nilsson [ID29](#), I. Ninca [ID48](#), H.R. Nindhito [ID56](#), G. Ninio [ID151](#), A. Nisati [ID75a](#),
 N. Nishu [ID2](#), R. Nisius [ID110](#), J-E. Nitschke [ID50](#), E.K. Nkadimeng [ID33g](#), T. Nobe [ID153](#), D.L. Noel [ID32](#),
 T. Nommensen [ID147](#), M.B. Norfolk [ID139](#), R.R.B. Norisam [ID96](#), B.J. Norman [ID34](#), M. Noury [ID35a](#),
 J. Novak [ID93](#), T. Novak [ID48](#), L. Novotny [ID132](#), R. Novotny [ID112](#), L. Nozka [ID122](#), K. Ntekas [ID160](#),
 N.M.J. Nunes De Moura Junior [ID83b](#), E. Nurse⁹⁶, J. Ocariz [ID127](#), A. Ochi [ID85](#), I. Ochoa [ID130a](#),
 S. Oerdek [ID48](#), J.T. Offermann [ID39](#), A. Ogrodnik [ID133](#), A. Oh [ID101](#), C.C. Ohm [ID144](#), H. Oide [ID84](#),
 R. Oishi [ID153](#), M.L. Ojeda [ID48](#), M.W. O’Keefe⁹², Y. Okumura [ID153](#), L.F. Oleiro Seabra [ID130a](#),
 S.A. Olivares Pino [ID137d](#), D. Oliveira Damazio [ID29](#), D. Oliveira Goncalves [ID83a](#), J.L. Oliver [ID160](#),
 Ö.O. Öncel [ID54](#), A.P. O’Neill [ID19](#), A. Onofre [ID130a,130e](#), P.U.E. Onyisi [ID11](#), M.J. Oreglia [ID39](#),
 G.E. Orellana [ID90](#), D. Orestano [ID77a,77b](#), N. Orlando [ID13](#), R.S. Orr [ID155](#), V. O’Shea [ID59](#),
 L.M. Osojnak [ID128](#), R. Ospanov [ID62a](#), G. Otero y Garzon [ID30](#), H. Otono [ID89](#), P.S. Ott [ID63a](#),
 G.J. Ottino [ID17a](#), M. Ouchrif [ID35d](#), J. Ouellette [ID29](#), F. Ould-Saada [ID125](#), M. Owen [ID59](#), R.E. Owen [ID134](#),
 K.Y. Oyulmaz [ID21a](#), V.E. Ozcan [ID21a](#), F. Ozturk [ID87](#), N. Ozturk [ID8](#), S. Ozturk [ID82](#), H.A. Pacey [ID126](#),
 A. Pacheco Pages [ID13](#), C. Padilla Aranda [ID13](#), G. Padovano [ID75a,75b](#), S. Pagan Griso [ID17a](#),
 G. Palacino [ID68](#), A. Palazzo [ID70a,70b](#), S. Palestini [ID36](#), J. Pan [ID172](#), T. Pan [ID64a](#), D.K. Panchal [ID11](#),
 C.E. Pandini [ID114](#), J.G. Panduro Vazquez [ID95](#), H.D. Pandya [ID1](#), H. Pang [ID14b](#), P. Pani [ID48](#),
 G. Panizzo [ID69a,69c](#), L. Paolozzi [ID56](#), C. Papadatos [ID108](#), S. Parajuli [ID44](#), A. Paramonov [ID6](#),
 C. Paraskevopoulos [ID10](#), D. Paredes Hernandez [ID64b](#), K.R. Park [ID41](#), T.H. Park [ID155](#), M.A. Parker [ID32](#),
 F. Parodi [ID57b,57a](#), E.W. Parrish [ID115](#), V.A. Parrish [ID52](#), J.A. Parsons [ID41](#), U. Parzefall [ID54](#),
 B. Pascual Dias [ID108](#), L. Pascual Dominguez [ID151](#), E. Pasqualucci [ID75a](#), S. Passaggio [ID57b](#), F. Pastore [ID95](#),
 P. Pasuwan [ID47a,47b](#), P. Patel [ID87](#), U.M. Patel [ID51](#), J.R. Pater [ID101](#), T. Pauly [ID36](#), J. Pearkes [ID143](#),
 M. Pedersen [ID125](#), R. Pedro [ID130a](#), S.V. Peleganchuk [ID37](#), O. Penc [ID36](#), E.A. Pender [ID52](#),
 K.E. Penski [ID109](#), M. Penzin [ID37](#), B.S. Peralva [ID83d](#), A.P. Pereira Peixoto [ID60](#), L. Pereira Sanchez [ID47a,47b](#),
 D.V. Perepelitsa [ID29,ai](#), E. Perez Codina [ID156a](#), M. Perganti [ID10](#), L. Perini [ID71a,71b,*](#), H. Pernegger [ID36](#),
 O. Perrin [ID40](#), K. Peters [ID48](#), R.F.Y. Peters [ID101](#), B.A. Petersen [ID36](#), T.C. Petersen [ID42](#), E. Petit [ID102](#),
 V. Petousis [ID132](#), C. Petridou [ID152,e](#), A. Petrukhin [ID141](#), M. Pettee [ID17a](#), N.E. Pettersson [ID36](#),
 A. Petukhov [ID37](#), K. Petukhova [ID133](#), R. Pezoa [ID137f](#), L. Pezzotti [ID36](#), G. Pezzullo [ID172](#), T.M. Pham [ID170](#),
 T. Pham [ID105](#), P.W. Phillips [ID134](#), G. Piacquadio [ID145](#), E. Pianori [ID17a](#), F. Piazza [ID123](#), R. Piegai [ID30](#),
 D. Pietreanu [ID27b](#), A.D. Pilkington [ID101](#), M. Pinamonti [ID69a,69c](#), J.L. Pinfeld [ID2](#),
 B.C. Pinheiro Pereira [ID130a](#), A.E. Pinto Pinoargote [ID100,135](#), L. Pintucci [ID69a,69c](#), K.M. Piper [ID146](#),
 A. Pirttikoski [ID56](#), D.A. Pizzi [ID34](#), L. Pizzimento [ID64b](#), A. Pizzini [ID114](#), M.-A. Pleier [ID29](#), V. Plesanovs⁵⁴,

V. Pleskot ¹³³, E. Plotnikova³⁸, G. Poddar ⁴, R. Poettgen ⁹⁸, L. Poggioli ¹²⁷, I. Pokharel ⁵⁵, S. Polacek ¹³³, G. Polesello ^{73a}, A. Poley ^{142,156a}, R. Polifka ¹³², A. Polini ^{23b}, C.S. Pollard ¹⁶⁷, Z.B. Pollock ¹¹⁹, V. Polychronakos ²⁹, E. Pompa Pacchi ^{75a,75b}, D. Ponomarenko ¹¹³, L. Pontecorvo ³⁶, S. Popa ^{27a}, G.A. Popeneciu ^{27d}, A. Poreba ³⁶, D.M. Portillo Quintero ^{156a}, S. Pospisil ¹³², M.A. Postill ¹³⁹, P. Postolache ^{27c}, K. Potamianos ¹⁶⁷, P.A. Potepa ^{86a}, I.N. Potrap ³⁸, C.J. Potter ³², H. Potti ¹, T. Poulsen ⁴⁸, J. Poveda ¹⁶³, M.E. Pozo Astigarraga ³⁶, A. Prades Ibanez ¹⁶³, J. Pretel ⁵⁴, D. Price ¹⁰¹, M. Primavera ^{70a}, M.A. Principe Martin ⁹⁹, R. Privara ¹²², T. Procter ⁵⁹, M.L. Proffitt ¹³⁸, N. Proklova ¹²⁸, K. Prokofiev ^{64c}, G. Proto ¹¹⁰, S. Protopopescu ²⁹, J. Proudfoot ⁶, M. Przybycien ^{86a}, W.W. Przygoda ^{86b}, J.E. Puddefoot ¹³⁹, D. Pudzha ³⁷, D. Pyatiizbyantseva ³⁷, J. Qian ¹⁰⁶, D. Qichen ¹⁰¹, Y. Qin ¹⁰¹, T. Qiu ⁵², A. Quadt ⁵⁵, M. Queitsch-Maitland ¹⁰¹, G. Quetant ⁵⁶, R.P. Quinn ¹⁶⁴, G. Rabanal Bolanos ⁶¹, D. Rafanoharana ⁵⁴, F. Ragusa ^{71a,71b}, J.L. Rainbolt ³⁹, J.A. Raine ⁵⁶, S. Rajagopalan ²⁹, E. Ramakoti ³⁷, I.A. Ramirez-Berend ³⁴, K. Ran ^{48,14e}, N.P. Rapheeha ^{33g}, H. Rasheed ^{27b}, V. Raskina ¹²⁷, D.F. Rassloff ^{63a}, A. Rastogi ^{17a}, S. Rave ¹⁰⁰, B. Ravina ⁵⁵, I. Ravinovich ¹⁶⁹, M. Raymond ³⁶, A.L. Read ¹²⁵, N.P. Readioff ¹³⁹, D.M. Rebuzzi ^{73a,73b}, G. Redlinger ²⁹, A.S. Reed ¹¹⁰, K. Reeves ²⁶, J.A. Reidelsturz ¹⁷¹, D. Reikher ¹⁵¹, A. Rej ⁴⁹, C. Rembser ³⁶, A. Renardi ⁴⁸, M. Renda ^{27b}, M.B. Rendel¹¹⁰, F. Renner ⁴⁸, A.G. Rennie ¹⁶⁰, A.L. Rescia ⁴⁸, S. Resconi ^{71a}, M. Ressegotti ^{57b,57a}, S. Rettie ³⁶, J.G. Reyes Rivera ¹⁰⁷, E. Reynolds ^{17a}, O.L. Rezanova ³⁷, P. Reznicek ¹³³, N. Ribaric ⁹¹, E. Ricci ^{78a,78b}, R. Richter ¹¹⁰, S. Richter ^{47a,47b}, E. Richter-Was ^{86b}, M. Ridel ¹²⁷, S. Ridouani ^{35d}, P. Rieck ¹¹⁷, P. Riedler ³⁶, E.M. Riefel ^{47a,47b}, J.O. Rieger ¹¹⁴, M. Rijssenbeek ¹⁴⁵, A. Rimoldi ^{73a,73b}, M. Rimoldi ³⁶, L. Rinaldi ^{23b,23a}, T.T. Rinn ²⁹, M.P. Rinnagel ¹⁰⁹, G. Ripellino ¹⁶¹, I. Riu ¹³, P. Rivadeneira ⁴⁸, J.C. Rivera Vergara ¹⁶⁵, F. Rizatdinova ¹²¹, E. Rizvi ⁹⁴, B.A. Roberts ¹⁶⁷, B.R. Roberts ^{17a}, S.H. Robertson ^{104,w}, D. Robinson ³², C.M. Robles Gajardo^{137f}, M. Robles Manzano ¹⁰⁰, A. Robson ⁵⁹, A. Rocchi ^{76a,76b}, C. Roda ^{74a,74b}, S. Rodriguez Bosca ^{63a}, Y. Rodriguez Garcia ^{22a}, A. Rodriguez Rodriguez ⁵⁴, A.M. Rodríguez Vera ^{156b}, S. Roe³⁶, J.T. Roemer ¹⁶⁰, A.R. Roepe-Gier ¹³⁶, J. Roggel ¹⁷¹, O. Røhne ¹²⁵, R.A. Rojas ¹⁰³, C.P.A. Roland ¹²⁷, J. Roloff ²⁹, A. Romaniouk ³⁷, E. Romano ^{73a,73b}, M. Romano ^{23b}, A.C. Romero Hernandez ¹⁶², N. Rompotis ⁹², L. Roos ¹²⁷, S. Rosati ^{75a}, B.J. Rosser ³⁹, E. Rossi ¹²⁶, E. Rossi ^{72a,72b}, L.P. Rossi ^{57b}, L. Rossini ⁵⁴, R. Rosten ¹¹⁹, M. Rotaru ^{27b}, B. Rottler ⁵⁴, C. Rougier ^{102,aa}, D. Rousseau ⁶⁶, D. Rousso ³², A. Roy ¹⁶², S. Roy-Garand ¹⁵⁵, A. Rozanov ¹⁰², Z.M.A. Rozario ⁵⁹, Y. Rozen ¹⁵⁰, X. Ruan ^{33g}, A. Rubio Jimenez ¹⁶³, A.J. Ruby ⁹², V.H. Ruelas Rivera ¹⁸, T.A. Ruggeri ¹, A. Ruggiero ¹²⁶, A. Ruiz-Martinez ¹⁶³, A. Rummeler ³⁶, Z. Rurikova ⁵⁴, N.A. Rusakovich ³⁸, H.L. Russell ¹⁶⁵, G. Russo ^{75a,75b}, J.P. Rutherford ⁷, S. Rutherford Colmenares ³², K. Rybacki⁹¹, M. Rybar ¹³³, E.B. Rye ¹²⁵, A. Ryzhov ⁴⁴, J.A. Sabater Iglesias ⁵⁶, P. Sabatini ¹⁶³, H.F-W. Sadrozinski ¹³⁶, F. Safai Tehrani ^{75a}, B. Safarzadeh Samani ¹³⁴, M. Safdari ¹⁴³, S. Saha ¹⁶⁵, M. Sahinsoy ¹¹⁰, A. Saibel ¹⁶³, M. Saimpert ¹³⁵, M. Saito ¹⁵³, T. Saito ¹⁵³, D. Salamani ³⁶, A. Salnikov ¹⁴³, J. Salt ¹⁶³, A. Salvador Salas ¹⁵¹, D. Salvatore ^{43b,43a}, F. Salvatore ¹⁴⁶, A. Salzburger ³⁶, D. Sammel ⁵⁴, D. Sampsonidis ^{152,e}, D. Sampsonidou ¹²³, J. Sánchez ¹⁶³, A. Sanchez Pineda ⁴, V. Sanchez Sebastian ¹⁶³, H. Sandaker ¹²⁵, C.O. Sander ⁴⁸, J.A. Sandesara ¹⁰³, M. Sandhoff ¹⁷¹, C. Sandoval ^{22b}, D.P.C. Sankey ¹³⁴, T. Sano ⁸⁸, A. Sansoni ⁵³, L. Santi ^{75a,75b}, C. Santoni ⁴⁰, H. Santos ^{130a,130b}, S.N. Santpur ^{17a}, A. Santra ¹⁶⁹, K.A. Saoucha ^{116b}, J.G. Saraiva ^{130a,130d}, J. Sardain ⁷, O. Sasaki ⁸⁴, K. Sato ¹⁵⁷, C. Sauer^{63b}, F. Sauerburger ⁵⁴, E. Sauvan ⁴, P. Savard ^{155,af}, R. Sawada ¹⁵³, C. Sawyer ¹³⁴, L. Sawyer ⁹⁷, I. Sayago Galvan¹⁶³, C. Sbarra ^{23b}, A. Sbrizzi ^{23b,23a}, T. Scanlon ⁹⁶, J. Schaarschmidt ¹³⁸, P. Schacht ¹¹⁰, U. Schäfer ¹⁰⁰, A.C. Schaffer ^{66,44}, D. Schaile ¹⁰⁹, R.D. Schamberger ¹⁴⁵, C. Scharf ¹⁸, M.M. Schefer ¹⁹,

V.A. Schegelsky [ID37](#), D. Scheirich [ID133](#), F. Schenck [ID18](#), M. Schernau [ID160](#), C. Scheulen [ID55](#), C. Schiavi [ID57b,57a](#), E.J. Schioppa [ID70a,70b](#), M. Schioppa [ID43b,43a](#), B. Schlag [ID143,n](#), K.E. Schleicher [ID54](#), S. Schlenker [ID36](#), J. Schmeing [ID171](#), M.A. Schmidt [ID171](#), K. Schmieden [ID100](#), C. Schmitt [ID100](#), N. Schmitt [ID100](#), S. Schmitt [ID48](#), L. Schoeffel [ID135](#), A. Schoening [ID63b](#), P.G. Scholer [ID54](#), E. Schopf [ID126](#), M. Schott [ID100](#), J. Schovancova [ID36](#), S. Schramm [ID56](#), F. Schroeder [ID171](#), T. Schroer [ID56](#), H-C. Schultz-Coulon [ID63a](#), M. Schumacher [ID54](#), B.A. Schumm [ID136](#), Ph. Schune [ID135](#), A.J. Schuy [ID138](#), H.R. Schwartz [ID136](#), A. Schwartzman [ID143](#), T.A. Schwarz [ID106](#), Ph. Schwemling [ID135](#), R. Schwienhorst [ID107](#), A. Sciandra [ID136](#), G. Sciolla [ID26](#), F. Scuri [ID74a](#), C.D. Sebastiani [ID92](#), K. Sedlaczek [ID115](#), P. Seema [ID18](#), S.C. Seidel [ID112](#), A. Seiden [ID136](#), B.D. Seidlitz [ID41](#), C. Seitz [ID48](#), J.M. Seixas [ID83b](#), G. Sekhniaidze [ID72a](#), S.J. Sekula [ID44](#), L. Selem [ID60](#), N. Semprini-Cesari [ID23b,23a](#), D. Sengupta [ID56](#), V. Senthikumar [ID163](#), L. Serin [ID66](#), L. Serkin [ID69a,69b](#), M. Sessa [ID76a,76b](#), H. Severini [ID120](#), F. Sforza [ID57b,57a](#), A. Sfyrta [ID56](#), E. Shabalina [ID55](#), R. Shaheen [ID144](#), J.D. Shahinian [ID128](#), D. Shaked Renous [ID169](#), L.Y. Shan [ID14a](#), M. Shapiro [ID17a](#), A. Sharma [ID36](#), A.S. Sharma [ID164](#), P. Sharma [ID80](#), S. Sharma [ID48](#), P.B. Shatalov [ID37](#), K. Shaw [ID146](#), S.M. Shaw [ID101](#), A. Shcherbakova [ID37](#), Q. Shen [ID62c,5](#), D.J. Sheppard [ID142](#), P. Sherwood [ID96](#), L. Shi [ID96](#), X. Shi [ID14a](#), C.O. Shimmin [ID172](#), J.D. Shinner [ID95](#), I.P.J. Shipsey [ID126](#), S. Shirabe [ID56,h](#), M. Shiyakova [ID38,u](#), J. Shlomi [ID169](#), M.J. Shochet [ID39](#), J. Shojaii [ID105](#), D.R. Shope [ID125](#), B. Shrestha [ID120](#), S. Shrestha [ID119,aj](#), E.M. Shrif [ID33g](#), M.J. Shroff [ID165](#), P. Sicho [ID131](#), A.M. Sickles [ID162](#), E. Sideras Haddad [ID33g](#), A. Sidoti [ID23b](#), F. Siegert [ID50](#), Dj. Sijacki [ID15](#), F. Sili [ID90](#), J.M. Silva [ID20](#), M.V. Silva Oliveira [ID29](#), S.B. Silverstein [ID47a](#), S. Simion [ID66](#), R. Simoniello [ID36](#), E.L. Simpson [ID59](#), H. Simpson [ID146](#), L.R. Simpson [ID106](#), N.D. Simpson [ID98](#), S. Simsek [ID82](#), S. Sindhu [ID55](#), P. Sinervo [ID155](#), S. Singh [ID155](#), S. Sinha [ID48](#), S. Sinha [ID101](#), M. Sioli [ID23b,23a](#), I. Siral [ID36](#), E. Sitnikova [ID48](#), S.Yu. Sivoklov [ID37,*](#), J. Sjölin [ID47a,47b](#), A. Skaf [ID55](#), E. Skorda [ID20](#), P. Skubic [ID120](#), M. Slawinska [ID87](#), V. Smakhtin [ID169](#), B.H. Smart [ID134](#), J. Smiesko [ID36](#), S.Yu. Smirnov [ID37](#), Y. Smirnov [ID37](#), L.N. Smirnova [ID37,a](#), O. Smirnova [ID98](#), A.C. Smith [ID41](#), E.A. Smith [ID39](#), H.A. Smith [ID126](#), J.L. Smith [ID92](#), R. Smith [ID143](#), M. Smizanska [ID91](#), K. Smolek [ID132](#), A.A. Snesarev [ID37](#), S.R. Snider [ID155](#), H.L. Snoek [ID114](#), S. Snyder [ID29](#), R. Sobie [ID165,w](#), A. Soffer [ID151](#), C.A. Solans Sanchez [ID36](#), E.Yu. Soldatov [ID37](#), U. Soldevila [ID163](#), A.A. Solodkov [ID37](#), S. Solomon [ID26](#), A. Soloshenko [ID38](#), K. Solovieva [ID54](#), O.V. Solovyanov [ID40](#), V. Solovyev [ID37](#), P. Sommer [ID36](#), A. Sonay [ID13](#), W.Y. Song [ID156b](#), J.M. Sonneveld [ID114](#), A. Sopczak [ID132](#), A.L. Soppio [ID96](#), F. Sopkova [ID28b](#), I.R. Sotarriva Alvarez [ID154](#), V. Sothilingam [ID63a](#), O.J. Soto Sandoval [ID137c,137b](#), S. Sottocornola [ID68](#), R. Soualah [ID116b](#), Z. Soumami [ID35e](#), D. South [ID48](#), N. Soybelman [ID169](#), S. Spagnolo [ID70a,70b](#), M. Spalla [ID110](#), D. Sperlich [ID54](#), G. Spigo [ID36](#), S. Spinali [ID91](#), D.P. Spiteri [ID59](#), M. Spousta [ID133](#), E.J. Staats [ID34](#), A. Stabile [ID71a,71b](#), R. Stamen [ID63a](#), A. Stampekis [ID20](#), M. Standke [ID24](#), E. Stanecka [ID87](#), M.V. Stange [ID50](#), B. Stanislaus [ID17a](#), M.M. Stanitzki [ID48](#), B. Stapf [ID48](#), E.A. Starchenko [ID37](#), G.H. Stark [ID136](#), J. Stark [ID102,aa](#), D.M. Starke [ID156b](#), P. Staroba [ID131](#), P. Starovoitov [ID63a](#), S. Stärz [ID104](#), R. Staszewski [ID87](#), G. Stavropoulos [ID46](#), J. Steentoft [ID161](#), P. Steinberg [ID29](#), B. Stelzer [ID142,156a](#), H.J. Stelzer [ID129](#), O. Stelzer-Chilton [ID156a](#), H. Stenzel [ID58](#), T.J. Stevenson [ID146](#), G.A. Stewart [ID36](#), J.R. Stewart [ID121](#), M.C. Stockton [ID36](#), G. Stoicea [ID27b](#), M. Stolarski [ID130a](#), S. Stonjek [ID110](#), A. Straessner [ID50](#), J. Strandberg [ID144](#), S. Strandberg [ID47a,47b](#), M. Stratmann [ID171](#), M. Strauss [ID120](#), T. Streblner [ID102](#), P. Strizenc [ID28b](#), R. Ströhmer [ID166](#), D.M. Strom [ID123](#), R. Stroynowski [ID44](#), A. Strubig [ID47a,47b](#), S.A. Stucci [ID29](#), B. Stugu [ID16](#), J. Stupak [ID120](#), N.A. Styles [ID48](#), D. Su [ID143](#), S. Su [ID62a](#), W. Su [ID62d](#), X. Su [ID62a,66](#), K. Sugizaki [ID153](#), V.V. Sulim [ID37](#), M.J. Sullivan [ID92](#), D.M.S. Sultan [ID78a,78b](#), L. Sultanaliev [ID37](#), S. Sultansoy [ID3b](#), T. Sumida [ID88](#), S. Sun [ID106](#), S. Sun [ID170](#), O. Sunneborn Gudnadottir [ID161](#), N. Sur [ID102](#), M.R. Sutton [ID146](#), H. Suzuki [ID157](#), M. Svatos [ID131](#), M. Swiatlowski [ID156a](#), T. Swirski [ID166](#), I. Sykora [ID28a](#), M. Sykora [ID133](#), T. Sykora [ID133](#), D. Ta [ID100](#), K. Tackmann [ID48,t](#), A. Taffard [ID160](#), R. Tafirout [ID156a](#), J.S. Tafoya Vargas [ID66](#), E.P. Takeva [ID52](#),

Y. Takubo ¹⁸⁴, M. Talby ¹⁰², A.A. Talyshev ³⁷, K.C. Tam ^{64b}, N.M. Tamir ¹⁵¹, A. Tanaka ¹⁵³,
 J. Tanaka ¹⁵³, R. Tanaka ⁶⁶, M. Tanasini ^{57b,57a}, Z. Tao ¹⁶⁴, S. Tapia Araya ^{137f},
 S. Tapprogge ¹⁰⁰, A. Tarek Abouelfadl Mohamed ¹⁰⁷, S. Tarem ¹⁵⁰, K. Tariq ^{14a}, G. Tarna ^{102,27b},
 G.F. Tartarelli ^{71a}, P. Tas ¹³³, M. Tasevsky ¹³¹, E. Tassi ^{43b,43a}, A.C. Tate ¹⁶², G. Tateno ¹⁵³,
 Y. Tayalati ^{35e,v}, G.N. Taylor ¹⁰⁵, W. Taylor ^{156b}, A.S. Tee ¹⁷⁰, R. Teixeira De Lima ¹⁴³,
 P. Teixeira-Dias ⁹⁵, J.J. Teoh ¹⁵⁵, K. Terashi ¹⁵³, J. Terron ⁹⁹, S. Terzo ¹³, M. Testa ⁵³,
 R.J. Teuscher ^{155,w}, A. Thaler ⁷⁹, O. Theiner ⁵⁶, N. Themistokleous ⁵², T. Theveneaux-Pelzer ¹⁰²,
 O. Thielmann ¹⁷¹, D.W. Thomas ⁹⁵, J.P. Thomas ²⁰, E.A. Thompson ^{17a}, P.D. Thompson ²⁰,
 E. Thomson ¹²⁸, Y. Tian ⁵⁵, V. Tikhomirov ^{37,a}, Yu.A. Tikhonov ³⁷, S. Timoshenko ³⁷,
 D. Timoshyn ¹³³, E.X.L. Ting ¹, P. Tipton ¹⁷², S.H. Tlou ^{33g}, A. Tnourji ⁴⁰, K. Todome ¹⁵⁴,
 S. Todorova-Nova ¹³³, S. Todt ⁵⁰, M. Togawa ⁸⁴, J. Tojo ⁸⁹, S. Tokár ^{28a}, K. Tokushuku ⁸⁴,
 O. Toldaiev ⁶⁸, R. Tombs ³², M. Tomoto ^{84,111}, L. Tompkins ^{143,n}, K.W. Topolnicki ^{86b},
 E. Torrence ¹²³, H. Torres ^{102,aa}, E. Torró Pastor ¹⁶³, M. Toscani ³⁰, C. Tosciri ³⁹, M. Tost ¹¹,
 D.R. Tovey ¹³⁹, A. Traeet ¹⁶, I.S. Trandafir ^{27b}, T. Trefzger ¹⁶⁶, A. Tricoli ²⁹, I.M. Trigger ^{156a},
 S. Trincaz-Duvoid ¹²⁷, D.A. Trischuk ²⁶, B. Trocmé ⁶⁰, C. Troncon ^{71a}, L. Truong ^{33c},
 M. Trzebinski ⁸⁷, A. Trzuppek ⁸⁷, F. Tsai ¹⁴⁵, M. Tsai ¹⁰⁶, A. Tsiamis ^{152,e}, P.V. Tsiareshka ³⁷,
 S. Tsigaridas ^{156a}, A. Tsigotis ^{152,r}, V. Tsiskaridze ¹⁵⁵, E.G. Tskhadadze ^{149a},
 M. Tsopoulou ^{152,e}, Y. Tsujikawa ⁸⁸, I.I. Tsukerman ³⁷, V. Tsulaia ^{17a}, S. Tsuno ⁸⁴, K. Tsuru ¹¹⁸,
 D. Tsybychev ¹⁴⁵, Y. Tu ^{64b}, A. Tudorache ^{27b}, V. Tudorache ^{27b}, A.N. Tuna ⁶¹,
 S. Turchikhin ^{57b,57a}, I. Turk Cakir ^{3a}, R. Turra ^{71a}, T. Turtuvshin ^{38,x}, P.M. Tuts ⁴¹,
 S. Tzamarias ^{152,e}, P. Tzani ¹⁰, E. Tzovara ¹⁰⁰, F. Ukegawa ¹⁵⁷, P.A. Ulloa Poblete ^{137c,137b},
 E.N. Umaka ²⁹, G. Unal ³⁶, M. Unal ¹¹, A. Undrus ²⁹, G. Unel ¹⁶⁰, J. Urban ^{28b},
 P. Urquijo ¹⁰⁵, P. Urrejola ^{137a}, G. Usai ⁸, R. Ushioda ¹⁵⁴, M. Usman ¹⁰⁸, Z. Uysal ^{21b},
 V. Vacek ¹³², B. Vachon ¹⁰⁴, K.O.H. Vadla ¹²⁵, T. Vafeiadis ³⁶, A. Vaitkus ⁹⁶, C. Valderanis ¹⁰⁹,
 E. Valdes Santurio ^{47a,47b}, M. Valente ^{156a}, S. Valentinetti ^{23b,23a}, A. Valero ¹⁶³,
 E. Valiente Moreno ¹⁶³, A. Vallier ^{102,aa}, J.A. Valls Ferrer ¹⁶³, D.R. Van Arneman ¹¹⁴,
 T.R. Van Daalen ¹³⁸, A. Van Der Graaf ⁴⁹, P. Van Gemmeren ⁶, M. Van Rijnbach ^{125,36},
 S. Van Stroud ⁹⁶, I. Van Vulpen ¹¹⁴, M. Vanadia ^{76a,76b}, W. Vandelli ³⁶, M. Vandenbroucke ¹³⁵,
 E.R. Vandewall ¹²¹, D. Vannicola ¹⁵¹, L. Vannoli ^{57b,57a}, R. Vari ^{75a}, E.W. Varnes ⁷,
 C. Varni ^{17b}, T. Varol ¹⁴⁸, D. Varouchas ⁶⁶, L. Varriale ¹⁶³, K.E. Varvell ¹⁴⁷, M.E. Vasile ^{27b},
 L. Vaslin ⁸⁴, G.A. Vasquez ¹⁶⁵, A. Vasyukov ³⁸, F. Vazeille ⁴⁰, T. Vazquez Schroeder ³⁶,
 J. Veatch ³¹, V. Vecchio ¹⁰¹, M.J. Veen ¹⁰³, I. Veliscek ¹²⁶, L.M. Veloce ¹⁵⁵, F. Veloso ^{130a,130c},
 S. Veneziano ^{75a}, A. Ventura ^{70a,70b}, S. Ventura Gonzalez ¹³⁵, A. Verbytskyi ¹¹⁰,
 M. Verducci ^{74a,74b}, C. Vergis ²⁴, M. Verissimo De Araujo ^{83b}, W. Verkerke ¹¹⁴,
 J.C. Vermeulen ¹¹⁴, C. Vernieri ¹⁴³, M. Vessella ¹⁰³, M.C. Vetterli ^{142,af}, A. Vgenopoulos ^{152,e},
 N. Viaux Maira ^{137f}, T. Vickey ¹³⁹, O.E. Vickey Boeriu ¹³⁹, G.H.A. Viehhauser ¹²⁶, L. Vigani ^{63b},
 M. Villa ^{23b,23a}, M. Villaplana Perez ¹⁶³, E.M. Villhauer ⁵², E. Vilucchi ⁵³, M.G. Vinciter ³⁴,
 G.S. Virdee ²⁰, A. Vishwakarma ⁵², A. Visibile ¹¹⁴, C. Vittori ³⁶, I. Vivarelli ¹⁴⁶,
 E. Voevodina ¹¹⁰, F. Vogel ¹⁰⁹, J.C. Voigt ⁵⁰, P. Vokac ¹³², Yu. Volkotrub ^{86a}, J. Von Ahnen ⁴⁸,
 E. Von Toerne ²⁴, B. Vormwald ³⁶, V. Vorobel ¹³³, K. Vorobev ³⁷, M. Vos ¹⁶³, K. Voss ¹⁴¹,
 J.H. Vossebeld ⁹², M. Vozak ¹¹⁴, L. Vozdecky ⁹⁴, N. Vranjes ¹⁵, M. Vranjes Milosavljevic ¹⁵,
 M. Vreeswijk ¹¹⁴, R. Vuillermet ³⁶, O. Vujanovic ¹⁰⁰, I. Vukotic ³⁹, S. Wada ¹⁵⁷, C. Wagner ¹⁰³,
 J.M. Wagner ^{17a}, W. Wagner ¹⁷¹, S. Wahdan ¹⁷¹, H. Wahlberg ⁹⁰, M. Wakida ¹¹¹, J. Walder ¹³⁴,
 R. Walker ¹⁰⁹, W. Walkowiak ¹⁴¹, A. Wall ¹²⁸, T. Wamorkar ⁶, A.Z. Wang ¹³⁶, C. Wang ¹⁰⁰,
 C. Wang ^{62c}, H. Wang ^{17a}, J. Wang ^{64a}, R.-J. Wang ¹⁰⁰, R. Wang ⁶¹, R. Wang ⁶,
 S.M. Wang ¹⁴⁸, S. Wang ^{62b}, T. Wang ^{62a}, W.T. Wang ⁸⁰, W. Wang ^{14a}, X. Wang ^{14c},
 X. Wang ¹⁶², X. Wang ^{62c}, Y. Wang ^{62d}, Y. Wang ^{14c}, Z. Wang ¹⁰⁶, Z. Wang ^{62d,51,62c},

Z. Wang ¹⁰⁶, A. Warburton ¹⁰⁴, R.J. Ward ²⁰, N. Warrack ⁵⁹, A.T. Watson ²⁰, H. Watson ⁵⁹, M.F. Watson ²⁰, E. Watton ^{59,134}, G. Watts ¹³⁸, B.M. Waugh ⁹⁶, C. Weber ²⁹, H.A. Weber ¹⁸, M.S. Weber ¹⁹, S.M. Weber ^{63a}, C. Wei ^{62a}, Y. Wei ¹²⁶, A.R. Weidberg ¹²⁶, E.J. Weik ¹¹⁷, J. Weingarten ⁴⁹, M. Weirich ¹⁰⁰, C. Weiser ⁵⁴, C.J. Wells ⁴⁸, T. Wenaus ²⁹, B. Wendland ⁴⁹, T. Wengler ³⁶, N.S. Wenke ¹¹⁰, N. Wermes ²⁴, M. Wessels ^{63a}, A.M. Wharton ⁹¹, A.S. White ⁶¹, A. White ⁸, M.J. White ¹, D. Whiteson ¹⁶⁰, L. Wickremasinghe ¹²⁴, W. Wiedenmann ¹⁷⁰, C. Wiel ⁵⁰, M. Wielers ¹³⁴, C. Wiglesworth ⁴², D.J. Wilbern ¹²⁰, H.G. Wilkens ³⁶, D.M. Williams ⁴¹, H.H. Williams ¹²⁸, S. Williams ³², S. Willocq ¹⁰³, B.J. Wilson ¹⁰¹, P.J. Windischhofer ³⁹, F.I. Winkel ³⁰, F. Winklmeier ¹²³, B.T. Winter ⁵⁴, J.K. Winter ¹⁰¹, M. Wittgen ¹⁴³, M. Wobisch ⁹⁷, Z. Wolffs ¹¹⁴, J. Wollrath ¹⁶⁰, M.W. Wolter ⁸⁷, H. Wolters ^{130a,130c}, A.F. Wongel ⁴⁸, E.L. Woodward ⁴¹, S.D. Worm ⁴⁸, B.K. Wosiek ⁸⁷, K.W. Woźniak ⁸⁷, S. Wozniowski ⁵⁵, K. Wraight ⁵⁹, C. Wu ²⁰, J. Wu ^{14a,14e}, M. Wu ^{64a}, M. Wu ¹¹³, S.L. Wu ¹⁷⁰, X. Wu ⁵⁶, Y. Wu ^{62a}, Z. Wu ¹³⁵, J. Wuerzinger ^{110,ad}, T.R. Wyatt ¹⁰¹, B.M. Wynne ⁵², S. Xella ⁴², L. Xia ^{14c}, M. Xia ^{14b}, J. Xiang ^{64c}, M. Xie ^{62a}, X. Xie ^{62a}, S. Xin ^{14a,14e}, A. Xiong ¹²³, J. Xiong ^{17a}, D. Xu ^{14a}, H. Xu ^{62a}, L. Xu ^{62a}, R. Xu ¹²⁸, T. Xu ¹⁰⁶, Y. Xu ^{14b}, Z. Xu ⁵², Z. Xu ^{14c}, B. Yabsley ¹⁴⁷, S. Yacoob ^{33a}, Y. Yamaguchi ¹⁵⁴, E. Yamashita ¹⁵³, H. Yamauchi ¹⁵⁷, T. Yamazaki ^{17a}, Y. Yamazaki ⁸⁵, J. Yan ^{62c}, S. Yan ¹²⁶, Z. Yan ²⁵, H.J. Yang ^{62c,62d}, H.T. Yang ^{62a}, S. Yang ^{62a}, T. Yang ^{64c}, X. Yang ³⁶, X. Yang ^{14a}, Y. Yang ⁴⁴, Y. Yang ^{62a}, Z. Yang ^{62a}, W-M. Yao ^{17a}, Y.C. Yap ⁴⁸, H. Ye ^{14c}, H. Ye ⁵⁵, J. Ye ^{14a}, S. Ye ²⁹, X. Ye ^{62a}, Y. Yeh ⁹⁶, I. Yeletsikh ³⁸, B.K. Yeo ^{17b}, M.R. Yexley ⁹⁶, P. Yin ⁴¹, K. Yorita ¹⁶⁸, S. Younas ^{27b}, C.J.S. Young ³⁶, C. Young ¹⁴³, C. Yu ^{14a,14e,ah}, Y. Yu ^{62a}, M. Yuan ¹⁰⁶, R. Yuan ^{62b}, L. Yue ⁹⁶, M. Zaazoua ^{62a}, B. Zabinski ⁸⁷, E. Zaid ⁵², Z.K. Zak ⁸⁷, T. Zakareishvili ^{149b}, N. Zakharchuk ³⁴, S. Zambito ⁵⁶, J.A. Zamora Saa ^{137d,137b}, J. Zang ¹⁵³, D. Zanzi ⁵⁴, O. Zaplatilek ¹³², C. Zeitnitz ¹⁷¹, H. Zeng ^{14a}, J.C. Zeng ¹⁶², D.T. Zenger Jr ²⁶, O. Zenin ³⁷, T. Ženiš ^{28a}, S. Zenz ⁹⁴, S. Zerradi ^{35a}, D. Zerwas ⁶⁶, M. Zhai ^{14a,14e}, B. Zhang ^{14c}, D.F. Zhang ¹³⁹, J. Zhang ^{62b}, J. Zhang ⁶, K. Zhang ^{14a,14e}, L. Zhang ^{14c}, P. Zhang ^{14a,14e}, R. Zhang ¹⁷⁰, S. Zhang ¹⁰⁶, S. Zhang ⁴⁴, T. Zhang ¹⁵³, X. Zhang ^{62c}, X. Zhang ^{62b}, Y. Zhang ^{62c,5}, Y. Zhang ⁹⁶, Y. Zhang ^{14c}, Z. Zhang ^{17a}, Z. Zhang ⁶⁶, H. Zhao ¹³⁸, T. Zhao ^{62b}, Y. Zhao ¹³⁶, Z. Zhao ^{62a}, A. Zhemchugov ³⁸, J. Zheng ^{14c}, K. Zheng ¹⁶², X. Zheng ^{62a}, Z. Zheng ¹⁴³, D. Zhong ¹⁶², B. Zhou ¹⁰⁶, H. Zhou ⁷, N. Zhou ^{62c}, Y. Zhou ⁷, C.G. Zhu ^{62b}, J. Zhu ¹⁰⁶, Y. Zhu ^{62c}, Y. Zhu ^{62a}, X. Zhuang ^{14a}, K. Zhukov ³⁷, V. Zhulanov ³⁷, N.I. Zimine ³⁸, J. Zinsser ^{63b}, M. Ziolkowski ¹⁴¹, L. Živković ¹⁵, A. Zoccoli ^{23b,23a}, K. Zoch ⁶¹, T.G. Zorbas ¹³⁹, O. Zormpa ⁴⁶, W. Zou ⁴¹, L. Zwalinski ³⁶.

¹Department of Physics, University of Adelaide, Adelaide; Australia.

²Department of Physics, University of Alberta, Edmonton AB; Canada.

^{3(a)}Department of Physics, Ankara University, Ankara; ^(b)Division of Physics, TOBB University of Economics and Technology, Ankara; Türkiye.

⁴LAPP, Université Savoie Mont Blanc, CNRS/IN2P3, Annecy; France.

⁵APC, Université Paris Cité, CNRS/IN2P3, Paris; France.

⁶High Energy Physics Division, Argonne National Laboratory, Argonne IL; United States of America.

⁷Department of Physics, University of Arizona, Tucson AZ; United States of America.

⁸Department of Physics, University of Texas at Arlington, Arlington TX; United States of America.

⁹Physics Department, National and Kapodistrian University of Athens, Athens; Greece.

¹⁰Physics Department, National Technical University of Athens, Zografou; Greece.

¹¹Department of Physics, University of Texas at Austin, Austin TX; United States of America.

¹²Institute of Physics, Azerbaijan Academy of Sciences, Baku; Azerbaijan.

- ¹³Institut de Física d'Altes Energies (IFAE), Barcelona Institute of Science and Technology, Barcelona; Spain.
- ¹⁴(^a)Institute of High Energy Physics, Chinese Academy of Sciences, Beijing; (^b)Physics Department, Tsinghua University, Beijing; (^c)Department of Physics, Nanjing University, Nanjing; (^d)School of Science, Shenzhen Campus of Sun Yat-sen University; (^e)University of Chinese Academy of Science (UCAS), Beijing; China.
- ¹⁵Institute of Physics, University of Belgrade, Belgrade; Serbia.
- ¹⁶Department for Physics and Technology, University of Bergen, Bergen; Norway.
- ¹⁷(^a)Physics Division, Lawrence Berkeley National Laboratory, Berkeley CA; (^b)University of California, Berkeley CA; United States of America.
- ¹⁸Institut für Physik, Humboldt Universität zu Berlin, Berlin; Germany.
- ¹⁹Albert Einstein Center for Fundamental Physics and Laboratory for High Energy Physics, University of Bern, Bern; Switzerland.
- ²⁰School of Physics and Astronomy, University of Birmingham, Birmingham; United Kingdom.
- ²¹(^a)Department of Physics, Bogazici University, Istanbul; (^b)Department of Physics Engineering, Gaziantep University, Gaziantep; (^c)Department of Physics, Istanbul University, Istanbul; Türkiye.
- ²²(^a)Facultad de Ciencias y Centro de Investigaciones, Universidad Antonio Nariño, Bogotá; (^b)Departamento de Física, Universidad Nacional de Colombia, Bogotá; Colombia.
- ²³(^a)Dipartimento di Fisica e Astronomia A. Righi, Università di Bologna, Bologna; (^b)INFN Sezione di Bologna; Italy.
- ²⁴Physikalisches Institut, Universität Bonn, Bonn; Germany.
- ²⁵Department of Physics, Boston University, Boston MA; United States of America.
- ²⁶Department of Physics, Brandeis University, Waltham MA; United States of America.
- ²⁷(^a)Transilvania University of Brasov, Brasov; (^b)Horia Hulubei National Institute of Physics and Nuclear Engineering, Bucharest; (^c)Department of Physics, Alexandru Ioan Cuza University of Iasi, Iasi; (^d)National Institute for Research and Development of Isotopic and Molecular Technologies, Physics Department, Cluj-Napoca; (^e)University Politehnica Bucharest, Bucharest; (^f)West University in Timisoara, Timisoara; (^g)Faculty of Physics, University of Bucharest, Bucharest; Romania.
- ²⁸(^a)Faculty of Mathematics, Physics and Informatics, Comenius University, Bratislava; (^b)Department of Subnuclear Physics, Institute of Experimental Physics of the Slovak Academy of Sciences, Kosice; Slovak Republic.
- ²⁹Physics Department, Brookhaven National Laboratory, Upton NY; United States of America.
- ³⁰Universidad de Buenos Aires, Facultad de Ciencias Exactas y Naturales, Departamento de Física, y CONICET, Instituto de Física de Buenos Aires (IFIBA), Buenos Aires; Argentina.
- ³¹California State University, CA; United States of America.
- ³²Cavendish Laboratory, University of Cambridge, Cambridge; United Kingdom.
- ³³(^a)Department of Physics, University of Cape Town, Cape Town; (^b)iThemba Labs, Western Cape; (^c)Department of Mechanical Engineering Science, University of Johannesburg, Johannesburg; (^d)National Institute of Physics, University of the Philippines Diliman (Philippines); (^e)University of South Africa, Department of Physics, Pretoria; (^f)University of Zululand, KwaDlangezwa; (^g)School of Physics, University of the Witwatersrand, Johannesburg; South Africa.
- ³⁴Department of Physics, Carleton University, Ottawa ON; Canada.
- ³⁵(^a)Faculté des Sciences Ain Chock, Réseau Universitaire de Physique des Hautes Energies - Université Hassan II, Casablanca; (^b)Faculté des Sciences, Université Ibn-Tofail, Kénitra; (^c)Faculté des Sciences Semlalia, Université Cadi Ayyad, LPHEA-Marrakech; (^d)LPMR, Faculté des Sciences, Université Mohamed Premier, Oujda; (^e)Faculté des sciences, Université Mohammed V, Rabat; (^f)Institute of Applied Physics, Mohammed VI Polytechnic University, Ben Guerir; Morocco.

- ³⁶CERN, Geneva; Switzerland.
- ³⁷Affiliated with an institute covered by a cooperation agreement with CERN.
- ³⁸Affiliated with an international laboratory covered by a cooperation agreement with CERN.
- ³⁹Enrico Fermi Institute, University of Chicago, Chicago IL; United States of America.
- ⁴⁰LPC, Université Clermont Auvergne, CNRS/IN2P3, Clermont-Ferrand; France.
- ⁴¹Nevis Laboratory, Columbia University, Irvington NY; United States of America.
- ⁴²Niels Bohr Institute, University of Copenhagen, Copenhagen; Denmark.
- ⁴³(^a)Dipartimento di Fisica, Università della Calabria, Rende;(^b)INFN Gruppo Collegato di Cosenza, Laboratori Nazionali di Frascati; Italy.
- ⁴⁴Physics Department, Southern Methodist University, Dallas TX; United States of America.
- ⁴⁵Physics Department, University of Texas at Dallas, Richardson TX; United States of America.
- ⁴⁶National Centre for Scientific Research "Demokritos", Agia Paraskevi; Greece.
- ⁴⁷(^a)Department of Physics, Stockholm University;(^b)Oskar Klein Centre, Stockholm; Sweden.
- ⁴⁸Deutsches Elektronen-Synchrotron DESY, Hamburg and Zeuthen; Germany.
- ⁴⁹Fakultät Physik , Technische Universität Dortmund, Dortmund; Germany.
- ⁵⁰Institut für Kern- und Teilchenphysik, Technische Universität Dresden, Dresden; Germany.
- ⁵¹Department of Physics, Duke University, Durham NC; United States of America.
- ⁵²SUPA - School of Physics and Astronomy, University of Edinburgh, Edinburgh; United Kingdom.
- ⁵³INFN e Laboratori Nazionali di Frascati, Frascati; Italy.
- ⁵⁴Physikalisches Institut, Albert-Ludwigs-Universität Freiburg, Freiburg; Germany.
- ⁵⁵II. Physikalisches Institut, Georg-August-Universität Göttingen, Göttingen; Germany.
- ⁵⁶Département de Physique Nucléaire et Corpusculaire, Université de Genève, Genève; Switzerland.
- ⁵⁷(^a)Dipartimento di Fisica, Università di Genova, Genova;(^b)INFN Sezione di Genova; Italy.
- ⁵⁸II. Physikalisches Institut, Justus-Liebig-Universität Giessen, Giessen; Germany.
- ⁵⁹SUPA - School of Physics and Astronomy, University of Glasgow, Glasgow; United Kingdom.
- ⁶⁰LPSC, Université Grenoble Alpes, CNRS/IN2P3, Grenoble INP, Grenoble; France.
- ⁶¹Laboratory for Particle Physics and Cosmology, Harvard University, Cambridge MA; United States of America.
- ⁶²(^a)Department of Modern Physics and State Key Laboratory of Particle Detection and Electronics, University of Science and Technology of China, Hefei;(^b)Institute of Frontier and Interdisciplinary Science and Key Laboratory of Particle Physics and Particle Irradiation (MOE), Shandong University, Qingdao;(^c)School of Physics and Astronomy, Shanghai Jiao Tong University, Key Laboratory for Particle Astrophysics and Cosmology (MOE), SKLPPC, Shanghai;(^d)Tsung-Dao Lee Institute, Shanghai;(^e)School of Physics and Microelectronics, Zhengzhou University; China.
- ⁶³(^a)Kirchhoff-Institut für Physik, Ruprecht-Karls-Universität Heidelberg, Heidelberg;(^b)Physikalisches Institut, Ruprecht-Karls-Universität Heidelberg, Heidelberg; Germany.
- ⁶⁴(^a)Department of Physics, Chinese University of Hong Kong, Shatin, N.T., Hong Kong;(^b)Department of Physics, University of Hong Kong, Hong Kong;(^c)Department of Physics and Institute for Advanced Study, Hong Kong University of Science and Technology, Clear Water Bay, Kowloon, Hong Kong; China.
- ⁶⁵Department of Physics, National Tsing Hua University, Hsinchu; Taiwan.
- ⁶⁶IJCLab, Université Paris-Saclay, CNRS/IN2P3, 91405, Orsay; France.
- ⁶⁷Centro Nacional de Microelectrónica (IMB-CNM-CSIC), Barcelona; Spain.
- ⁶⁸Department of Physics, Indiana University, Bloomington IN; United States of America.
- ⁶⁹(^a)INFN Gruppo Collegato di Udine, Sezione di Trieste, Udine;(^b)ICTP, Trieste;(^c)Dipartimento Politecnico di Ingegneria e Architettura, Università di Udine, Udine; Italy.
- ⁷⁰(^a)INFN Sezione di Lecce;(^b)Dipartimento di Matematica e Fisica, Università del Salento, Lecce; Italy.
- ⁷¹(^a)INFN Sezione di Milano;(^b)Dipartimento di Fisica, Università di Milano, Milano; Italy.

- 72^(a) INFN Sezione di Napoli; ^(b) Dipartimento di Fisica, Università di Napoli, Napoli; Italy.
- 73^(a) INFN Sezione di Pavia; ^(b) Dipartimento di Fisica, Università di Pavia, Pavia; Italy.
- 74^(a) INFN Sezione di Pisa; ^(b) Dipartimento di Fisica E. Fermi, Università di Pisa, Pisa; Italy.
- 75^(a) INFN Sezione di Roma; ^(b) Dipartimento di Fisica, Sapienza Università di Roma, Roma; Italy.
- 76^(a) INFN Sezione di Roma Tor Vergata; ^(b) Dipartimento di Fisica, Università di Roma Tor Vergata, Roma; Italy.
- 77^(a) INFN Sezione di Roma Tre; ^(b) Dipartimento di Matematica e Fisica, Università Roma Tre, Roma; Italy.
- 78^(a) INFN-TIFPA; ^(b) Università degli Studi di Trento, Trento; Italy.
- 79 Universität Innsbruck, Department of Astro and Particle Physics, Innsbruck; Austria.
- 80 University of Iowa, Iowa City IA; United States of America.
- 81 Department of Physics and Astronomy, Iowa State University, Ames IA; United States of America.
- 82 Istinye University, Sariyer, Istanbul; Türkiye.
- 83^(a) Departamento de Engenharia Elétrica, Universidade Federal de Juiz de Fora (UFJF), Juiz de Fora; ^(b) Universidade Federal do Rio De Janeiro COPPE/EE/IF, Rio de Janeiro; ^(c) Instituto de Física, Universidade de São Paulo, São Paulo; ^(d) Rio de Janeiro State University, Rio de Janeiro; Brazil.
- 84 KEK, High Energy Accelerator Research Organization, Tsukuba; Japan.
- 85 Graduate School of Science, Kobe University, Kobe; Japan.
- 86^(a) AGH University of Krakow, Faculty of Physics and Applied Computer Science, Krakow; ^(b) Marian Smoluchowski Institute of Physics, Jagiellonian University, Krakow; Poland.
- 87 Institute of Nuclear Physics Polish Academy of Sciences, Krakow; Poland.
- 88 Faculty of Science, Kyoto University, Kyoto; Japan.
- 89 Research Center for Advanced Particle Physics and Department of Physics, Kyushu University, Fukuoka ; Japan.
- 90 Instituto de Física La Plata, Universidad Nacional de La Plata and CONICET, La Plata; Argentina.
- 91 Physics Department, Lancaster University, Lancaster; United Kingdom.
- 92 Oliver Lodge Laboratory, University of Liverpool, Liverpool; United Kingdom.
- 93 Department of Experimental Particle Physics, Jožef Stefan Institute and Department of Physics, University of Ljubljana, Ljubljana; Slovenia.
- 94 School of Physics and Astronomy, Queen Mary University of London, London; United Kingdom.
- 95 Department of Physics, Royal Holloway University of London, Egham; United Kingdom.
- 96 Department of Physics and Astronomy, University College London, London; United Kingdom.
- 97 Louisiana Tech University, Ruston LA; United States of America.
- 98 Fysiska institutionen, Lunds universitet, Lund; Sweden.
- 99 Departamento de Física Teórica C-15 and CIAFF, Universidad Autónoma de Madrid, Madrid; Spain.
- 100 Institut für Physik, Universität Mainz, Mainz; Germany.
- 101 School of Physics and Astronomy, University of Manchester, Manchester; United Kingdom.
- 102 CPPM, Aix-Marseille Université, CNRS/IN2P3, Marseille; France.
- 103 Department of Physics, University of Massachusetts, Amherst MA; United States of America.
- 104 Department of Physics, McGill University, Montreal QC; Canada.
- 105 School of Physics, University of Melbourne, Victoria; Australia.
- 106 Department of Physics, University of Michigan, Ann Arbor MI; United States of America.
- 107 Department of Physics and Astronomy, Michigan State University, East Lansing MI; United States of America.
- 108 Group of Particle Physics, University of Montreal, Montreal QC; Canada.
- 109 Fakultät für Physik, Ludwig-Maximilians-Universität München, München; Germany.
- 110 Max-Planck-Institut für Physik (Werner-Heisenberg-Institut), München; Germany.

- ¹¹¹Graduate School of Science and Kobayashi-Maskawa Institute, Nagoya University, Nagoya; Japan.
- ¹¹²Department of Physics and Astronomy, University of New Mexico, Albuquerque NM; United States of America.
- ¹¹³Institute for Mathematics, Astrophysics and Particle Physics, Radboud University/Nikhef, Nijmegen; Netherlands.
- ¹¹⁴Nikhef National Institute for Subatomic Physics and University of Amsterdam, Amsterdam; Netherlands.
- ¹¹⁵Department of Physics, Northern Illinois University, DeKalb IL; United States of America.
- ¹¹⁶(^a)New York University Abu Dhabi, Abu Dhabi;(^b)University of Sharjah, Sharjah; United Arab Emirates.
- ¹¹⁷Department of Physics, New York University, New York NY; United States of America.
- ¹¹⁸Ochanomizu University, Otsuka, Bunkyo-ku, Tokyo; Japan.
- ¹¹⁹Ohio State University, Columbus OH; United States of America.
- ¹²⁰Homer L. Dodge Department of Physics and Astronomy, University of Oklahoma, Norman OK; United States of America.
- ¹²¹Department of Physics, Oklahoma State University, Stillwater OK; United States of America.
- ¹²²Palacký University, Joint Laboratory of Optics, Olomouc; Czech Republic.
- ¹²³Institute for Fundamental Science, University of Oregon, Eugene, OR; United States of America.
- ¹²⁴Graduate School of Science, Osaka University, Osaka; Japan.
- ¹²⁵Department of Physics, University of Oslo, Oslo; Norway.
- ¹²⁶Department of Physics, Oxford University, Oxford; United Kingdom.
- ¹²⁷LPNHE, Sorbonne Université, Université Paris Cité, CNRS/IN2P3, Paris; France.
- ¹²⁸Department of Physics, University of Pennsylvania, Philadelphia PA; United States of America.
- ¹²⁹Department of Physics and Astronomy, University of Pittsburgh, Pittsburgh PA; United States of America.
- ¹³⁰(^a)Laboratório de Instrumentação e Física Experimental de Partículas - LIP, Lisboa;(^b)Departamento de Física, Faculdade de Ciências, Universidade de Lisboa, Lisboa;(^c)Departamento de Física, Universidade de Coimbra, Coimbra;(^d)Centro de Física Nuclear da Universidade de Lisboa, Lisboa;(^e)Departamento de Física, Universidade do Minho, Braga;(^f)Departamento de Física Teórica y del Cosmos, Universidad de Granada, Granada (Spain);(^g)Departamento de Física, Instituto Superior Técnico, Universidade de Lisboa, Lisboa; Portugal.
- ¹³¹Institute of Physics of the Czech Academy of Sciences, Prague; Czech Republic.
- ¹³²Czech Technical University in Prague, Prague; Czech Republic.
- ¹³³Charles University, Faculty of Mathematics and Physics, Prague; Czech Republic.
- ¹³⁴Particle Physics Department, Rutherford Appleton Laboratory, Didcot; United Kingdom.
- ¹³⁵IRFU, CEA, Université Paris-Saclay, Gif-sur-Yvette; France.
- ¹³⁶Santa Cruz Institute for Particle Physics, University of California Santa Cruz, Santa Cruz CA; United States of America.
- ¹³⁷(^a)Departamento de Física, Pontificia Universidad Católica de Chile, Santiago;(^b)Millennium Institute for Subatomic physics at high energy frontier (SAPHIR), Santiago;(^c)Instituto de Investigación Multidisciplinario en Ciencia y Tecnología, y Departamento de Física, Universidad de La Serena;(^d)Universidad Andres Bello, Department of Physics, Santiago;(^e)Instituto de Alta Investigación, Universidad de Tarapacá, Arica;(^f)Departamento de Física, Universidad Técnica Federico Santa María, Valparaíso; Chile.
- ¹³⁸Department of Physics, University of Washington, Seattle WA; United States of America.
- ¹³⁹Department of Physics and Astronomy, University of Sheffield, Sheffield; United Kingdom.
- ¹⁴⁰Department of Physics, Shinshu University, Nagano; Japan.

- ¹⁴¹Department Physik, Universität Siegen, Siegen; Germany.
- ¹⁴²Department of Physics, Simon Fraser University, Burnaby BC; Canada.
- ¹⁴³SLAC National Accelerator Laboratory, Stanford CA; United States of America.
- ¹⁴⁴Department of Physics, Royal Institute of Technology, Stockholm; Sweden.
- ¹⁴⁵Departments of Physics and Astronomy, Stony Brook University, Stony Brook NY; United States of America.
- ¹⁴⁶Department of Physics and Astronomy, University of Sussex, Brighton; United Kingdom.
- ¹⁴⁷School of Physics, University of Sydney, Sydney; Australia.
- ¹⁴⁸Institute of Physics, Academia Sinica, Taipei; Taiwan.
- ¹⁴⁹^(a)E. Andronikashvili Institute of Physics, Iv. Javakhishvili Tbilisi State University, Tbilisi;^(b)High Energy Physics Institute, Tbilisi State University, Tbilisi;^(c)University of Georgia, Tbilisi; Georgia.
- ¹⁵⁰Department of Physics, Technion, Israel Institute of Technology, Haifa; Israel.
- ¹⁵¹Raymond and Beverly Sackler School of Physics and Astronomy, Tel Aviv University, Tel Aviv; Israel.
- ¹⁵²Department of Physics, Aristotle University of Thessaloniki, Thessaloniki; Greece.
- ¹⁵³International Center for Elementary Particle Physics and Department of Physics, University of Tokyo, Tokyo; Japan.
- ¹⁵⁴Department of Physics, Tokyo Institute of Technology, Tokyo; Japan.
- ¹⁵⁵Department of Physics, University of Toronto, Toronto ON; Canada.
- ¹⁵⁶^(a)TRIUMF, Vancouver BC;^(b)Department of Physics and Astronomy, York University, Toronto ON; Canada.
- ¹⁵⁷Division of Physics and Tomonaga Center for the History of the Universe, Faculty of Pure and Applied Sciences, University of Tsukuba, Tsukuba; Japan.
- ¹⁵⁸Department of Physics and Astronomy, Tufts University, Medford MA; United States of America.
- ¹⁵⁹United Arab Emirates University, Al Ain; United Arab Emirates.
- ¹⁶⁰Department of Physics and Astronomy, University of California Irvine, Irvine CA; United States of America.
- ¹⁶¹Department of Physics and Astronomy, University of Uppsala, Uppsala; Sweden.
- ¹⁶²Department of Physics, University of Illinois, Urbana IL; United States of America.
- ¹⁶³Instituto de Física Corpuscular (IFIC), Centro Mixto Universidad de Valencia - CSIC, Valencia; Spain.
- ¹⁶⁴Department of Physics, University of British Columbia, Vancouver BC; Canada.
- ¹⁶⁵Department of Physics and Astronomy, University of Victoria, Victoria BC; Canada.
- ¹⁶⁶Fakultät für Physik und Astronomie, Julius-Maximilians-Universität Würzburg, Würzburg; Germany.
- ¹⁶⁷Department of Physics, University of Warwick, Coventry; United Kingdom.
- ¹⁶⁸Waseda University, Tokyo; Japan.
- ¹⁶⁹Department of Particle Physics and Astrophysics, Weizmann Institute of Science, Rehovot; Israel.
- ¹⁷⁰Department of Physics, University of Wisconsin, Madison WI; United States of America.
- ¹⁷¹Fakultät für Mathematik und Naturwissenschaften, Fachgruppe Physik, Bergische Universität Wuppertal, Wuppertal; Germany.
- ¹⁷²Department of Physics, Yale University, New Haven CT; United States of America.
- ^a Also Affiliated with an institute covered by a cooperation agreement with CERN.
- ^b Also at An-Najah National University, Nablus; Palestine.
- ^c Also at Borough of Manhattan Community College, City University of New York, New York NY; United States of America.
- ^d Also at Center for High Energy Physics, Peking University; China.
- ^e Also at Center for Interdisciplinary Research and Innovation (CIRI-AUTH), Thessaloniki; Greece.
- ^f Also at Centro Studi e Ricerche Enrico Fermi; Italy.
- ^g Also at CERN, Geneva; Switzerland.

- h* Also at Département de Physique Nucléaire et Corpusculaire, Université de Genève, Genève; Switzerland.
- i* Also at Departament de Física de la Universitat Autònoma de Barcelona, Barcelona; Spain.
- j* Also at Department of Financial and Management Engineering, University of the Aegean, Chios; Greece.
- k* Also at Department of Physics, Ben Gurion University of the Negev, Beer Sheva; Israel.
- l* Also at Department of Physics, California State University, Sacramento; United States of America.
- m* Also at Department of Physics, King's College London, London; United Kingdom.
- n* Also at Department of Physics, Stanford University, Stanford CA; United States of America.
- o* Also at Department of Physics, University of Fribourg, Fribourg; Switzerland.
- p* Also at Department of Physics, University of Thessaly; Greece.
- q* Also at Department of Physics, Westmont College, Santa Barbara; United States of America.
- r* Also at Hellenic Open University, Patras; Greece.
- s* Also at Institutio Catalana de Recerca i Estudis Avancats, ICREA, Barcelona; Spain.
- t* Also at Institut für Experimentalphysik, Universität Hamburg, Hamburg; Germany.
- u* Also at Institute for Nuclear Research and Nuclear Energy (INRNE) of the Bulgarian Academy of Sciences, Sofia; Bulgaria.
- v* Also at Institute of Applied Physics, Mohammed VI Polytechnic University, Ben Guerir; Morocco.
- w* Also at Institute of Particle Physics (IPP); Canada.
- x* Also at Institute of Physics and Technology, Ulaanbaatar; Mongolia.
- y* Also at Institute of Physics, Azerbaijan Academy of Sciences, Baku; Azerbaijan.
- z* Also at Institute of Theoretical Physics, Ilia State University, Tbilisi; Georgia.
- aa* Also at L2IT, Université de Toulouse, CNRS/IN2P3, UPS, Toulouse; France.
- ab* Also at Lawrence Livermore National Laboratory, Livermore; United States of America.
- ac* Also at National Institute of Physics, University of the Philippines Diliman (Philippines); Philippines.
- ad* Also at Technical University of Munich, Munich; Germany.
- ae* Also at The Collaborative Innovation Center of Quantum Matter (CICQM), Beijing; China.
- af* Also at TRIUMF, Vancouver BC; Canada.
- ag* Also at Università di Napoli Parthenope, Napoli; Italy.
- ah* Also at University of Chinese Academy of Sciences (UCAS), Beijing; China.
- ai* Also at University of Colorado Boulder, Department of Physics, Colorado; United States of America.
- aj* Also at Washington College, Chestertown, MD; United States of America.
- ak* Also at Yeditepe University, Physics Department, Istanbul; Türkiye.
- * Deceased